



# MEMBRANE SENSORS FOR STATIC AND HYDRODYNAMIC POTENTIOMETRIC ASSESSMENT OF CETIRIZINE DRUG IN PHARMACEUTICAL FORMULATIONS

Saad S. M. Hassan<sup>[a]\*</sup>, Ayman H. Kamel<sup>[a]\*</sup>, Heba Abd El-Naby<sup>[a]</sup>

**Keywords:** Cetirizine; Potentiometric sensors; Flow injection; Pharmaceutical analysis

The construction and electrochemical response characteristics of poly(vinyl chloride) (PVC) membrane sensors for the determination of cetirizine drug were described. These sensors were based on the use of the ion-association complexes of the cetirizinium cation (Cet<sup>+</sup>) with phosphomolybdic acid [H<sub>3</sub>Mo<sub>12</sub>O<sub>40</sub>] (PMA) (sensor I), tetraphenylborate (TPB) (sensor II) and ammonium reineckate (NH<sub>4</sub>)<sub>2</sub>[Cr(NCS)<sub>4</sub>(NH<sub>3</sub>)<sub>2</sub>] (sensor III) counter anions as ion-exchange sites in a PVC matrix plasticized with dioctylphthalate (DOP). The sensors revealed fast, stable and Nernstian response between 9.0x10<sup>-7</sup> - 1.0x10<sup>-3</sup> mol L<sup>-1</sup> and 5.2x10<sup>-6</sup> - 1.0x10<sup>-3</sup> mol L<sup>-1</sup> with slope of 59.3±0.2, 60.6±0.3 and 61.5±0.2 mV and detection limits 5.3x10<sup>-7</sup>, 3.8x10<sup>-6</sup> and 5.2x10<sup>-6</sup> mol L<sup>-1</sup> for sensor I, II and III respectively. The intrinsic characteristics of the detectors in a low dispersion manifold under hydrodynamic mode of operation are determined and compared with data obtained under batch mode of operation. Validation of the method reveals good performance characteristics including long life span, good selectivity for Cet<sup>+</sup> over a wide variety of other organic compounds, long term stability, high reproducibility, fast response, low detection limit, wide measurement range, acceptable accuracy and precision. Applications of the sensors for the determination of Cet<sup>+</sup> in pharmaceutical samples were also reported. The sensors offered several advantages over many of those previously described and were amenable for quality control/quality assurance assessment of the homogeneity, stability and purity of ephedrine drug tablets.

\*Corresponding Authors

Tel.: +201222162766.

E-mail address: [saadsmhassan@yahoo.com](mailto:saadsmhassan@yahoo.com) (S.S.M.Hassan)

Tel.: +201000743328

E-mail address: [ahkamel76@yahoo.com](mailto:ahkamel76@yahoo.com) (A. H. Kamel)

[a] Chemistry Department, Faculty of Science, Ain Shams University, Abbasia, Cairo, Egypt

## Introduction

Cetirizine drug is considered as a member of the second generation antihistamines and used for the symptomatic relief of hypersensitivity reactions including rhinitis and chronic urticaria.<sup>1,2</sup> Its H<sub>1</sub>-antagonist activity is primarily due to its R- enantiomer, levocetirizine which can be considered as the third-generation non-sedative antihistamine, developed from the second-generation antihistamine cetirizine. Chemically, levocetirizine is the active enantiomer of cetirizine, in which it works by blocking histamine receptors.<sup>3</sup> It also reduces asthma attacks in children by 70%<sup>4</sup>, and slightly crosses the blood-brain barrier only, eliminating the sedative side-effect common with older antihistamines; however it still causes mild drowsiness.<sup>5</sup> Several analytical techniques have been reported for the determination of cetirizine which include liquid chromatography<sup>6-10</sup>, gas chromatography,<sup>11</sup> spectrophotometry,<sup>12-14</sup> capillary electrophoresis<sup>15</sup> and voltammetry.<sup>16</sup> Most of these methods, however, utilize expensive instrumentation, suffer from lack of selectivity, involve careful control of the reaction conditions or derivatization reactions, and require time-consuming pretreatment steps which affect their usefulness for routine analysis. On the other hand, application of potentiometric sensors in the field of pharmaceutical and biomedical analysis have been advocated.<sup>17-19</sup> The approach provides simple, fast, and selective technique for various drugs.<sup>20,21</sup>

Some potentiometric sensors for assessment of cetirizine were reported.<sup>22-24</sup> Advantages and limitations of these sensors for cetirizine were presented in Table 1.

The present work describes preparation, characterization and application of three potentiometric tubular membrane sensors for static and continuous monitoring of cetirizine in pharmaceutical preparations. The sensors exhibit high accuracy, high analytical throughput and good response stability with short measurement time, low limit of detection and high selectivity in the presence of many interferents.

## Experimental

### Equipments

Potentiometric measurements were performed at 25±1°C with an Orion digital pH/mV meter (model SA 720) using cetirizine PVC membrane sensors in conjunction with an Orion Ag/AgCl double junction reference electrode (model 90-02) filled with 10% (m/v) KNO<sub>3</sub> solution in the outer compartment and Ross glass pH combination electrode (Orion 81-02) was used for pH measurements. The potentials were measured for stirred solutions using the following electrochemical cell Ag/AgCl/10<sup>-3</sup> mol L<sup>-1</sup> Cet<sup>+</sup>/membrane/sample test solution/Ag/AgCl double junction reference electrode.

### Materials and methods

All reagents were of analytical grade and used as received without further purification. Doubly distilled water was used throughout. High molecular weight poly(vinyl chloride)

PVC, tetrahydrofuran (THF) were obtained from Aldrich. Dioctylphthalate (DOP) and sodium tetraphenyl borate (Na-TPB) were obtained from Fluka (Ronkonoma, NY). Phosphomolybdic acid and ammonium reineckate were obtained from Sigma Chemical Co. (St. Louis, MO). Pure grade of cetirizine dihydrochloride was supplied by Drug Control Authority, Al-Haram, Giza, Egypt. A  $10^{-2}$  mol L $^{-1}$  stock solution of the drug was freshly prepared by dissolving 0.461 g in 100 mL acetate buffer (0.05 mol L $^{-1}$ ) of pH 4.2. Working solutions ( $10^{-5}$ -  $10^{-3}$  mol L $^{-1}$ ) were prepared by accurate dilutions.

### Sensor preparation and EMF measurements

The ion-exchangers of cetirizinium phosphomolybdate (Cet/PMA) (sensor I), cetirizinium tetraphenylborate (Cet/TPB) (sensor II) and cetirizinium reineckate (Cet/Ren) (sensor III) were prepared by mixing equal volumes of  $10^{-2}$  mol L $^{-1}$  cetirizine dihydrochloride with  $10^{-1}$  mol L $^{-1}$  phosphomolybdic acid, sodium tetraphenylporate and ammonium renickate, respectively. The precipitate of each ion pair was then filtered, washed thoroughly with double distilled water, dried at room temperature for 24 hour.

The sensors prepared by dissolving 10 mg of each ion-associate with 350 mg of the plasticizer DOP and 190 mg PVC in ca. 4 mL tetrahydrofuran (THF). The solution mixture was poured into a 5 cm Petri-dish. All membrane solutions were left to stand overnight at room temperature to evaporate the solvent slowly. The resulting membrane was peeled off from the Petri-dish and discs of 9 mm i.d were cut out and glued onto a 7-mm i.d PVC body using THF. The tube was filled with  $10^{-2}$  mol L $^{-1}$  Cet $^{+}$  as internal solution and 3mm diameter Ag/AgCl coated wire was used as an internal reference electrode. The electrodes were constructed in the conventional mode by the general procedure previously described.<sup>25-26</sup> The sensors were conditioned by soaking in a  $10^{-2}$  mol L $^{-1}$  aqueous Cet $^{+}$  solution for at least 3 hr before use and were stored in distilled water between measurements. They were calibrated by immersion with an Ag/AgCl double junction reference electrode into a 25 mL beaker containing 10 mL of 0.05 mol L $^{-1}$  acetate buffer solution of pH 4.2. Portions (0.5-1.0 mL) of  $10^{-5}$ - $10^{-2}$  mol L $^{-1}$  standard Cet $^{+}$  solutions were successively added and the potential response of stirred solutions was measured after stabilization to  $\pm 0.2$  mV. A calibration was constructed by plotting the EMF reading against the logarithm of Cet $^{+}$  concentrations. The plot was used for subsequent determination of unknown cetirizine drug.

### Flow injection setup and measurements

The flow injection analysis (FIA) system manifold consisted of a two-channel Ismatech MS-REGLO model peristaltic pump. The manifold was connected with polyethylene tubing (Tygon, 0.7 mm i.d.) and an Omnifit injection valve (Rheodyne, Model 7125) with sample loop of 500  $\mu$ L volume. A carrier solution consists of 0.05 mol L $^{-1}$  acetate buffer of pH 4.2 was propelled by means of a peristaltic pump through PTEE tubing (1.13 mm i.d.). The length of the tubing from the injection valve to the sensing cell was 35 cm. A tubular detector was constructed as described previously.<sup>27</sup> The coating solution was prepared by thoroughly shaken 10 mg of the ion pair with 350 mg

DOP plasticizer and mixed with 190 mg PVC powder and 6 ml THF. This cocktail was deposited, using a micro dropper, three to four times in a hole (3 mm wide $\times$ 5 mm length) made in the middle of a 15 cm Tygon tube (ALKEM, P/N A003494 red/red 0.071 i.d.). The tube was inserted and sealed with Araldite in 100  $\mu$ L pipette tip (7 cm long, 0.4 cm diameter).

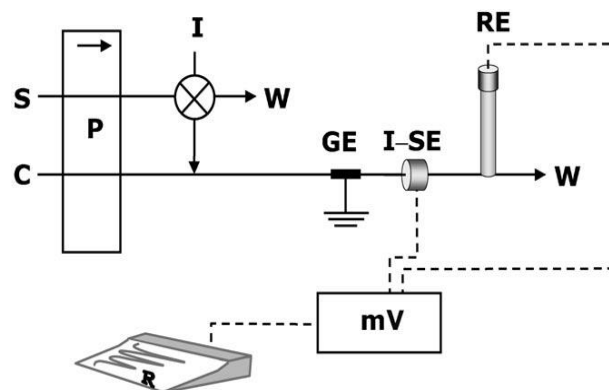


**Figure 1.** Schematic diagram of the flow injection system. P: peristaltic pump, S: sample, C: buffer solution carrier, I: injection valve, GE: grounding electrode, I-SE: Cetirizine selective electrode, RE: reference electrode, W: waste, mV: deci/milli-voltmeter, R: data acquisition system connected to a computer

The tubular sensor was inserted into the flow injection system as schematically shown in Fig. 1. The end of the tube was placed in a Petri dish where a double junction Ag/AgCl reference electrode was placed downstream from the indicator sensor just before the solution went to waste. The sample loop (500  $\mu$ L) of the injection valve was filled and the valve was rotated to allow the sample to be carried out by 0.05 mol L $^{-1}$  acetate buffer stream (pH 4.2) to the flow-through cell by a flow rate 6.5 mL min $^{-1}$ . The potential signals were recorded using an Orion pH/mV meter (model SA 720) connected to a PC through the interface ADC 16 (Pico Technology, UK) and PicoLog for windows (version 5.07) software. The average peak height of 3 replicate runs on each sample was measured and compared with a calibration plot under the same condition.

### Analytical application

Potentiometric analysis was conducted on oral dosage forms of pharmaceutical preparations, commercially designated as Cetrak syrup (Pharco. pharm.co. Alex.), Alerid syrup (Global Napi pharm. Co., Egypt) and Zyrtec drop (Glaxosmithkline.pharm.co., Egypt). Portions of (0.01-11.5) mL aliquot of the pure sample was diluted with 0.05 mol L $^{-1}$  acetate solution of pH 4.2 in 25 mL measuring flask. For drug measurements, a 10 mL aliquot of the drug solution was potentiometrically measured.

### Results and discussion

#### Characterization of cetirizine ion-pair complexes

Cetirizine was reacted with phosphomolybdic acid, sodium tetraphenylborate and ammonium reineckate forming cetirizinium-phosphomolybdate [Cet] $_{2}$ [PM],

**Table1.** General performance characteristics of some potentiometric cetirizine sensors.

Sensor	Slope mV decade <sup>-1</sup>	Linear Range, mol L <sup>-1</sup>	Detection limit, µg mL <sup>-1</sup>	pH range	Response time, s	Interferents	Ref.
<b>Cet./TPB coated wire</b>	66.8	3.16x10 <sup>-5</sup> - 3.1x10 <sup>-3</sup>	14.6	1.5–2.8	<10	Maltose (-2.7), Lactose (-2.6), Starch (-2.5), K <sup>+</sup> (-2.5), Li <sup>+</sup> (-2.5)	[22]
<b>β-cyclodextrin PVC electrode</b>	60.2	5.0x10 <sup>-6</sup> - 1.0x10 <sup>-1</sup>	2.3	2 – 4	10	Vitamin C(-1.1),Glucose(-2.1), Histidine(-2.1)	[23]
<b>β-cyclodextrin carbon paste electrode</b>	57.4	5.0x10 <sup>-6</sup> - 1.0x10 <sup>-1</sup>	3.2	2 – 4	10	Vitamin C (1.6),Glucose (-2.1), Histidine (-2.2)	[23]
<b>Molecularly imprinted polymer (MIP)</b>	28.0	1x10 <sup>-6</sup> - 1x10 <sup>-2</sup>	0.32	1.9 – 4.5	20	Hydroxyzine (-2.2), Piperazine (-3.2), Triethylamine (-3.3)	[24]
<b>Cet./PMA</b>	59.3	9.0x10 <sup>-7</sup> - 1.0x10 <sup>-3</sup>	0.24	3.4 - 6.0	10	Quinine(-1.2),Caffeine (-2.2),Ephedrine (-1.5)	This work
<b>Cet./TPB</b>	60.57	5.2x10 <sup>-6</sup> - 1.0x10 <sup>-3</sup>	1.7	3.3 – 4.6	10	Quinine(-1.8), Caffeine (-2.5), Ephedrine (-1.4),	This work
<b>Cet./Ren</b>	61.5	5.2x10 <sup>-6</sup> - 1.0x10 <sup>-3</sup>	2.4	3.0 -4.5	10	Quinine(-1.6), Caffeine (-2.2), Ephedrine (-1.6)	This work

cetirizinium-tetraphenylborate [Cet][TPB] and cetirizinium-reineckate [Cet][Ren] ion associate complexes. The precipitates were isolated and characterized by elemental analysis.

The elemental analysis obtained for the solid complex agree fairly well with the formula 2:1 of Cet:PMA (Calculated, C: 19.36%, H: 2.303%, N: 2.529%, found, C:19.1%, H: 2.304%, N:2.52%), 1:1 of Cet:TPB (Calculated, C: 76.15%, H: 6.48%, N: 3.95 % found, C: 76.27%, H: 5.87%, N: 4.01 %) and with the formula 1:1 of Cet:Reineckate (Calculated, C:41.28%, H: 4.82%, N: 15.41% found, C: 41.15%, H: 4.84%, N: 15.78%).

### Response characteristics of the electrode system

The electrochemical response characteristics of [Cet]<sub>2</sub>[PM], [Cet][TPB] and [Cet][Ren] PVC membrane sensors were evaluated according to IUPAC recommendations.<sup>28</sup>

The composition of the sensors was 33% PVC the plastic matrix, 66% DOP the solvent mediator and 2% of the ion pair. The calibration graphs were liner over the concentration rang 9.0x10<sup>-7</sup> - 1.0x10<sup>-3</sup>, 5.2x10<sup>-6</sup> – 1.0x10<sup>-3</sup> and 5.1x10<sup>-6</sup> – 1.0 x10<sup>-3</sup> mol L<sup>-1</sup> with slopes 59.3±0.2, 60.6±0.3 and 61.5±0.2 mV decade<sup>-1</sup> and detection limits 5.3x10<sup>-7</sup>, 3.8x10<sup>-6</sup> and 5.2x10<sup>-6</sup> mol L<sup>-1</sup>for sensors I, II and III, respectively. The potentiometric response characteristics of the electrodes assembled with the different membranes

are shown in Fig. 2. The validity of the proposed potentiometric method for determining cetirizine was assessed by measuring the range, lower limit of detection (LOD), accuracy (recovery), precision or repeatability (CV<sub>w</sub>), between-day variability (CV<sub>b</sub>), linearity (correlation coefficient) and sensitivity (slope).<sup>27</sup> Data obtained with six batches (six determinations each) of Cet<sup>+</sup> solutions are shown in Table 2.

The accuracy (trueness) and precision (relative standard deviation, RSD) of the results obtained by sensors I and II were calculated according to equations 1 and 2.<sup>29</sup>

$$\text{Accuracy, \%} = \frac{x}{\mu} 100 \quad (1)$$

$$\text{Precision, \%} = \frac{SD}{x} 100 \quad (2)$$

where:  $x$ ,  $\mu$  and  $SD$  are the average measured concentration found, reference-value and standard deviation, respectively. The results obtained are given in Table 1.

### Effect of pH and response time

The influence of pH on the potentiometric response of the proposed sensors was examined with standard 10<sup>-4</sup> and 10<sup>-3</sup> mol L<sup>-1</sup> Cet<sup>+</sup> solutions over a pH range of 2–9. The pH of

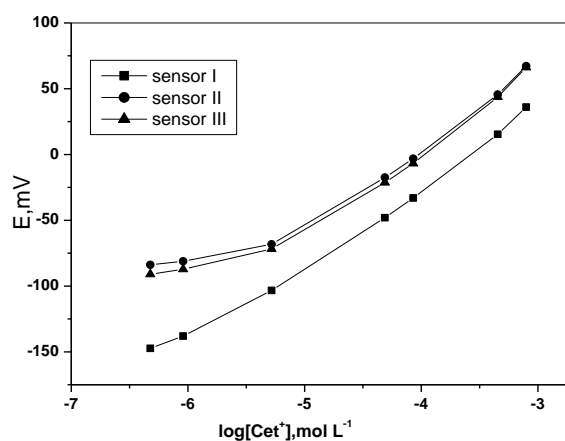


**Figure 2.** Potentiometric response of cetirizine membrane based sensors plasticized in DOP.

the solution was adjusted with either hydrochloric acid and/or sodium hydroxide solutions. It was apparent that sensor I revealed good stability with pH range 3.4 - 6.0 but sensor II, III revealed good stability with pH range 3.3 - 4.6, 3.0 - 4.5 respectively. The potentials of all sensors considerably declined with negative drift at higher pH values due to progressive precipitation of the free cetirizine base. One of the important features of electrochemical sensor is the response time which can be evaluated by measuring the time required to achieve a steady-state potential with in  $\pm 0.2$  mV of the final equilibrium value after successive immersion in a series of  $\text{Cet}^+$  solution, each have a 10 fold difference from low to high concentrations. The response time was  $< 10$  s for all cetirizine solutions in the linear range of calibration curves indicating fast response to these sensors. After several calibrations for each sensor, low potential drift, long-term stability and negligible change in sensors response were observed. When not in use, the sensors were stored and conditioned in  $10^{-3}$  mol  $\text{L}^{-1}$   $\text{Cet}^+$ . For all sensors examined, the detection limits, response times, linear range and calibration slopes were reproducible within  $\pm 3\%$  of their original values over a period of at least 8 weeks.

### Selectivity

The selectivity is the most important characteristic of any sensor, which defines the extent to which it may be used to estimate the particular ionic species in real samples to be selective over all the other ions likely to be present in actual samples along with determined species. Selectivity coefficients of the sensors were determined using the

separate solution method (SSM) and static mode of measurements<sup>28</sup>, determined at  $1.0 \times 10^{-3}$  mol  $\text{L}^{-1}$  concentration of both  $\text{Cet}^+$  and the interfering species in 0.05 mol  $\text{L}^{-1}$  acetate buffer of pH 4.2, are listed in Table 3. The selectivity order for these sensors were  $\text{Cet}^+ > \text{Quinine} > \text{Ephedrine} > \text{fexofenadine} > \text{K}^+ > \text{Histidine} > \text{Caffeine} = \text{Glutamine} > \text{Ba}^{2+}$  (sensor I),  $\text{Cet}^+ > \text{Ephedrine} > \text{Quinine} > \text{Fexofenadine} = \text{Histidine} > \text{Glutamine} > \text{Caffeine} > \text{K}^+ > \text{Ba}^{2+}$  (sensor II),  $\text{Cet}^+ > \text{Quinine} > \text{Ephedrine} > \text{Fexofenadine} > \text{Histidine} > \text{Glutamine} > \text{Caffeine} > \text{K}^+ > \text{Ba}^{2+}$  (sensor III). The results show, on the one hand, reasonable selectivity by all membranes for  $\text{Cet}^+$  compared with many other common inorganic and organic cations and on the other hand, slightly better selectivity by sensor II over sensors I and III especially for quinine, caffeine and fexofenadine. For the effect of ephedrine on the response of the sensors, sensor III exhibit better selectivity than sensors I and II.

Interferent	$\lg K^{pot}_{Cet, J}$		
	Sensor I	Sensor II	Sensor III
Cetirizine	0	0	0
Quinine	-1.2	-1.8	-1.6
Caffeine	-2.2	-2.5	-2.2
Ephedrine	-1.5	-1.4	-1.6
Histidine	-2.1	-2.0	-2.0
Glutamine	-2.2	-2.2	-2.1
Fexofenadine	-1.8	-2.0	-1.9
$\text{K}^+$	-2.1	-3	-2.4
$\text{Ba}^{2+}$	-4	-4.2	-3.5

### Hydrodynamic monitoring of cetirizine

For continuous cetirizinium measurements, a tubular-type

Parameter	Sensor I	Sensor II	Sensor III
Slope, $\text{mV decade}^{-1}$	$59.3 \pm 0.2$	$60.6 \pm 0.3$	$61.5 \pm 0.2$
Correlation coefficient, $r$	0.995	0.998	0.998
Linear range, $\text{mol L}^{-1}$	$9 \times 10^{-7} - 1.0 \times 10^{-3}$	$5.2 \times 10^{-6} - 1.0 \times 10^{-3}$	$5.2 \times 10^{-6} - 1.0 \times 10^{-3}$
Detection limit, $\mu\text{g mL}^{-1}$	0.24	1.75	2.40
Working range, pH	3.4 - 6	3.3 - 4.6	3.0 - 4.5
Response time, s	$< 10$	$< 10$	$< 10$
Standard deviation, $\sigma_v$ , mV	0.9	1.1	1.1
Accuracy, %	99	97.3	97
Precision, $\text{Cv}_w$ , %	2.5	2.4	4.9

detector incorporating a Cet/PMA, Cet/TPB and Cet/Rein based membrane sensors were prepared and used under hydrodynamic mode of operation for continuous  $\text{Cet}^+$  quantification.

**Table 2.** Potentiometric response characteristics of cetirizine membrane based sensors.

**Table 3.** Selectivity coefficient values for cetirizine selective electrodes as calculated by separate solution method

**Table 4.** Potentiometric response characteristics of cetirizine membrane sensors based on Cet/PMA, Cet/TPB and Cet/Rein ion pairs using FI operation

Parameter	Sensor I	Sensor II	Sensor III
Slope, mV decade <sup>-1</sup>	65.6±0.6	66.6±0.4	40.9±0.8
Correlation coefficient, <i>r</i>	0.990	0.977	0.986
Detection limit, mol	1.6x10 <sup>-5</sup>	6.3x10 <sup>-5</sup>	5.0x10 <sup>-5</sup>

L <sup>-1</sup>			
Flow rate, ml min <sup>-1</sup>	6.5	6.5	6.5
Carrier acetate buffer (pH)	4.2	4.2	4.2
Sample rate, h <sup>-1</sup>	20-22	28-30	25-28

Table 5. Static determination of cetirizine in some pharmaceutical formulations using the proposed sensors.

Pharmaceutical Product and source	Nominal content taken (mg mL <sup>-1</sup> )	Sensor I Found (mg mL <sup>-1</sup> )	Recovery %	Sensor II Found (mg mL <sup>-1</sup> )	Recovery %	Sensor III Found (mg mL <sup>-1</sup> )	Recovery %
Cetrak(syrup) Pharco.pharm.co.,Alex.	1.0	0.96	96.0 ±0.5	0.90	90.0 ±1.0	1.01	101 ±0.9
Alerid(syrup), Global napi pharm. Co. Egypt	1.0	0.90	90.0 ±0.8	0.96	96 ±0.6	0.84	84.0 ±1.2
Zyrtec(drops), Glaxosmith-kline Pharm.co., Egypt	10.0	10.50	105 ±0.4	9.12	91.2 ±0.9	10.80	108 ±0.7

Sample		Sensor I			Sensor II			Sensor III		
		Nominal content <sup>a</sup> (µg mL <sup>-1</sup> )	Found (µg mL <sup>-1</sup> )	Recovery, %	Nominal content <sup>a</sup> (µg mL <sup>-1</sup> )	Found, µg mL <sup>-1</sup>	Recovery, %	Nominal content <sup>a</sup> , µg mL <sup>-1</sup>	Found µg mL <sup>-1</sup>	Recovery, %
Cetrak (syrup), Pharco. Pharm. Co. Alex.	C1	46	47	102.0	46	50	108.7	50	47	94.0
	C2	460	470	102	460	410	89.1	461	371	80.4
Alerid(syrup) Global Napi Pharm. Co.Egypt	A1	46	44	895.6	4.62	4.56	98.7	50	54	108.0
	A2	460	470	102	460	432	93.9	460	480	104.3
Zyrtec(drops), Glaxosmithkline.Ph arm. Co., Egypt	Z1	90	80	88.8	4.6	4.1	89.0	92	92	100.0
	Z2	460	490	106.5	460	430	93.5	460	510	110.0

Table 6. Hydrodynamic determination of cetirizine in some pharmaceutical formulations using the proposed sensors.

B

C

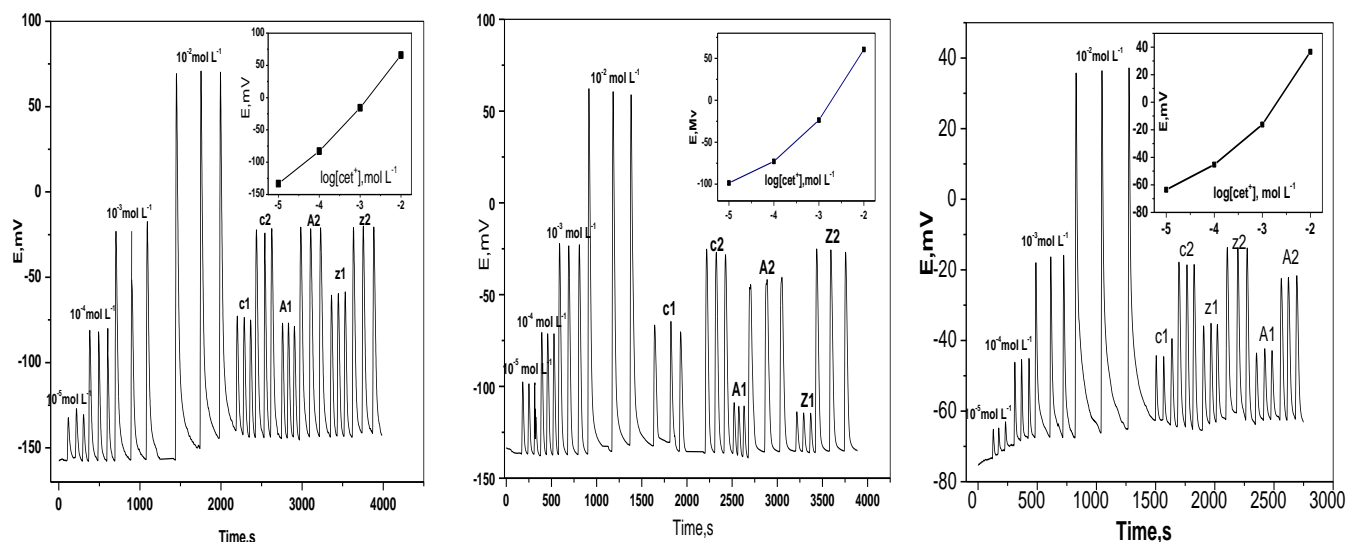


**Figure 3.** Transient potentiometric

signals obtained in triplicate for: (a) Cet/PMA, (b) Cet/TPB and (c) Cet/Ren membrane based sensor. Conditions: carrier solution,  $0.05 \text{ mol L}^{-1}$  acetate buffer pH 4.2 flow rate,  $6.5 \text{ mL min}^{-1}$ ; sample volume,  $500 \mu\text{L}$

A sample loop ( $500 \mu\text{L}$ ) for cetirizine solution ranging from  $1.0 \times 10^{-5}$  to  $1.0 \times 10^{-2} \text{ mol L}^{-1}$  at pH 4.2 with a  $0.05 \text{ mol L}^{-1}$  acetate carrier buffer, flow rate  $6.5 \text{ mL min}^{-1}$  was chosen to study the potentiometric response (slope in  $\text{mV decade}^{-1}$ ) of the proposed sensors. Main analytical features recorded under optimum flow conditions were presented in Table 4. The Sensors gave slopes of  $65.6 \pm 0.6$ ,  $66.6 \pm 0.4$  and  $40.9 \pm 0.8 \text{ mV decade}^{-1}$  with detection limits of  $1.6 \times 10^{-5}$ ,  $6.3 \times 10^{-5}$  and  $5.0 \times 10^{-5} \text{ mol L}^{-1}$  and sampling rate 20-22, 28-30 and 25-28 sample  $\text{h}^{-1}$ , for sensors I, II and III, respectively. Typical FI-diagrams for the sensors are shown in Fig. 3.

#### Assessment of cetirizine in Dosage forms

A number of pharmaceutical additives and diluents commonly used in drug formulations have been examined for their effect on the assay method. Amount of sucrose, glucose, lactose, starch and magnesium stearate in far greater excess than normally found in pharmaceutical preparations were added to both  $\text{Cet}^+$  and the blank. No interferences were noticed.

The contents of cetirizine in various dosage forms were determined with all proposed sensors by both batch and flow injection systems. The results are shown in both Tables 5 and 6. The determinations were made on various types of samples, prepared as described before. The mean results obtained with the proposed sensor on several independent preparations ( $n=5$ ) which show an average recovery of 97.0% for sensor I, 92.4% for sensor II and 97.6% for sensor III with a mean standard deviation of  $\pm 1.5\%$ ,  $\pm 2.2\%$  and  $\pm 1.9\%$ . No interference was caused by active or inactive ingredients and diluents commonly used in drug formulation. Results obtained for determination of cetirizine in some pharmaceutical preparations by FIA show an average recovery of 99.4%, 87.7% and 92.9% with a mean standard deviation of  $\pm 2.4\%$ ,  $\pm 2.2\%$  and  $\pm 1.7\%$  for sensors I, II and III, respectively (Table 6).

#### Conclusions

A fast and simple potentiometric method is used for determination of cetirizine under static (manual) and hydrodynamic (FIA) mode of operations. The potentiometric detection system facilitated the determination of cetirizine with high sampling rates, and a low consumption of sample volume. Tubular membrane sensors are incorporated in flow-through cells and used as detectors for flow injection analysis (FIA) of cetirizine. The electrode methods are more precise and not liable to interferences by the active ingredients, excipients and diluents commonly used in cetirizine drug formation.

#### References

- <sup>1</sup>The Merck Index Merck research Laboratories. 13th edition, **2001**, Martindale J.O'Neil, Merck & Co., Inc., White house Station, NJ. USA. 6281 and 2030.
- <sup>2</sup>Martindale, *The Extra Pharmacopoeia*, The Pharmaceutical Press, London, Ed: J.E.F. Reynolds, **1997**.
- <sup>3</sup>Tillement, J. P., Testa, B., Brée, F., *Biochem. Pharmacol.*, **2003**, 66, 1123.
- <sup>4</sup>Pasquali, M., Baiardini, I., Rogkakou, A., Riccio, A. M., Gamalero, C., Descalzi, D., Folli, C., Passalacqua, G., *Clin. & Experim. Aller.*, **2006**, 36, 1161.
- <sup>5</sup>Gupta, A., Chatelain, P., Massingham, R., Jonsson, E. N., Hammarlund-Udenaes, M., *Drug Metab. Dispos.*, **2006**, 34, 318.
- <sup>6</sup>Dharuman, J., Vasudhevan, M., Ajithlal, T., *J. Chromatog. B*, **2011**, 879, 2624.
- <sup>7</sup>Karakus, S., Kucukguzel, I., Kucukguzel, S. G., *J. Pharm. & Biomed. Anal.*, **2008**, 46, 295.
- <sup>8</sup>Hadad, G. M., Emara, S., Mahmoud, W. M. M., *Talanta*, **2009**, 79, 1360.

- <sup>9</sup>Kang, S. W., Jang, H. J., Moorea, V. S., Parkb, Ji, Kimb, K., Youmc, J., Hanc,S. B., *J. Chromatog. B*, **2010**, 878, 3351.
- <sup>10</sup>Morita , M. R., Berton, D., Boldin, R., Barros , F. A. P., Meurer , E. C., Amarante , A. R., Campos, D. R., Calafatti, S. A., Pereira, R., Abib Jr., E., , Pedrazolli Jr., J., *J. Chromatog. B*, **2008**, 862, 132.
- <sup>11</sup>Baltes, E., Coupez, R., Brouwers, L., Gobert, J., *J. Chromatogr. Biomed.*, **1988**, 74, 149.
- <sup>12</sup>Prabu, S. L., , Shirwaikar, A. A., Shirwaikar, A., Kumar, C. D., G. A. Kumar, G. A., *Indian J. Pharm. Sci.*, **2008**, 70, 236 .
- <sup>13</sup>Choudhari, V., Kale, A., Abnawe, S., Kuchekar, B., Gawli, V., Patil, N., *J. Pharm. Tech. Res.*, **2010**, 2, 4 .
- <sup>14</sup>El Walily, A. F. M., Korany, M. A., El Gindy, A., Bedair, M. F., *J. Pharm. & Biomed. Anal.*, **1998**, 17, 435.
- <sup>15</sup>Bajerski, L., de Silva Sangoi, M., Barth, T., Diefenbach, I. F., Simone Gonçalves Cardoso, S. L. D. E., *Quim. Nova*, **2010**, 33, 114 .
- <sup>16</sup>Patil, R. H., Hegde, R. N., Nandibewoor, S. T., *J. Colloids and Surfaces B: Bioint.*, **2011**, 83, 133 .
- <sup>17</sup>Kamel, A. H., *J. Pharm. & Biomed. Anal.*, **2007**, 45, 341.
- <sup>18</sup>Hassan, S. S. M., Sayour, H. E. M., Kamel, A. H., *Anal. Chim. Acta*, **2009**, 640, 75.
- <sup>19</sup>Kamel, A. H., Mahmoud, W. H., Mostafa, M. S., *Anal. Meth.* , **2011**, 957, 9 .
- <sup>20</sup>Kamel, A. H., Mahmoud, W. H., Mostafa, M. S., *Eur. Chem. Bull.*, **2013**, 2, 88-93
- <sup>21</sup>Hassan, S. S. M., Kamel, A. H., Abd El-Naby, H., *Talanta*, **2013**, 103 ,330–336.
- <sup>22</sup>Shoukry, A. F., Abdel-Ghani, N. T., Issa, Y. M., Ahmed, H. M., *Electroanalysis*, **1998**, 11, 443.
- <sup>23</sup>Rizk, N. M. H., Abbas, S. S., EL-Sayed, F. A., Abo-Bakr, A., *Int. J. Electrochem. Sci.*, **2009**, 4, 396 .
- <sup>24</sup>Javanbakht, M., Eynollahi Fard, S., Abdouss, M., Mohammadi, A., Ganjali, M. R., Norouzi, P., Safaraliev, L., *Electroanalysis*, **2008**, 20, 2023.
- <sup>25</sup>Abdel Aziz, A. A, Kamel, A. H., *Talanta*, **2010**, 80, 1356.
- <sup>26</sup>Kamel, A. H., Mahmoud, W. H., Mostafa, M. S., *Electroanalysis*, **2010**, 22, 2453 (2010)
- <sup>27</sup>Kamel, A. H., Sayour, H. E. M., *Electroanalysis* **2009**, 21, 2701.
- <sup>28</sup>Umezawa, Y., Buhlmann, P., Umezawa, K., Tohoda, K., Amemiya, S., *Pure Appl. Chem.*, **2000**, 72, 1851.
- <sup>29</sup>Taylor, J. K., *Quality Assurance of Chemical Measurements* CRC Press, Florida, **1987**

Received: 06.01.2013.

Accepted: 13.01.2013.



# BIOSORPTION OF $Zn^{2+}$ AND $Cd^{2+}$ IN A TWO-METAL SYSTEM BY *NANNOCHLOROPSIS SALINA*

Yusafir Hala<sup>[a]</sup>, M. Syahrul<sup>[a]</sup>, Emma Suryati<sup>[b]</sup>, Paulina Taba<sup>[a]</sup>, Nunuk H. Soekamto<sup>[a]</sup>

**Keywords:** *Nannochloropsis salina*, zinc, cadmium, two-metal system, Conwy, biosorption.

Although  $Zn^{2+}$  and  $Cd^{2+}$  ions in waters are pollutant with a large amount due to mining and industrial activities, information relating to the use of marine microalgae *Nannochloropsis salina* to absorb both types of metals is still very little. A marine microalga, *N. salina*, was used as biosorbent for the metal ions in water. Concentration of each ion ( $Zn^{2+}$  and  $Cd^{2+}$ ) was  $10 \text{ mg L}^{-1}$  and the concentration ratio of  $Zn^{2+}$  to  $Cd^{2+}$  in the two-metal system (a combination of  $Zn^{2+}$  and  $Cd^{2+}$  in the culture medium) was 1:1. Experimental conditions were as follows: salinity = 25 ‰, temperature = 20 °C, and pH = 7. Addition of each ion individually or the combination of ions was conducted when the optimum growth of microalgae was achieved (i.e. at the 8<sup>th</sup> day after cultivation). The *N. salina* growth after the exposure of metal ions was observed daily and the metal ion concentration adsorbed was determined by using atomic absorption spectrophotometer. Results showed that *N. salina* can be used as biosorbent for  $Zn^{2+}$  and  $Cd^{2+}$  both in single metal ion and two-metal system. Biosorption of  $Zn^{2+}$  by *N. salina* was higher than that of  $Cd^{2+}$  in the single metal ion. The amount of  $Zn^{2+}$  adsorbed in the two-metal system was higher than the one in the single metal ion. However, the opposite trend was observed in the case of  $Cd^{2+}$  ion.

\* Corresponding Author

E-Mail: eddievedder\_jie@yahoo.com

[a] Faculty of Mathematic and Natural Sciences Hasanuddin University, Makassar, Indonesia.

[b] Research Institute for Coastal Aquaculture, Maros, Indonesia

## Introduction

Heavy metals are main contaminants for environment due to the rapid development of industrialization to meet the desires of human life. Heavy metals enter to the human body through the process of digestion and respiration. Chromium, zinc, copper, and manganese are essential metals needed for a variety of physiological functions.<sup>1</sup> In the group of heavy metals, cadmium is recognized as one of the metals considered very toxic and has no role in biological functions. Naturally, the abundance of cadmium is small, but the activities of mining, industry and agriculture have increased the concentration of this metal in the environment.<sup>2</sup> However, zinc is one of the essential metals needed by the human body to function metalloenzyme, but in large quantities, these metals are potentially toxic<sup>1</sup> and inhibit the process of diversity in bacteria.<sup>3</sup> The recovery of heavy metals from industrial waste is important to the community as the effort to recycle and conserve the essential metals,<sup>4</sup> but metal remediation by physico-chemical methods is still expensive and not environmentally friendly. Biotechnological approaches are an attractive alternative and acceptable as a means of bioremediation in waters recently.<sup>5</sup> Natural materials are potential to be used for environmental cleanup of heavy metal contamination.

Microalgae, as aquatic microorganisms, are able to adsorb and accumulate heavy metals in their bodies. Previous research suggested that there was an interaction occurs

between Zn ions with microalgae, where Zn showed significant toxic effects, followed by Ni and Pb.<sup>6</sup> Marine microalgae, *N. salina* was significantly able to adsorb Pb, Cd, and Zn ions,<sup>7</sup> and  $Zn^{2+}$  inhibited the growth of *N. salina* especially at the beginning time of contact. Microalgae can be used as biosorbent for  $Zn^{2+}$  ions with removal efficiency of 94.10% at a concentration of  $10 \text{ mg L}^{-1}$ .<sup>8</sup>

In a multi-metal ion system, antagonistic and synergic interaction may occur in relation to the increased growth of microalgae in marine waters.<sup>9</sup> In the three biosorbents system, adsorption of Pb ions decreased with the presence of Cd and Zn ions in the system, due to competition, both between Cd and Pb ions, as well as between Zn and Pb ions.<sup>10</sup> The presence of other metal ions slightly increases the total biosorption capacity of biomass.<sup>11</sup>

Based on the above description, research on biosorption of  $Zn^{2+}$  and  $Cd^{2+}$  ions in the two-metal system has been done using marine microalgae, *N. salina*, through the observation of its growth and determination of metal concentrations adsorbed after the optimum growth was achieved. The study was expected to be one of the alternative solutions for the heavy metals pollution in waters.

## Materials and Methods

### Materials

Material used in this research was sterile sea water, a unialgal strain of *N. Salina*, and Conwy cultivated medium with the composition shown in Table 1, obtained from the Research Institute for Coastal Aquaculture (Balitbang BAP) Maros Indonesia;  $HNO_3$  solution (p.a grade); double distilled water; aluminium foil. The stock solution of  $Zn^{2+}$



and  $Cd^{2+}$  ions were prepared by dissolving given amounts of  $Zn(NO_3)_2$  and  $CdSO_4 \cdot 8H_2O$ , respectively, in double distilled water. The solutions of different concentrations used in various experiments were obtained by dilution of the stock solutions.

**Table 1.** Composition of Medium Conwy<sup>12</sup>

Materials	Amount, g
<b>Stock A</b>	
FeCl <sub>2</sub> ·6H <sub>2</sub> O	1.3
MnCl <sub>2</sub> ·4 H <sub>2</sub> O	0.36
H <sub>3</sub> BO <sub>3</sub>	33.6
EDTA (Na-salt)	45
NaH <sub>2</sub> PO <sub>4</sub> ·2H <sub>2</sub> O	20
NaNO <sub>3</sub>	100
Double distilled water	1 L
<b>Stock B</b>	
ZnCl <sub>2</sub>	2.1
CoCl <sub>2</sub> ·6H <sub>2</sub> O	2
(NH <sub>4</sub> ) <sub>6</sub> MoO <sub>24</sub> ·4H <sub>2</sub> O	0.9
CuSO <sub>4</sub> ·5H <sub>2</sub> O	2
Double distilled water	100 mL
<b>Stock C</b>	
Vitamin B <sub>12</sub>	10
Vitamin B <sub>1</sub>	200
Double distilled water	100 L
<b>Stock D</b>	
Na <sub>2</sub> SiO <sub>3</sub> ·5H <sub>2</sub> O	4.00
Double distilled water	100 mL

Equipment used is Marienfeld LOT-No 4551 haemocytometer, hand counter, Amara aerator, All America No. 1925X autoclave, atomic absorption spectrophotometer (AAS), Buck Scientific Model 205 VGP, Phase Contrast Microscope Olympus IX71 with magnification of 40 times, Hettich Micro 22R stirrer, Memmert oven, and Millipore cellulose nitrate membrane filter (0.45 μm).

## Methods

### Optimum growth of *N. salina*

Sterile sea water with salinity of 25 ‰ was put into 3 Erlenmeyer flasks. One mL of medium (Conwy) and a unialgal strain *N. salina* with initial population of approximately  $26 \times 10^4$  cell mL<sup>-1</sup> were added into each Erlenmeyer flask. Each mixture was added with the sterile sea water until the volume of solution become 500 mL. The solution was stirred, connected to the aerator and covered with aluminium foil. The growth of *N. salina* was observed with a haemocytometer everyday to obtain the optimum growth of *N. salina*.

### Exposure of metal ions into the *N. salina* culture

When the optimum growth was achieved, each metal ion ( $Zn^{2+}$  and  $Cd^{2+}$ ) with a concentration of 10 mg L<sup>-1</sup> and a mixture of the ions in two-metal system with the ratio of 1:1 were added into the 3 Erlenmeyer flasks containing cultured marine microalgae of *N. salina*, respectively. Further growth

of *N. salina* was observed everyday. After that, separation of solution from the residual marine microalgae was conducted by using a stirrer Hettich Micro 22R for 15 min at 4 °C and 6000 rpm. Furthermore, 2 drops of 2 M HNO<sub>3</sub> was added into each Erlenmeyer flask to prevent precipitation of metal ions. The concentration of each ion in the solution was measured by the AAS. The concentration of metal ion adsorbed ( $C_a$ ) can be calculated by equation (1) and the removal efficiency ( $R_e$ ) was determined by equation (2).  $C_a$  is the difference between initial metal ion concentration ( $C_i$ ) and metal ion concentration in the solution after biosorption ( $C_f$ ).

$$C_a = C_i - C_f \quad (1)$$

$$R_e = \frac{C_a}{C_i} 100 \quad (2)$$

## Result and Discussions

### Optimum growth of *N. salina*

The optimum growth of marine microalgae, *N. salina*, was achieved on the 8<sup>th</sup> day with a population number of  $105 \times 10^4$  cells mL<sup>-1</sup>. Figure 1 shows the relationship between population numbers of *N. salina* against days of growth. Naturally, the growth of *N. salina* will decrease after the optimum growth is achieved. This is because the amount of nutrients in the medium decreases with increasing population number of *N. salina*. The decrease in population is also supported by the accumulation of organic compounds from the dried biomass settling at the bottom of the media. Biomass serves as a new competitor to the *N. salina* cells that are still alive for dissolved oxygen and nutrients in the growth medium.<sup>9</sup>

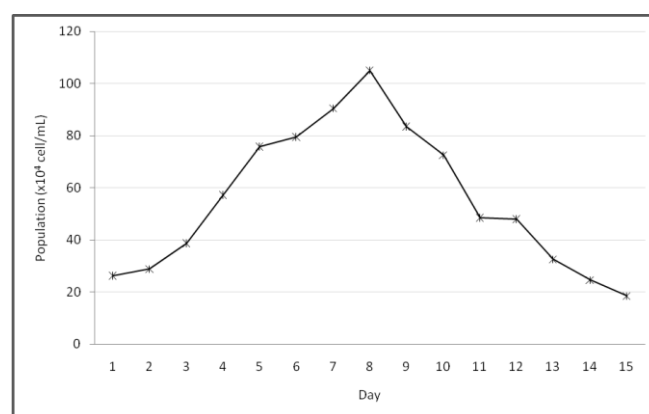


**Figure 1.** The population number of marine microalgae, *N. Salina*, as a function of the growth time.

Natural water is often contaminated by dissolved organic materials that could potentially form complexes with metal ions. Complex organic materials and metals that form can alter the toxicity of heavy metals. The composition of organic matter depends on the environment, it can contain various ligands, such as,  $-SO_4$ ,  $-PO_4$ ,  $-OH$ ,  $-COOH$ ,  $-SH$ , and  $-NH_2$ .<sup>2</sup>

Exposure of Zn<sup>2+</sup> and Cd<sup>2+</sup> ions individually and both ions in the two-metal system causes the drastic decrease in the *N. salina* growth compare to the control (Figure 2). This is caused by the binding of metal ions on the surface of microalgae cells containing a layer of fat, because the body surface of microalgae is covered by cell membranes so that the potency for interaction with metal ions in water is high.<sup>13</sup> The high surface area of cells containing various functional groups, such as the N-terminal of the –NH<sub>2</sub>, C-terminal from the group –COO–, S-terminal of the –SH side chain functional groups of amino acid residues, causes the potency of active sides to bind metal ions.<sup>14</sup>

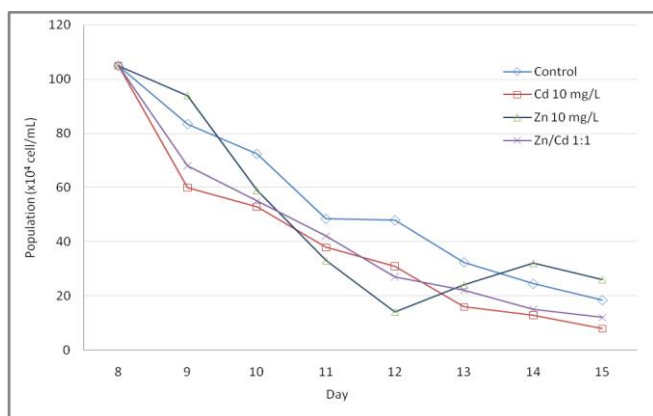


**Figure 2.** The growth of marine microalgae *N. salina* after exposure: Zn<sup>2+</sup> 10 mg L<sup>-1</sup>; Cd<sup>2+</sup> 10 mg L<sup>-1</sup>; and combination of Zn<sup>2+</sup>/Cd<sup>2+</sup> 1:1.

The presence of Cd<sup>2+</sup> ions both in the single metal ion and two-metal system showed a mixture of metal ions have the lower growth trend compared to the control, but Zn<sup>2+</sup> showed an increase in the population at the 13<sup>th</sup> day and the 14<sup>th</sup> day after cultivation. This is because Zn<sup>2+</sup> is one of essential metals that give contribution to the growth of *N. salina* after equilibrium is achieved. Interaction of Zn<sup>2+</sup> ion with functional groups of –OH and –COO– on *N. salina* will form more stable complexes than Cd<sup>2+</sup> ion. According to Lesage et al.,<sup>15</sup> metal concentration at equilibrium (2 h) in the two-metal system is lower than the initial concentration, due to competition on the active site of biosorbent. In the previous study, exposure of Zn<sup>2+</sup> ion showed dominant adsorption occurred at the early contact between the metal ions with *N. salina*.<sup>8</sup> This is because the adsorption of metal ions by the active group, takes place at the cell surface followed by a slow transport step of the ion into the cell membrane and then into the cytoplasm.<sup>14</sup> The particle size was not a significant effect on the total sorption capacity.<sup>16</sup>

In addition, the metal ions in solution undergo equilibrium with ligands produced and excreted by algae.<sup>17</sup> The antagonistic effects between cadmium and essential metals could result in an inhibition of the different enzyme activities. The toxic effects of cadmium will increase with the deficiency of essential metals.<sup>2</sup> Accumulation of some metals on algae occurs through active biological intracellular transport. Toxic heavy metal ions to be sequestered from the cytoplasm of cells through three possible ways, namely: by chelating intracellular biological polymers; deposition of heavy metals on the surface of the cell wall, or by surface adsorption of metal ion binding by chemical functional groups in the cell wall.<sup>18</sup>

## Removal efficiency of metal ions

According to equation (1), the concentration of metal ions adsorbed and removal efficiency for each metal ion individually and in the two-metal system is presented in Table 2. Table 2 shows that the removal efficiency of individual Zn<sup>2+</sup> ion is higher than that of individual Cd<sup>2+</sup>, while in the two-metal system, the removal efficiency of Zn<sup>2+</sup> ion is slightly higher than that in the single metal ion. In contrast, Cd<sup>2+</sup> shows the different result, in which the removal efficiency of Cd<sup>2+</sup> ion in the two-metal system is considerably lower than that in the single metal ion.

**Table 2.** Removal efficiency of Zn<sup>2+</sup> and Cd<sup>2+</sup> adsorbed individually and in the two-metal system after biosorption by *N. salina*

Initial conc., C <sub>i</sub> (mg L <sup>-1</sup> )	Conc. after biosorption (mg L <sup>-1</sup> )		Metal ions	Removal efficiency, R <sub>e</sub> (%)
	Solution, C <sub>f</sub>	Adsorbed, C <sub>a</sub>		
Zn <sup>2+</sup> : 10	0.42	9.58	Zn <sup>2+</sup>	95.77
Cd <sup>2+</sup> : 10	0.71	9.29	Cd <sup>2+</sup>	92.92
Zn <sup>2+</sup> /Cd <sup>2+</sup> 1:1	0.11	9.89	Zn <sup>2+</sup>	98.89
	1.31	8.69	Cd <sup>2+</sup>	86.92

The high concentration of cadmium in the medium results in the decrease of the growth of microalgae and physiological changes associated with the *N. salina* growth. Inhibition of the microalgae growth is caused by inhibition of more specific metabolic processes, particularly those having metalloenzyme or enzymes with sulphhydryl functional group.<sup>2</sup>

## Conclusion

The optimum growth of *N. salina* with a population of 105 x 10<sup>4</sup> cells mL<sup>-1</sup> was obtained at the 8<sup>th</sup> day after cultivation. Marine microalga of *N. salina* can be used as biosorbent for Zn<sup>2+</sup> and Cd<sup>2+</sup> both in single metal ion and two-metal system. Biosorption of Zn<sup>2+</sup> by *N. salina* was higher than that of Cd<sup>2+</sup> in the single metal ion. The amount of Zn<sup>2+</sup> adsorbed in the two-metal system was higher than the one in the single metal ion. However, the amount of Cd<sup>2+</sup> adsorbed in the two-metal system was lower than that in the single metal ion.

## References

- Sathawara, N. G., Parikh, D. J., Agarwal, Y. K. *Bull. Environ. Contam. Toxicol.*, **2004**, 73, 756-761.
- Torres, E., Cid, A., Herrero, C., and Abalde, J. *Water, Air, Soil Pollut.*, **2000**, 117, 1-14.
- Pringault, O., Viret, H., Duran, R. *Environ. Sci. Pollut. Res.*, **2012**, 19, 879–892
- Hashim, M. A and Chu K. H. *Chem. Eng. J.*, **2004**, 97, 249-255.
- Iyer, A., Mody K., and Jha B. *Marine Pollut. Bull.*, **2005**, 50, 340–343.
- Nayar, S., Goh, B. P. L., and Chou, L. M. *Ecotoxicol. Environ. Safety*, **2004**, 59, 349-369.

- <sup>7</sup> Tambung, A., Patabang, A., Astri, Hala, Y., dan Taba, P., Kajian interaksi ion logam Pb, Cd, dan Zn dengan fitoplankton *Nannochloropsis salina*, *Mar. Chim. Acta*, Ed. Khusus Seminar Nasional FK3TI, Oktober **2007**, 42-46.
- <sup>8</sup> Hala, Y., Syahrul, M., Suryati, E., Taba, P. 2012. Biosorption of  $Zn^{2+}$  with *Nannochloropsis salina*, Presented on the 2<sup>nd</sup> international seminar on new paradigm and innovation on natural sciences and its application (INSPINSA-2), Semarang, Indonesia, October 4, **2012**.
- <sup>9</sup> Gonzalez Davila, M. *Marine Chem.*, **1995**, *48*, 215-236.
- <sup>10</sup> Vilar, V. J. P., Botelho, C. M. S., and Boaventura, R. A. R. *J. Hazard. Mater.*, **2008**, *154*, 711-720.
- <sup>11</sup> Say, R., Denizli, A., Arica, M. Y. *Bioresour. Technol.*, **2001**, *76*, 67-70.
- <sup>12</sup> Fogg, G. E. *Algae culture and phytoplankton ecology.*, 3<sup>rd</sup>. Ed., **1985**, The University of Wisconsin Press.
- <sup>13</sup> Fhencel, T. *Ann. Rev. Ecol.*, **1988**, *10(2)*, 165-173.
- <sup>14</sup> Chu, K. H and Hashim M. A. *J. Environ. Sci.*, **2007**, *19*, 928-932.
- <sup>15</sup> Lesage, E., Mundia, C., Rousseau, D. P. L., Van de Moortel, A. M. K., Du Laing, G., Meers, E., Tack, F. M. G., De Pauw, N., Verloo, M. G. *Ecol. Eng.*, **2007**, *30*, 320-325.
- <sup>16</sup> Pavasant, P., Apiratikul, R., Sungkhum, V., Suthiparinyanont, P., Wattanachira, S.. *Bioresour. Technol.*, **2006**, *97(18)*, 2321-2329.
- <sup>17</sup> Santana-Casiano, J. M., Gonzalez-Davila, M., Perez-Pefia, J., Millerob, F. J. *Marine Chem.*, **1995**, *48*, 115-129.
- <sup>18</sup> Moreno-Garrido, I., Blasco J., Gonzalez-Delvalle M., Lubian L. M. *Ecotoxicol. Environ. Restor.*, **1998**, *1*, 43-47.

Received: 19.12.2012.

Accepted: 13.01.2013.



# CLEAN AND EFFICIENT MICROWAVE ASSISTED SYNTHESIS OF SOME NEW PYRIMIDINE, PYRAZOLINE AND ISOXAZOLINE DERIVATIVES FROM 3-(3-NITROPHENYL)-N- PHENYL-PROP-2-ENAMIDE

Urvashi Tiwari<sup>[a]</sup>, Chetna Ameta<sup>[a]</sup>, Sanyogita Sharma<sup>[b]</sup>, Meenakshi Sharma<sup>[c]</sup>, Arpit Kumar  
Pathak<sup>[a]</sup>, Pinki B. Punjabi<sup>[a]\*</sup>

**Keywords:** Microwave irradiation, Chalcones, Isoxazoles, Pyrazoles, Pyrimidines

A rapid and efficient method for the preparation of some new pyrimidine, pyrazoline and isoxazoline derivatives by the reaction of chalcones with hydroxylamine, urea and hydrazine hydrate under microwave exposure has been reported. The products have been isolated, purified and characterized by spectral methods like IR, NMR and mass spectrometry. The antibacterial and antifungal activities of the final products against various bacteria and fungi have also been reported.

\*Corresponding Authors

\*E-mail: [pb\\_punjabi@yahoo.com](mailto:pb_punjabi@yahoo.com)

- [a] Microwave Chemistry Laboratory, Department of Chemistry, Mohanlal Sukhadia University, Udaipur - 313 001, Rajasthan, India  
[b] Department of Chemistry, Pacific Institute of Technology, "Pacific Hills" Pratapnagar Extension, Airport Road, Debari, Udaipur, India  
[c] Department of Chemistry, Banasthali Vidyapeeth, Banasthali, Rajasthan, India

## Introduction

Increasing globalization and industrialization is causing harm to our ecosystem, which is gradually getting polluted. The implementation of green chemistry and green manufacturing technologies will help to decrease the causes for these climate changes which are dreaded for environmental and human health challenges that we are facing and feeling now-a-days. Green chemistry techniques are now being used across the world to develop new materials in every field of chemistry. MAOS (Microwave Assisted Organic Synthesis)<sup>1</sup> strategies offer feasible solutions to minimize environmental deterioration as their benefits are manifold: it frequently leads to dramatically reduction in reaction time, higher yields, cleaner reaction profiles and above all, eco-friendliness. This is a technique which gives "yes or no answer" for a particular chemical transformation within 5 to 10 minutes as compared to several hours in conventional protocol in industry and academia.<sup>2,3</sup> A heterocyclic compound is one which possesses a cyclic structure with hetero atoms in the ring in addition to c- atom. Nitrogen and oxygen containing heterocyclic compounds have received considerable attention due to their wide range of pharmacological activities.<sup>4-8</sup>

As our interest is to synthesize heterocyclic templates capable of bearing some potential pharmacophores which can enhance the inherent biological activity, Therefore systematic propagation of heterocyclic rings in chalcones

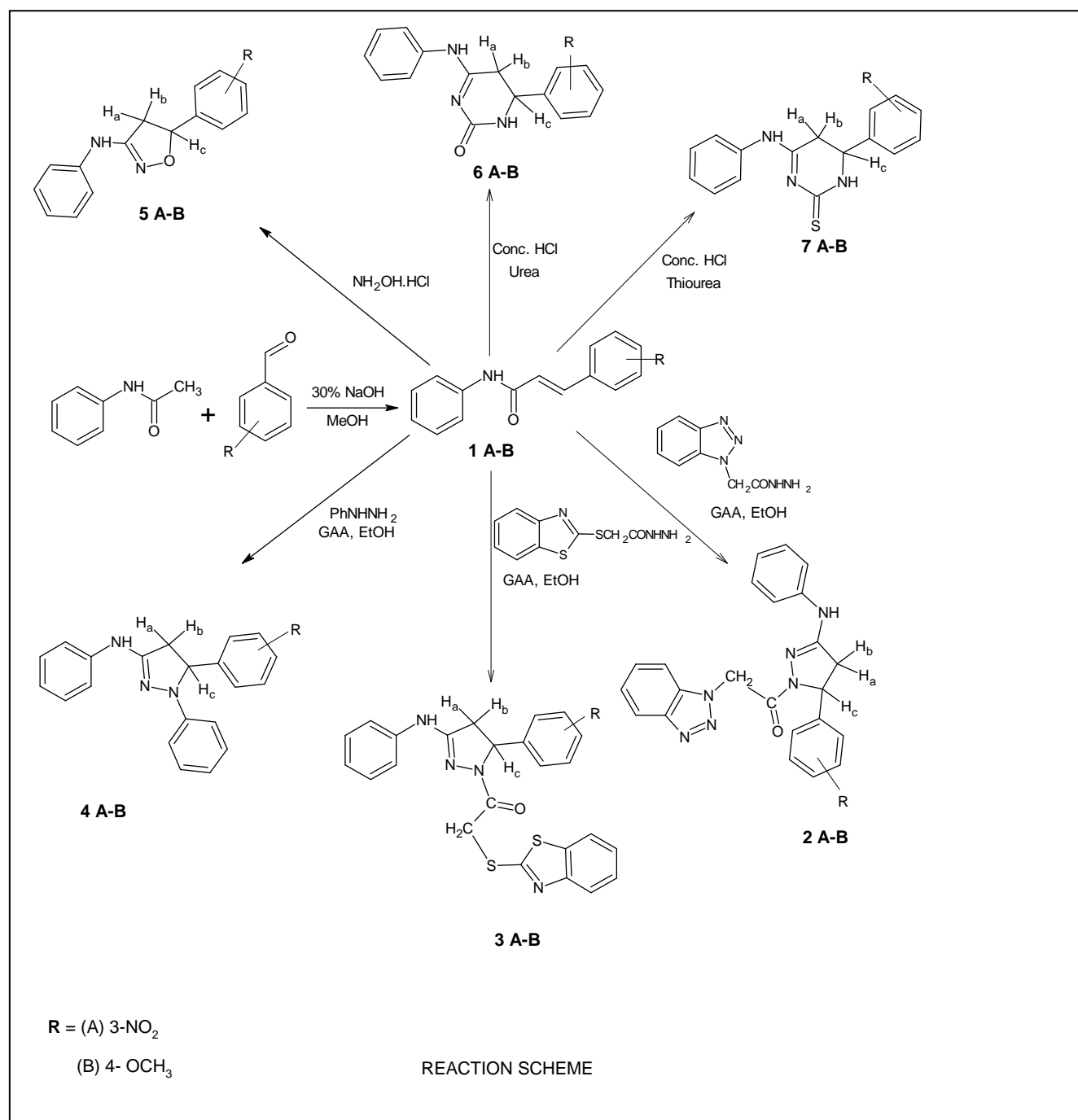
with the installation of biological active heterocyclic units such as isoxazoles, pyrimidines and pyrazoles has been carried out. Pyrimidines are found to be endowed with potential biological activity such as antitumor,<sup>9</sup> antiviral,<sup>10</sup> anticancer,<sup>11</sup> antibacterial,<sup>12</sup> antimicrobial<sup>13</sup> and many others.

Isoxazoles have been reported to possess bactericidal,<sup>14</sup> fungicidal<sup>15</sup> and antimicrobial activity.<sup>16</sup> Pyrazoles display a number of antimicrobial activities like anticancer,<sup>17</sup> antidiabetic<sup>18</sup> and antidepressant.<sup>19</sup> Therefore, it was thought worthwhile to synthesize these nuclei from 3-(substituted phenyl)-N-phenyl prop-2-enamide, in order to explore the pharmacological activities of these compounds.

## Results and Discussion

Acetanilide on condensation with substituted aldehydes in presence of 30% NaOH afforded compound **1A-B**, which were used as intermediates for the synthesis of pyrazolines, pyrimidines and isoxazolines following three different pathways. Compounds **1A-B** gave characteristic IR bands in the region between 3310-3315 cm<sup>-1</sup> for (N-H str.), 3014 – 3018 cm<sup>-1</sup> (C-H str., Ar-H), 1660 -1666 cm<sup>-1</sup> (C=O str.), 1595 -1605 cm<sup>-1</sup> (C=C str.) and <sup>1</sup>H NMR signals for multiplet of nine integrating aromatic protons at (δ) 6.20 - 7.40, doublet of C-H vinyl group at (δ) 6.302 -5.20, singlet at (δ) 5.24 – 5.95 for N-H group and signal at (δ) 3.5 for OCH<sub>3</sub>. Further, compounds **1A** and **1B** were confirmed by the characteristics IR bands at 1540, 1499 cm<sup>-1</sup> (NO<sub>2</sub> str.) and 1218 cm<sup>-1</sup> (C-O-C str.).

Chalcones are convenient starting material for the synthesis of pyrazolines, pyrimidines and isoxazolines due to their α, β-unsaturated moiety. The absence of carbonyl stretching frequency in the region of 1665 cm<sup>-1</sup> confirms the formation of products. In the first path way compound **1A** and **1B** were treated with hydrazides of benzotriazole, mercaptobenzthiazole and phenylhydrazine hydrate resulting in the formation of pyrazoline containing nuclei



**2A-B**, **3A-B** and **4A-B**, respectively. Compound **2A** showed characteristic IR absorption bands in the region 2962cm<sup>-1</sup> (CH<sub>2</sub> str.) and 1683 cm<sup>-1</sup> (C=N str.), 1606 & 1415 cm<sup>-1</sup> (NO<sub>2</sub> str.) and signals at 6.40 ppm (dd, 1H, H<sub>c</sub>), 4.54 ppm (dd, 1H, H<sub>a</sub>), 3.48 ppm (dd, 1H, H<sub>b</sub>) and 3.24 ppm (s, 2H, CH<sub>2</sub>) in <sup>1</sup>H NMR spectrum in addition to -NH and aromatic protons, which supports the synthesis of compound **2A** and pyrazoline ring.

Similarly other synthesized pyrazoline derivatives commonly gave characteristics IR absorption bands in the region between 2940 -2970 cm<sup>-1</sup> for C-H str. of CH<sub>2</sub>, 1610 - 1690 cm<sup>-1</sup> (C=N str.) and signals at (δ) 3.50 -3.20 ppm (dd, 1H, H<sub>b</sub>), 4.54 -4.30 ppm (dd, 1H, H<sub>a</sub>) and 6.42 -6.20 ppm (dd, 1H, H<sub>c</sub>) which, further confirmed the formation of pyrazoline ring in respective compound **3A-B** and **4A-B**.

In second pathway, isoxazoline derivatives **5A-B** have been synthesized by treating compounds **1A-B** and hydroxylamine hydrochloride in basic medium. Compound **5A** showed absorption bands in the region of 3348 cm<sup>-1</sup> (N-H str.), 2931cm<sup>-1</sup> (C-H str. CH<sub>2</sub>) 1638 cm<sup>-1</sup>(C=N str.), 1450 & 1352 cm<sup>-1</sup> (NO<sub>2</sub> str.). <sup>1</sup>H NMR signals were found at (δ) 6.8- 7.39 (m, 9H, Ar-H), 6.16 (dd, 1H, H<sub>c</sub>), 5.4 (s, 1H, NH), 4.38 (dd, 1H, H<sub>a</sub>) and 3.40 (dd, 1H, H<sub>b</sub>) confirmed synthesis of compound **5A**. The compound **5B** also showed IR band at 1210 cm<sup>-1</sup> (C-O-C str.) and NMR signal at (δ) 3.3 singlet of three integrating protons for OCH<sub>3</sub>.

In third pathway, reaction of compounds **1A-B** with urea and thiourea in acidic medium afforded the corresponding compounds **6A-B** and **7A-B** bearing pyrimidine ring.

**Table 1.** Physical and analytical data of synthesized compounds

Compound	Molecular Formula	Mol. weight	M.P., °C	Yield, %	Elemental analysis, calculated/(found) %		
					C	H	N
<b>1A</b>	C <sub>15</sub> H <sub>12</sub> N <sub>2</sub> O <sub>3</sub>	268	92	70	67.16 (67.06)	4.51 (4.44)	10.44(10.36)
<b>1B</b>	C <sub>16</sub> H <sub>15</sub> NO <sub>2</sub>	253	76	75	75.87(75.79)	5.97(5.90)	5.53(5.45)
<b>2A</b>	C <sub>23</sub> H <sub>19</sub> N <sub>7</sub> O <sub>3</sub>	441	210	68	62.58(62.49)	4.34(4.25)	22.21(22.16)
<b>2B</b>	C <sub>24</sub> H <sub>22</sub> N <sub>6</sub> O <sub>2</sub>	426	228	72	67.59(67.50)	5.20(5.11)	19.71(19.63)
<b>3A</b>	C <sub>24</sub> H <sub>19</sub> N <sub>5</sub> O <sub>3</sub> S <sub>2</sub>	489	182	78	58.88(58.79)	3.91(3.82)	14.31(14.22)
<b>3B</b>	C <sub>25</sub> H <sub>22</sub> N <sub>4</sub> O <sub>2</sub> S <sub>2</sub>	474	210	65	63.27(63.18)	4.67(4.58)	11.81(11.73)
<b>4A</b>	C <sub>21</sub> H <sub>18</sub> N <sub>4</sub> O <sub>2</sub>	358	158	77	70.38(70.30)	5.06(5.00)	15.63(15.56)
<b>4B</b>	C <sub>22</sub> H <sub>21</sub> N <sub>3</sub> O	343	160	70	76.94(76.85)	6.16(6.09)	12.24(12.14)
<b>5A</b>	C <sub>15</sub> H <sub>13</sub> N <sub>3</sub> O <sub>3</sub>	283	196	75	63.60(63.51)	4.63(4.55)	14.83(14.74)
<b>5B</b>	C <sub>16</sub> H <sub>16</sub> N <sub>2</sub> O <sub>2</sub>	268	206	80	71.62(71.56)	6.01(5.92)	10.44(10.32)
<b>6A</b>	C <sub>16</sub> H <sub>14</sub> N <sub>4</sub> O <sub>3</sub>	310	208	64	61.93(61.84)	4.55(4.42)	18.06(17.93)
<b>6B</b>	C <sub>17</sub> H <sub>17</sub> N <sub>3</sub> O <sub>2</sub>	295	210	69	69.14(69.05)	5.80(5.70)	14.23(14.14)
<b>7A</b>	C <sub>16</sub> H <sub>14</sub> N <sub>4</sub> O <sub>2</sub> S	326	160	71	58.88(58.79)	4.32(4.22)	17.17(17.09)
<b>7B</b>	C <sub>17</sub> H <sub>17</sub> N <sub>3</sub> OS	311	156	67	65.57(65.48)	5.50(5.41)	13.49(13.38)

**Table 2.** Antimicrobial activity of synthesized compounds (500 ppm)

Compound	Code	Antibacterial activity (Activity index)				Antifungal activity (Activity index)	
		<i>K.pneumoniae</i>	<i>P. aeruginosa</i>	<i>E.Coli</i>	<i>B.subtilis</i>	<i>C.albicans</i>	<i>A. fumigatus</i>
<b>2A</b>	A	14	14	20	10	15	16
<b>2B</b>	B	22	12	18	15	12	-
<b>3A</b>	C	12	20	22	19	18	12
<b>3B</b>	D	18	14	16	17	-	17
<b>4A</b>	E	23	-	12	21	12	-
<b>4B</b>	F	20	-	14	16	-	11
<b>5A</b>	G	-	18	08	19	12	08
<b>5B</b>	H	10	24	13	18	10	-
<b>6A</b>	I	-	15	23	20	16	-
<b>6B</b>	J	14	20	18	16	10	15
<b>7A</b>	K	13	-	16	22	11	12
<b>7B</b>	L	16	18	19	14	-	-
Standard 1	1	24	25	25	24	-	-
Standard 2	2	-	-	-	-	20	NA

Standard: 1 = Ciprofloxacin, 2 = Fluconazole dispersible; NA: Nil activity

Their IR, <sup>1</sup>H NMR and mass spectral studies confirmed the structure of these compounds. **6A-B** gave IR bands at 1692 cm<sup>-1</sup> (CONH str. ), 1618 cm<sup>-1</sup> (C=N str.), 1728 cm<sup>-1</sup> (C=O str.) and 1350 & 1487 cm<sup>-1</sup> (NO<sub>2</sub> str.) and <sup>1</sup>H NMR signals at (δ) 6.06 (dd, 1H, H<sub>c</sub>), 5.30 (s, 1H, NH), 3.30 (dd, 1H, H<sub>b</sub>), 4.26 (dd, 1H, H<sub>a</sub>) and 5.8 (d, 1H, CONH ) confirmed the synthesis of compound **6A-B** and pyrimidine ring. Similarly, compound **7A-B** gave some characteristic bands in the region between 3370 – 3380 cm<sup>-1</sup> (N-H str.), 1670 -1672 cm<sup>-1</sup> (CSNH str.) , 3080 -3090 cm<sup>-1</sup> (C –H str., Ar- H), 1608 -1612 cm<sup>-1</sup> (C=N str.) and <sup>1</sup>H NMR signals at (δ) 6.06 -6.08 (dd, 1H, H<sub>c</sub>), 4.20 -4.30 (dd, 1H, H<sub>a</sub>), 3.28 - 3.32 (dd, 1H, H<sub>b</sub>) and 5.0 -5.4 (s, 1H, CSNH) which, further confirmed the synthesis of compounds **7A-B**.

The synthesized compounds have also been characterized by their mass spectral and elemental analysis studies.

### Antimicrobial activity

The antimicrobial activity of synthesized compounds has been investigated against four bacterial strains i.e., *E. coli*, *B. subtilis*, *K. pneumoniae* and *P. aeruginosa* and two fungal strains *C. albicans* and *A. fumigatus*. (**Table 2**)

Sabourad dextrose agar media following agar well diffusion method at 500 µg / mL using DMSO as solvent. The zone of inhibition was measured in mm. Standard drugs used were ciprofloxacin (antibacterial) and fluconazole dispersible (antifungal). Compounds **3A**, **6A**, **7B** and **4A**, **6A**, **7A** showed better activity against *E.coli* and *B. subtilis*, respectively. The rest compounds shows moderate to good activity. Compounds **2B**, **4A**, **4B** and **3A**, **5B**, **6B** showed significant activity against *K. pneumoniae* and *P. aeruginosa*, respectively. Compounds **3A**, **6A** showed good activity against *C. albicans* and all synthesized compounds showed moderate to good activity against *A. fumigatus* as compared to standard drug, which was active against *A. fumigatus*.

## Experimental Section

### General Procedure

All reactions were carried out in a domestic microwave oven (Kenstar, Model No. OM-26 EGO). Melting points are uncorrected and determined in open capillaries. Reactions were monitored by thin layer chromatography using silica gel-G as adsorbent using ethyl acetate: n-hexane (7: 3) as

eluent and products were detected by iodine vapors. IR spectra (KBr pellets) were recorded on Perkin-Elmer 1800 (FTIR) spectrometer.  $^1\text{H}$  NMR spectra (DMSO- $d_6$ ) were taken on a Bruker DRX spectrometer (300 MHz FT NMR) using TMS as internal standard and chemical shift were expressed in  $\delta$ . Mass spectra were taken on a Jeol SX-102/PA-6000 (EI) spectrometer. Elemental analysis was carried out on C, H, N analyzer (Elemental Vario Carlo Alba 1108). The results were found to be in good agreement with the calculated values ( $\pm 0.2\%$ ).

#### Synthesis of **1A** and **1B**

It is prepared by the reaction of mixture of acetanilide (0.01 mol), aldehydes (0.01 mol), aqueous NaOH (30%) in methanol (50 mL). The reaction mixture was stirred for 1hr. Then the reaction mixture was irradiated for 6-8 minutes in MW at 600 W. After completion of reaction, the viscous mass was poured into ice cold water with vigorous stirring and left over night for complete precipitation. The resultant solid was dried and recrystallized from ethanol.

#### Synthesis of **2A**, **2B**, **3A**, **3B**, **4A** and **4B**

Equimolar amounts of chalcone 1A-B (0.01 mol), substituted hydrazides (0.01 mol) in ethanol (50 mL) were taken in an Erlenmeyer flask and 2-3 mL of glacial acetic acid was added to it. The reaction mixture was mixed thoroughly and irradiated for 6-8 minutes at 720 W with intermitted irradiation for 30 sec. interval. On completion of reaction (as monitored by TLC) resultant mass was poured into ice cold water with vigorous stirring. The solid obtained was filtered, washed with ethanol and recrystallized from ethanol.

#### Synthesis of **5A** and **5B**

It is prepared by reacting purified mixture of chalcone (0.01 mol), hydroxylamine hydrochloride (0.01 mol) and of NaOH (30%) in ethanol (50 mL) under microwave irradiation for 4-6 minutes at 720W. Completion of reaction was monitored by TLC. Excess of solvent was removed by evaporation; obtained mass was poured into ice water with vigorous stirring. It was kept over night. The resultant solid product was filtered, washed and recrystallized from acetone.

#### Synthesis of **6A**, **6B**, **7A** and **7B**

It is prepared by reacting purified mixture of chalcone (1A-B) (0.01 mol), compounds urea or thiourea (0.01 mol) in ethanol (50 mL) and 2-3 drops of conc. HCl. Reaction mass was irradiated for 7-10 minute in microwave at 960 W. Excess of solvent was removed, poured in ice-cold water, filtered, recrystallized from ethanol.

### Spectral Data

#### 3-(3-Nitrophenyl)-N-phenyl prop-2-enamide (**1A**)

IR (KBr,  $\text{cm}^{-1}$ ): 3315 (NH), 3018 (C-H str. Ar-H), 1666 (C=O), 1602 (C=C), 1540, 1499 ( $\text{NO}_2$ );  $^1\text{H}$  NMR ( $\delta$ ): 6.35-7.40 (m, 9H, Ar), 6.30 (d, 1H, CH vinyl), 5.95 (d, 1H, CH vinyl), 5.26 (s, 1H, NH); Mass (m/z): 268 [M] $^+$ .

#### 3-(4-Methoxyphenyl)-N-phenyl prop-2-enamide (**1B**)

IR (KBr,  $\text{cm}^{-1}$ ): 3311 (NH), 3014 (C-H str., ArH), 1599 (C=O), 1218 (C-O-C);  $^1\text{H}$  NMR ( $\delta$ ): 6.20-7.30 (m, 9H Ar-H), 6.10 (d, 1H, CH vinyl), 5.92 (d, 1H, CH vinyl), 5.24 (s, 1H, NH), 3.5 (s, 3H,  $\text{OCH}_3$ ); Mass (M/Z): 253 [M] $^+$ .

#### 2-(1H-benzotriazol-1-yl)-1-[5-(3-nitrophenyl)-3-(phenylamino)-4,5-dihydro-1H-pyrazol-1-yl]ethanone (**2A**)

IR (KBr,  $\text{cm}^{-1}$ ): 3348 (NH), 3022 (C-H str., ArH), 2962 ( $\text{CH}_2$ ), 1815 (C=O), 1683 (C=N), 1606, 1415 ( $\text{NO}_2$ );  $^1\text{H}$ NMR ( $\delta$ ): 6.64-7.96 (m, 13H, Ar), 6.40 (dd, 1H,  $\text{H}_c$ ), 5.33 (s, 1H, NH), 4.54 (dd, 1H,  $\text{H}_a$ ), 3.48 (dd, 1H,  $\text{H}_b$ ), 3.24 (s, 2H,  $\text{CH}_2$ ); Mass (m/z): 441[M] $^+$ .

#### 2-(1H-benzotriazol-1-yl)-1-[5-(4-methoxyphenyl)-3-(phenylamino)-4,5-dihydro-1H-pyrazol-1-yl]ethanone (**2B**)

IR (KBr,  $\text{cm}^{-1}$ ): 3345 (NH), 3018 (C-H str., Ar-H), 2954 ( $\text{CH}_2$ ), 1812 (C=O), 1678 (C=N), 1225 (C-O-C);  $^1\text{H}$  NMR ( $\delta$ ): 6.50-7.86 (m, 13H, Ar), 6.36 (dd, 1H,  $\text{H}_a$ ), 3.46 (dd, 1H,  $\text{H}_b$ ), 3.22 (s, 2H,  $\text{CH}_2$ ), 3.60 (s, 3H,  $\text{-OCH}_3$ ); Mass (m/z): 426 [M] $^+$ .

#### 2-(1,3-Benzothiazol-2-yl sulfanyl)-1-[5-(3-nitrophenyl)-3-(phenylamino)-4,5-dihydro-1H-pyrazol-1-yl] ethanone (**3A**)

IR (KBr,  $\text{cm}^{-1}$ ): 3348 (NH), 3018 (C-H str. Ar-H), 2950 ( $\text{CH}_2$ ), 1820 (C=O), 1650 (C=N), 1600, 1410 ( $\text{NO}_2$ );  $^1\text{H}$  NMR ( $\delta$ ): 6.65-7.35 (m, 13H, Ar-H), 6.21(dd, 1H,  $\text{H}_c$ ), 5.22 (s, 1H, NH), 4.40 (dd, 1H,  $\text{H}_a$ ), 3.20 (dd, 1H,  $\text{H}_b$ ), 2.78 (t, 1H,  $\text{H}_c$ ), 2.89 (s, 2H,  $\text{CH}_2$ ); Mass (m/z): 489 [M] $^+$ .

#### 2-(1,3-Benzothiazol-2-yl-sulfanyl)-1-[5-(4-methoxyphenyl)-3-(phenylamino)-4,5-dihydro-1H-pyrazol-1-yl]ethanone (**3B**)

IR (KBr,  $\text{cm}^{-1}$ ): 3344 (NH), 3015 (C-H str., Ar-H), 2946 ( $\text{CH}_2$ ), 1816 (C=O), 1647 (C=N), 1220 (C-O-C);  $^1\text{H}$ NMR ( $\delta$ ): 6.42-7.98 (m, 13H, Ar-H), 6.15 (dd, 1H,  $\text{H}_c$ ), 5.18 (s, 1H, NH), 4.32 (dd, 1H,  $\text{H}_a$ ), 3.14 (dd, 1H,  $\text{H}_b$ ), 2.84 (s, 2H,  $\text{CH}_2$ ), 3.80 (s, 3H,  $\text{OCH}_3$ ); Mass (m/z): 474 [M] $^+$ .

#### 5-(3-Nitrophenyl)-N,1-diphenyl-4,5-dihydro-1H-pyrazol-3-amine (**4A**)

IR (KBr,  $\text{cm}^{-1}$ ): 3351 (NH), 3096(C-H str., Ar-H), 2949 ( $\text{CH}_2$ ), 1610 (C=N), 1338, 1487 ( $\text{NO}_2$ );  $^1\text{H}$ NMR ( $\delta$ ): 6.25-7.40 (m, 14H, Ar-H), 6.34 (dd, 1H,  $\text{H}_c$ ), 5.1 (s, 1H, NH), 4.50 (dd, 1H,  $\text{H}_a$ ), 3.46 (dd, 1H,  $\text{H}_b$ ); Mass (m/z): 358[M] $^+$ .

#### 5-(4-Methoxyphenyl)-N,1-diphenyl-4,5-dihydro-1H-pyrazol-3-amine (**4B**)

IR (KBr,  $\text{cm}^{-1}$ ): 3350 (NH), 3090(C-H str., Ar-H), 2946 ( $\text{CH}_2$ ), 1615 (C=N), 1214 (C-O-C);  $^1\text{H}$  NMR ( $\delta$ ): 6.30-7.20 (m, 14H, Ar-H), 6.20 (dd, 1H,  $\text{H}_c$ ), 5.5 (s, 1H, NH), 4.40 (dd, 1H,  $\text{H}_a$ ), 3.42 (dd, 1H,  $\text{H}_b$ ), 3.3 (s, 3H,  $\text{-OCH}_3$ ); Mass (m/z): 343 [M] $^+$ .

**5-(3-Nitrophenyl)-N-phenyl-4,5-dihydro-1,2-oxazol-3-amine (5A)**

IR (KBr,  $\text{cm}^{-1}$ ): 3348 (NH), 3089 (C-H str., Ar-H), 2931 ( $\text{CH}_2$ ), 1638 (C=N), 1450, 1352 ( $\text{NO}_2$ );  $^1\text{H NMR}$  ( $\delta$ ): 6.82-7.39 (m, 9H, Ar), 6.16 (dd, 1H,  $\text{H}_c$ ), 5.4 (s, 1H, NH), 4.38 (dd, 1H,  $\text{H}_a$ ), 3.40 (dd, 1H,  $\text{H}_b$ ); Mass (m/z): 283 [M] $^+$ .

**5-(4-Methoxyphenyl)-N-phenyl-4,5-dihydro-1,2-oxazol-3-amine (5B)**

IR (KBr,  $\text{cm}^{-1}$ ): 3344 (NH), 3080 (C-H str., Ar-H), 2930 ( $\text{CH}_2$ ), 1630 (C=N), 1210 (C-O-C);  $^1\text{H NMR}$  ( $\delta$ ): 6.95-7.25 (m, 9H, Ar-H), 6.10 (dd, 1H,  $\text{H}_c$ ), 4.9 (s, 1H, NH), 4.30 (dd, 1H,  $\text{H}_a$ ), 3.36 (dd, 1H,  $\text{H}_b$ ), 3.3 (s, 3H,  $-\text{OCH}_3$ ); Mass (m/z): 268 [M] $^+$ .

**6-(3-Nitrophenyl)-4-(phenylamino)-5,6-dihydropyrimidin-2-(1H)-one (6A)**

IR (KBr,  $\text{cm}^{-1}$ ): 3380 (NH), 3080 (C-H str., Ar-H), 1692 (CONH), 1618 (C=N), 1350, 1487 ( $\text{NO}_2$ ), 1728 (C=O);  $^1\text{H NMR}$  ( $\delta$ ): 6.80-7.48 (m, 9H, Ar-H), 6.06 (dd, 1H,  $\text{H}_c$ ), 5.3 (s, 1H, NH), 3.30 (dd, 1H,  $\text{H}_b$ ), 4.26 (dd, 1H,  $\text{H}_a$ ), 5.8 (d, 1H, CONH); Mass (m/z): 310 [M] $^+$ .

**6-(4-Methoxyphenyl)-4-(phenylamino)-5,6-dihydropyrimidin-2-(1H)-one (6B)**

IR (KBr,  $\text{cm}^{-1}$ ): 1680 (CONH), 3060 (C-H str., Ar-H), 1720 (C=O), 1610 (C=N), 1218 (C-O-C);  $^1\text{H NMR}$  ( $\delta$ ): 6.60-7.30 (m, 9H, Ar-H), 6.04 (dd, 1H,  $\text{H}_c$ ), 5.1 (s, 1H, NH), 3.28 (dd, 1H,  $\text{H}_b$ ), 4.20 (dd, 1H,  $\text{H}_a$ ), 5.6 (d, 1H, CONH); Mass (m/z): 295 [M] $^+$ .

**6-(3-Nitrophenyl)-4-(phenylamino)-5,6-dihydropyrimidine-2-(1H)-thione (7A)**

IR (KBr,  $\text{cm}^{-1}$ ): 3387 (NH), 3089 (C-H str., Ar-H), 1672 (CSNH), 1612 (C=N), 1389, 1428 ( $\text{NO}_2$ );  $^1\text{H NMR}$  ( $\delta$ ): 6.28-7.46 (m, 9H, Ar-H), 6.08 (dd, 1H,  $\text{H}_c$ ), 5.1 (s, 1H, NH), 3.32 (dd, 1H,  $\text{H}_b$ ), 4.30 (dd, 1H,  $\text{H}_a$ ), 5.0 (d, 1H, CSNH); Mass (m/z): 326 [M] $^+$ .

**6-(4-Methoxyphenyl)-4-(phenylamino)-5,6-dihydropyrimidine-2-(1H)-thione (7B)**

IR (KBr,  $\text{cm}^{-1}$ ): 1670 (CSNH), 3080 (C-H str., Ar-H), 1608 (C=N), 3378 (NH);  $^1\text{H NMR}$  ( $\delta$ ): 6.20-7.40 (m, 9H, Ar-H), 6.06 (dd, 1H,  $\text{H}_c$ ), 5.2 (s, 1H, NH), 4.20 (dd, 1H,  $\text{H}_a$ ), 3.28 (dd, 1H,  $\text{H}_b$ ), 5.4 (s, 1H, CSNH); Mass (m/z): 311 [M] $^+$ .

**Conclusion**

The purpose of the research is the development of new potent bioactive molecules with less toxic, safer and easily available methods. From the literature survey it is evident that Microwave Induced Organic Reaction Enhancement (MORE) chemistry offers a simple, nonconventional technique for the synthesis of wide variety of compounds including biologically important heterocyclic compounds, co-ordination compounds etc.

The results of the antimicrobial screening indicated that the synthesized derivatives in which 3- $\text{NO}_2$  substituted

benzene rings attached to the pyrazoline moiety show excellent activity whereas 4- $\text{OCH}_3$  substituted benzene rings attached to the pyrimidine moiety show good activity against *K. pneumoniae* as compared to other compounds. Compounds containing isoxazole moiety are moderately active against both bacteria and fungi.

**Acknowledgement**

We are thankful to Prof. Suresh C. Ameta for giving valuable suggestions during the progress of the work and to the Head, Department of Chemistry, M. L. Sukhadia University, Udaipur for providing laboratory facilities. Our thanks are also due to the Director, SAIF, CDRI, Lucknow, India for providing spectral and analytical data and Prof. Kanika Sharma, Head, Biotechnology Department, M. L. Sukhadia University, Udaipur for antimicrobial activity.

**References**

- Croignani, S., Launay, D., Linclau, B., Bradley, M., *Mol. Divers.*, **2003**, *7*, 3.
- Shmidt, M. S., Reverdito, A. M., Kremenchuzky, L., Perillo, I. A., Blanco, M. M., *Molecules*, **2008**, *13*, 831.
- Martin, B., Sektjic, H., Chassaing, C., *Org. Lett.*, **2003**, *5*, 1851.
- Chaudhary, A., Sharma, N., Sharma, P., Jasuja, N. D., Sharma, G., Joshi, S. C., Singh, R.V., *Rasayan J. Chem.*, **2000**, *1*, 648.
- Singh, A. K., Parthasarthy, R., Lohani, M., *J. Chem. Pharm. Res.*, **2012**, *4*, 779.
- Malladi, S., Isloora, A. M., Peethambar, S. K., Ganesh, B. M., Goud, P. S., *Der Pharma Chemica*, **2012**, *4*, 43.
- Rao, R. M., Sreeramulu, J., Ravindranath, L. K., Reddy, G. N., Hanumantharayudu, K., Reddy, G. N., Jayaraju, A., Madhusudhan, P., *J. Chem. Pharm. Res.*, **2012**, *4*, 272.
- Sharshira, E. M., Hamada, N. M. M., *Molecules*, **2012**, *17*, 4962.
- Baraldi, P. G., Pavani, M. G., Nunez, M., Brigidi, P., Vitali, B., Gambari, R., Romagnoli, R., *Bioorg. Med. Chem.*, **2002**, *10*, 449.
- Kumar, A., Sinha, S., Chauhan, M. S., *Bioorg. Med. Chem. Lett.*, **2002**, *12*, 667.
- Rostom, S. A., Ashour, H. M., Abd, E. L., Razik, H. A., *Arch. Pharm.*, **2009**, *5*, 299.
- Parekh, A. K., Desai, K. K., *Eur. J. Chem.*, **2005**, *2*, 109.
- Vaghasta, S. J., Shah, V. H., *J. Serb. Chem. Soc.*, **2007**, *72*, 109.
- Shah, T. K., Desai, V., *J. Serb. Chem. Soc.*, **2007**, *72*(5), 443
- Ai-Shihry, S. S., *Molbank*, **2005**, M447.
- Bhambi, D., Salvi, V. K., Jat, J. L., Ojha, S., Talesara, G. L., *J. Sulfur Chem.*, **2007**, *28*, 155.
- Manna, F., Chimenti, F., Fioravanti, R., Bolasco, A., Seecci, D., Chimenti, P., Ferlini, C., Scambia, G., *Bioorg. Med. Chem. Lett.*, **2005**, *15*, 4632.
- Ahn, J. H., Kim, H. M., Jung, S. H., Kang, S. K., Kim, K. R., Rhee, S. D., Yang, S. D., Cheon, H. G., Kim S. S., *Bioorg. Med. Chem. Lett.*, **2004**, *14*, 4461.
- Prasad, Y. R., Rao, A. L., Prasoon, L., Murali, K., Kumar P. R., *Bioorg. Med. Chem. Lett.*, **2005**, *15*, 5030.

Received: 02.01.2013.

Accepted: 21.01.2013.





# STRUCTURAL AND DIFFUSIONAL STUDY OF PURE ETHANOL AND WATER ON Pt (III) SURFACE USING MOLECULAR DYNAMICS SIMULATION

Kholmirzo Kholmurodov,<sup>[a]\*</sup> Ermuhammad Dushanov,<sup>[b]</sup> Kenji Yasuoka,<sup>[c]</sup> Hagar Hassan,<sup>[d]</sup> Ahmed Galal,<sup>[e]</sup> and Nasser Sweilam<sup>[f]</sup>

**Keywords:** Molecular dynamics simulation, Ethanol, Water, Pt (111), Diffusion coefficient, Activation energy of diffusion.

Molecular dynamics simulations were performed on ethanol–water–Pt system for studying the structural and diffusion behaviour of both ethanol and water molecules on the surface of Pt (111). This work is concerned with the differences between pure liquids and solutions in their diffusional behaviour. The self-diffusion coefficients and activation energies of diffusion of pure ethanol and water on Pt (111) surface were calculated and compared with the corresponding values of their mixtures. The results showed that the values of both the diffusion coefficients and activation energies are strongly affected by the purity of chemical species under investigation. A comparison between two different metal surfaces was also investigated and the results revealed that the nature of metal surface has a strong effect on the adsorption and diffusional behaviour of liquids based on their affinity towards a specific type of surfaces in addition to the hydrophobicity and hydrophilicity of the metal surface.

\* Corresponding Author

- [a] Laboratory of Radiation Biology, Joint Institute for Nuclear Research & Dubna International University, Dubna, Moscow Region, Russia. E-mail: mirzo@jinr.ru.  
[b] Laboratory of Radiation Biology, Joint Institute for Nuclear Research & Institute of Nuclear Physics, Tashkent, Uzbekistan. E-mail: eric.dushanov@gmail.com.  
[c] Department of Mechanical Engineering, Keio University, Japan. E-mail: yasuoka@mech.keio.ac.jp.  
[d] Chemistry Department, Faculty of Science, Cairo University, Egypt. E-mail: hagar@sci.cu.edu.eg.  
[e] Chemistry Department, Faculty of Science, Cairo University, Egypt. E-mail: galal@sci.cu.edu.eg.  
[f] Mathematics Department, Faculty of Science, Cairo University, Egypt. E-mail: nsweilam@sci.cu.edu.eg.

## 1. Introduction

Methanol and ethanol are known to be among the most promising renewable resources that can replace petrochemicals.<sup>1</sup> Among the renewable energetic resources, ethanol is a green fuel that can be used directly as a fuel or as a gasoline enhancer since it is not toxic, does not contaminate with water resources,<sup>2</sup> and it can be produced in large quantities from the agriculture products.<sup>3</sup>

Metal surfaces such Au nanotubes were used to study the structure of water, ethanol and water–ethanol mixtures.<sup>4</sup> Platinum is the most known surface used for oxidation of ethanol in fuel cell applications through the activation of the dissociative adsorption of ethanol.<sup>5</sup> Platinum surfaces are used as a catalyst to activate carbon–carbon and carbon–oxygen bond breakage which are the elementary steps in oxidation of alcohols.<sup>6</sup> The structural properties of liquids and solutions at molecular level can be investigated by

means of molecular dynamics (MD) simulation that acts as a powerful tool to simulate the behaviour of such systems alone or in the presence of solid surfaces.<sup>7,8</sup> MD simulation can provide information about the structure and dynamics of the system and the event which can take place on the surface within a few picoseconds.<sup>9</sup> Also, MD simulation allows the computation of some kinetics and structural properties such as diffusion coefficient, activation energy of diffusion and radial distribution functions that help in getting some information about the structure of both solid and liquid structures.<sup>10</sup>

Alcohol–water mixture often shows quite different properties than the corresponding pure components. Of particular interest, are the structure and diffusion properties, which play important roles in the theoretical study and technological applications involving mass transfer.<sup>2</sup> In our previous work,<sup>2</sup> we investigated the behaviour and structure of 50-50 % ethanol–water mixture in absence and presence of a platinum surface by means of the MD simulation technique. We found that the presence of metal surface such as Pt enhances the diffusion property of both ethanol and water. Moreover, ethanol provided different affinity to Pt surface than that provided by water molecules.

Few studies concerning ethanol, water and their mixtures were previously cited using MD simulation tool, for example: Wang Yao-Chun et al. investigated the behaviour of pure water molecules, ethanol molecules, and water–ethanol mixture with various weight fractions inside Au nanotubes.<sup>4</sup> Ming-Mei Yang et al. used density functional theory (DFT) to study the adsorption behaviour of ethanol on Rh (III)<sup>11</sup> and D.J. Cooke et al. studied the interface between the {10 4} surface of calcite and pure ethanol, pure water, and 50:50 mixture (by amount) of water and ethanol.<sup>12</sup>

This work is a continuation to our study of the behaviour of a mixture of solvents at solid Pt surfaces.<sup>2</sup> The aim of this work is to study the behaviour of both pure ethanol and pure water on the surface of Pt (111) and to compare this results with that of 50-50% (by molecules) ethanol–water mixture. Moreover, the comparison of the behaviour of these solvents will be studied at two different surfaces Pt surface (this work) and Au nanotube as indicated by Wang Yao-Chun et al.<sup>4</sup> This will be important to reveal the effect of changing the structure of the metallic substrate with respect to different interfacial forces and interactions at the interface such as hydrophobicity/hydrophilicity and electrostatic interactions.

## 2. Simulation method

We have studied the molecular dynamics of pure ethanol and pure water separately on the presence of a platinum surface at various temperatures between 250 to 600 K using the DL\_POLY\_2.0 code, which was developed by the Molecular Simulation Group at the Daresbury Laboratory (England) with the support of the Research Council for the Engineering and Physical Sciences (project CCP5 of the simulation of condensed phases). DL\_POLY is a general-purpose MD simulation package developed by W. Smith, T.P. Forester and I.T. Todorov.<sup>13,14</sup>

Ethanol and water molecules are described using the force field from the DL\_POLY database,<sup>13,14</sup> where bonding, angular, and dihedral parameters are incorporated into standard molecular mechanics potentials. All nonbonding interactions are accounted for via Lennard–Jones (LJ) potentials and Coulombic interactions based on the partial charges associated in each atom. The computer simulations have been performed for a MD cell of a volume  $V = (54.92, 54.92, 63.8) \text{ \AA}^3$  under the energy and temperature control. The temperature of the system was varied from 250 to 600 K using the annealing process starting with 250 K then raises the temperature by 25 K in each simulation. The number of molecules of both ethanol and water is 2304 molecules while that of Pt is 588 ( $\text{Pt}_4$ ) molecules, for a total of 2352 atoms. The metallic substrate used was cubic Pt, which has the formula  $\text{Pt}_4$ ; in this case we have four atoms for one unit cell in the face centered-cubic structure that form (111) orientation. Pt (111) surface was arranged in six layers numbering a total of 2352 atoms. The surface area was  $3016.43 \text{ \AA}^2$ ; and the lattice constant was  $a = 3.923 \text{ \AA}$ . All the parameters of platinum were taken from EIM databases and datasets website supported by the Russian Foundation for Basic Research.<sup>15</sup> Our Pt (111) surface has the characteristics described by us  $z = 4$  and symmetry  $Fm\bar{3}m$ .

The integration of the equations of motion was performed using the Verlet integration scheme in quaternion. The integration step was 1 fs (femtosecond); a canonical (nvt) ensemble was used for the simulated system, and the Nose–Hoover algorithm was employed to keep the desired temperature. The intermolecular chemical bonds were estimated on the basis of the Shake algorithm with an accuracy of  $10^{-8}$ . The Ewald summation with a convergence parameter of  $10^{-6}$  was used for the calculation of electrostatic forces in the periodic system.<sup>13,14</sup> All simulations were periodic in three dimensions.

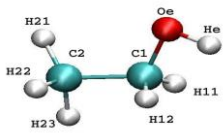
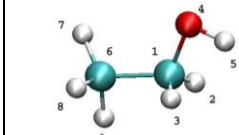
Water was represented by the constrained OW–HW bond potential; thus a SPC model was used. Tables 1 and 2 contain bond lengths and intermolecular Lennard–Jones parameters for ethanol, water molecules, and a Pt surface, respectively.

**Table 1.** The effective charges of atoms of ethanol, water and a Pt surface.

Atom	$q/e$ , proton charge
C1	0.05
C2	−0.27
Oe	−0.66
He	0.43
H	0.09
OW	−0.82
HW	0.41
Pt	0.00

**Table 2.** The intermolecular Lennard–Jones parameters for ethanol, water, and a Pt surface, in a cell volume  $V = (54.92, 54.92, 63.801) \text{ \AA}^3$ .

Group	$\epsilon/k$ (kcal·mol <sup>−1</sup> )	$\sigma$ (Å)
C–C	0.12	3.30
C–H	0.00	2.54
C <sub>1</sub> –Oe	0.16	3.08
H–H	0.00	1.78
H–O	0.00	2.32
Oe–Oe	0.20	2.85
C–Pt	0.94	2.90
Oe–Pt	0.92	2.70
C–OW	0.14	3.43
Oe–OW	0.18	3.20
OW–OW	0.16	3.17

An organic force field used to describe the ethanol molecules is presented in Table 3. As it was mentioned above for the organic force field in describing the ethanol molecule both DL\_FIELD and DL\_POLY data bases were employed as references. These ethanol force field data are already fitted and tabulated in the data bases of both DL\_FIELD and DL\_POLY. Also these force field parameters are available in CHARMM database that were derived from quantum mechanical calculations.<sup>16,17</sup> It is worth noting that CHARMM was also ported to other force field formats and widely used by AMBER, GROMACS, and DL\_POLY general-purpose MD simulation programs. Many authors used these force field parameters to describe the modelling of the water–metal and organics–metal systems (such as water, benzene, phenol, amino acids on the Pt (111), Au (111), Ni (111), etc. surfaces).<sup>18–29</sup> Therefore, we can take these force field parameters as satisfactory to describe the surface–organic and surface–water interactions, including the behaviour of the interfaces as well.

**Table 3.** The potential parameters used for ethanol molecules.

Harmonic bond potential = $K(r_{ij} - r_0)^2 / 2$		
Bond	$K$ (kcal·mol <sup>-1</sup> ·Å)	$r_0$ (Å)
C <sub>1</sub> -C <sub>2</sub>	222	1.52
C-H	309	1.11
C <sub>1</sub> -O <sub>e</sub>	428	1.42
O <sub>e</sub> -H <sub>e</sub>	545	0.94
Angular potential = $K(\theta_{ijk} - \theta_0)^2 / 2$		
Group	$K$ (kcal·mol <sup>-1</sup> ·rad <sup>-2</sup> )	$\theta_0$ (°)
H <sub>1</sub> -C <sub>1</sub> -O <sub>e</sub>	45.90	109.44
H <sub>1</sub> -C <sub>1</sub> -C <sub>2</sub>	34.60	109.46
H <sub>1</sub> -C <sub>1</sub> -H <sub>1</sub>	35.50	120.00
O <sub>e</sub> -C <sub>1</sub> -C <sub>2</sub>	75.70	109.00
He-O <sub>e</sub> -C <sub>1</sub>	57.50	109.50
H <sub>2</sub> -C <sub>2</sub> -H <sub>2</sub>	35.50	109.50
H <sub>2</sub> -C <sub>2</sub> -C <sub>1</sub>	34.60	109.46
Dihedral potential = $K(\varphi_{ijkn} - \varphi_0)^2 / 2$		
Group	$K$ (kcal·mol <sup>-1</sup> )	$\varphi_0$ (°)
C <sub>2</sub> -C <sub>1</sub> -O <sub>e</sub> -H <sub>e</sub>	1.30	180
H <sub>12</sub> -C <sub>1</sub> -O <sub>e</sub> -H <sub>e</sub>	0.14	60
H <sub>11</sub> -C <sub>1</sub> -O <sub>e</sub> -H <sub>e</sub>	0.14	-60
O <sub>e</sub> -C <sub>1</sub> -C <sub>2</sub> -H <sub>21</sub>	0.16	180
O <sub>e</sub> -C <sub>1</sub> -C <sub>2</sub> -H <sub>22</sub>	0.16	60
O <sub>e</sub> -C <sub>1</sub> -C <sub>2</sub> -H <sub>23</sub>	0.16	-60
H <sub>11</sub> -C <sub>1</sub> -C <sub>2</sub> -H <sub>21</sub>	0.16	-60
H <sub>11</sub> -C <sub>1</sub> -C <sub>2</sub> -H <sub>22</sub>	0.16	180
H <sub>11</sub> -C <sub>1</sub> -C <sub>2</sub> -H <sub>23</sub>	0.16	60
H <sub>12</sub> -C <sub>1</sub> -C <sub>2</sub> -H <sub>21</sub>	0.16	60
H <sub>12</sub> -C <sub>1</sub> -C <sub>2</sub> -H <sub>22</sub>	0.16	-60
H <sub>13</sub> -C <sub>1</sub> -C <sub>2</sub> -H <sub>23</sub>	0.16	-180

The configuration energy of the molecular model is represented as a sum of the energies of the bonding ( $E_{val}$ ) and non-bonding ( $E_{nb}$ ) interactions:

$$E = E_{val} + E_{nb}. \quad (1)$$

The energy of the valence (bonding) interactions  $E_{val}$  is given by the following formula:

$$E_{val} = E_{bond} + E_{ang} + E_{dih} + E_{teth}, \quad (2)$$

where  $E_{bond}$  is the energy of chemical bonds,  $E_{ang}$  is the energy of angular bonds,  $E_{dih}$  is the energy of dihedral bonds, and  $E_{tether}$  is tether energy.

The energy of the non-valence (non-bonded) interactions is a sum of the energies of the van-der-Waals (vdW), electrostatics (Coulombic), and hydrogen bonds:

$$E_{nb} = E_{vdW} + E_{coul} \quad (3)$$

During the MD simulations, the following potential types, which represent the topology of the molecular field for an ethanol–water system, were used:<sup>13,14</sup>

Harmonic bond potential: 
$$U(r_{ij}) = \frac{1}{2} K(r_{ij} - r_0)^2 \quad (4)$$

Harmonic bond angle: 
$$U(\theta_{ijk}) = \frac{1}{2} K(\theta_{ijk} - \theta_0)^2 \quad (5)$$

Harmonic dihedral: 
$$U(\varphi_{ijkn}) = \frac{1}{2} K(\varphi_{ijkn} - \varphi_0)^2 \quad (6)$$

The Lennard–Jones potential: 
$$U_{ij}(r_{ij}) = 4\varepsilon_{ij} \left[ \left( \frac{\sigma_{ij}}{r_{ij}} \right)^{12} - \left( \frac{\sigma_{ij}}{r_{ij}} \right)^6 \right] \quad (7)$$

Coulombic interaction: 
$$U(r_{ij}) = \frac{1}{4\pi\varepsilon_0} \frac{q_i q_j}{r_{ij}} \quad (8)$$

Quartic tether potential: 
$$U(r) = \frac{1}{2} k r_0^2 + \frac{1}{4} k' r_0^4 \quad (9)$$

For the Lennard-Jones potential (7),  $\sigma_{ij}$  is the size parameter,  $\varepsilon_{ij}$  the energy parameter, and Lorentz-Berthelot mixing rules were used:  $\sigma_{ij} = (\sigma_i + \sigma_j)/2$  and  $\varepsilon_{ij} = \sqrt{\varepsilon_i \varepsilon_j}$ .

For the Coulombic potential (8),  $q_i$  is the charge of site  $i$  and  $r_{ij}$  the distance between sites  $i$  and  $j$ .

The tether potential (9) suggests that the momentum has no longer been a conserved quantity of the simulation. The force on the atom “ $i$ ” arising from the tether potential is obtained using the general formula:

$$\underline{F}_i = -\frac{1}{r_{i0}} \left[ \frac{\partial}{\partial r_{i0}} U(r_{i0}) \right] \underline{r}_{i0} \quad (10)$$

The atomic sites to be tethered to a fixed point in space,  $r_{i0}$ , are taken as their position at the beginning of the simulation. This is also known as position restraining. Tethering potential is applied for the surface atoms only. Under a tethering potential the surface atoms would allow, nevertheless, to vibrate around their equilibrium positions. We choose the values of  $k=0.2$  and  $k'=0.4$  to avoid the destruction of our surface during heating and annealing processes.

One of the potentials used in MD simulation using DL\_POLY to describe the metal surface is the one described by Sutton and Chen (SC or st-ch):<sup>30</sup>

$$U = \sum_i U_i \quad (11)$$

$$U_i = \left[ \frac{1}{2} \sum_{j \neq i} \left( \frac{a}{r_{ij}} \right)^n - c \sqrt{\rho_i} \right] \quad (12)$$

Here  $\rho_i$  is a density-like term for atom  $i$ :

$$\rho_i = \sum_{j \neq i} \left( \frac{a}{r_{ij}} \right)^m \quad (13)$$

In this equation the potential has three dimensionless parameters adjustable for the metal materials. They are  $c$ ,  $n$ , and  $m$ , and can be chosen for various materials, especially metals. The variable  $\varepsilon$  sets the energy parameter and  $a$  is the lattice constant. In this work we used such kind of potential to describe Pt (111) surface and Table 4 contains the SC potential parameters used.

**Table 4.** The Sutton-Chen (st-ch) potential parameters of platinum.

$\varepsilon$ (kcal·mol <sup>-1</sup> )	$a$ (Å)	$N$	$M$	$c$
0.226	3.92	11.0	7.0	71.336

### 3. Results and Discussion

Figure 1 shows three MD simulated snapshots of the pure ethanol (A), pure water (B) and 50-50% (by molecules) ethanol–water mixture (C).

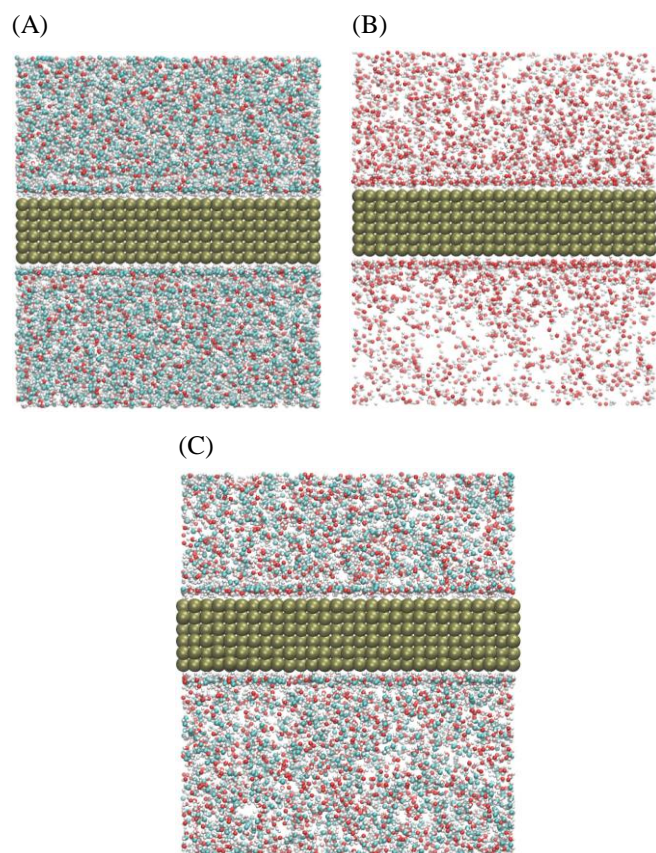


**Figure 1.** The snapshots of 100% ethanol (A), 100% water (B) and 50-50% (by molecules) ethanol–water mixture (C).

#### 3.1. Diffusion coefficient and activation energy of diffusion

Mechanistic studies of ethanol chemical interactions with metal and metal oxide single crystal surfaces are of fundamental importance. However, while there are many studies of ethanol chemisorption over for example Ni,<sup>31</sup> Pd<sup>32–34</sup> and Cu<sup>35–37</sup> single crystals, those over platinum are limited to the Pt (111)<sup>38–40</sup> and Pt (331)<sup>41</sup> surfaces.

We have estimated the self-diffusion coefficient of both pure ethanol and pure water in presence of Pt (III) surface at 298 K. From our previous work,<sup>2</sup> the calculated diffusion coefficients of water and ethanol in the mixture were enhanced in presence of Pt surface. The values for the self-diffusion coefficients are estimated for each liquid separately, and the results of the calculations are summarized in Table 5. We observed that, the value of diffusion coefficient of pure ethanol is much lower than its value in the mixture unlike water molecules that showed higher value of diffusion coefficient for the pure liquid compared to its corresponding value in the mixture. These results can be attributed to the hydrogen bonding in the liquid phase that plays an important role on the molecular level and should affect the value of diffusion coefficient. Thus, in case of pure ethanol the only way to form hydrogen

bond is by forming intermolecular hydrogen bonds with other ethanol molecules to form dimer or trimer and also they have high chance to form 1D chain. Formation of 1D chain of ethanol molecules can lead to a decrease in the mobility of ethanol molecules in the vicinity of simulation box that renders the molecules much slower than in case of a mixture of ethanol–water. On the other hand, the ability of ethanol molecules to form hydrogen bond with other ethanol molecules decreases in ethanol–water mixture. Another contributing factor to this observation is the ability of ethanol molecules to form hydrogen bonds with water molecules. Moreover, the molecular mass of ethanol–water dimers is relatively smaller than that of an ethanol–ethanol dimer.

**Table 5.** The values of diffusion coefficient and activation energy of ethanol and water in pure liquids and in solution of 50-50% (by molecules) ethanol–water mixture.

Simulated system	Diffusion coefficient ( $D$ ) / $\text{m}^2 \cdot \text{s}^{-1} \times 10^{-9}$	Activation Energy ( $E_a$ ) / $\text{Kcal} \cdot \text{mol}^{-1}$
Pure Ethanol	0.26	3.411
Pure Water	3.86	3.718
50% ethanol in ethanol–water mixture	1.07	2.470
50% water in ethanol–water mixture	2.10	2.980

The same explanation can be applied to explain the calculated values of diffusion coefficients in case of pure water and ethanol–water mixtures. Unlike the case of ethanol, the presence of ethanol molecules with water molecules will likely lead to the formation of hydrogen bonds between “mixed” molecules which results in slower mobility of the structures thus formed.

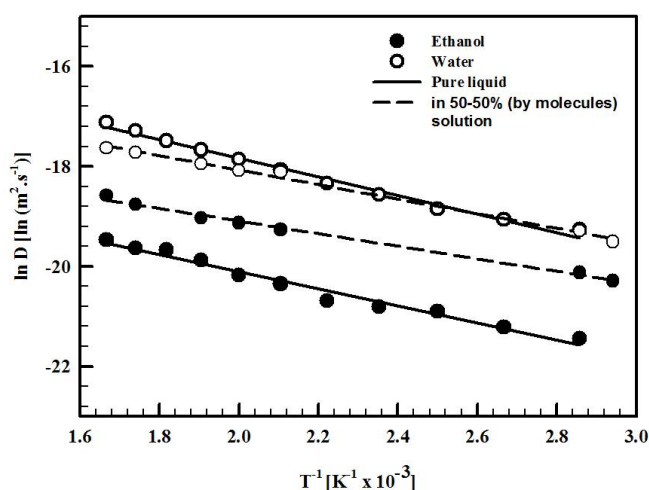


**Figure 2.** Arrhenius plot of pure liquids (solid lines) and ethanol–water mixture (dashed lines).

On the other hand, it is believed that the self-diffusion coefficients of both pure ethanol and pure water obey Arrhenius relation with temperature. Thus, we simulated both pure water and pure ethanol interactions with Pt at various temperatures, ranging from 250–600 K using annealing process as referred before in the simulation method. In this temperature range, the self-diffusion coefficients of ethanol and water were calculated by plotting

a graph of  $\ln D$  as function of the reciprocal of temperature in Kelvin (Figure 2) we observed that both water and ethanol give a straight line which indicates that they obey Arrhenius relation. And the value of activation energy of diffusion can be calculated from the following relation:<sup>42</sup>

$$D = D_0 e^{-\frac{E_a}{RT}}$$

where,  $D$  is the diffusion coefficient,  $D_0$  is the Arrhenius constant,  $R$  is the universal gas constant,  $T$  is the temperature and  $E_a$  is the activation energy of diffusion.

We calculated the activation energy of diffusion ( $E_a$ ) from the slope of Arrhenius plot and the results are in Table 5. The values of  $E_a$ 's are in agreement with the values of diffusion coefficients as activation energy of diffusion of pure ethanol is higher than that of ethanol molecules in solution of ethanol and water.

### 3.2. Interaction of ethanol and water with Pt (111) surface

The interfacial structure and adsorption behaviour of both ethanol and water can be investigated by calculating the normalized ethanol and water density profile as a function of the distance from Pt (111) surface. In the density profile, the higher density of liquid molecules indicates stronger interaction with the surface. Figure 3 shows the density profiles of 100% water (A), 100% ethanol (B) and 50-50% (by molecules  $\approx$  72-28% weight fraction) ethanol–water mixture). The density profile of pure water shows two peaks, a well-defined first adsorption layer from 5-8 Å and one more diffuse layer from 8-10 Å which indicates that water molecules can adsorb directly on the surface of Pt (111) forming a shell-like adsorption layer. The high density of the first peak indicates that water molecules interact strongly with Pt surface which is in agreement with the hydrophilic nature of Pt surface.<sup>43</sup> While the density profile of pure ethanol shows only one adsorption peak of lower density than that of water which indicates that for pure liquids, water interacts with Pt (111) stronger than ethanol. This can be attributed to the strong hydrogen bonding of ethanol molecules with each other where, they can form dimer, trimer or/and 1D chains as previously mentioned. These 1D chains lead to decreasing the interaction of ethanol molecules with Pt surface, in addition, the steric hindrance of ethanol molecules relative to the simple structure of water molecules can affect the approaching of the molecules to the metal surface.

By comparing these results with our previous results of ethanol–water mixture we observed two differences: the first is in the height of the first adsorption peaks where, ethanol molecules show stronger interaction with Pt (111) surface than that of water in the mixture. The opposite behaviour was observed in case of pure water. We attributed this result to the fact that ethanol molecules in the mixture preferentially adsorb onto Pt (111) (selective–competitive adsorption).<sup>2</sup>

The second observed difference between the density profiles of pure liquids and that of mixture is in the position of adsorption peaks of both water and ethanol. The ability of ethanol molecules to approach the Pt (111) surface increases in the mixture compared to the case of pure liquids that also can be attributed to decreasing the probability of forming hydrogen bonds with the same kind of molecules which may

prevent ethanol molecules to form 1D and also water molecules to form clusters. It is worth to mention that at relatively large distances from the surface the relative density of pure liquids or even mixture approaches unity that is consistent with the bulk of solution. Also for pure water and for water and ethanol molecules in the mixture the first minimum approaches zero which means there is little or no movement of liquid molecules between the adsorption layer and the bulk of solution within the time scale of solution. While for the case of pure ethanol there is no well-defined adsorption peak for ethanol molecules and there is no distinction between the adsorption and diffusion layers which indicates that the thickness of diffusion layer is much larger than in case of pure water or in case of a mixture.

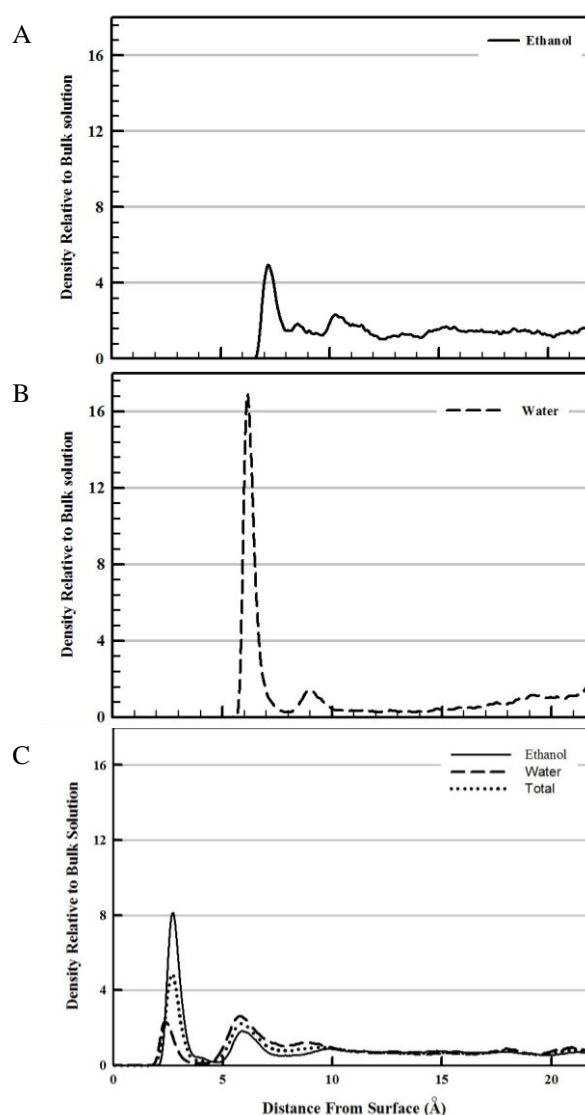


**Figure 3.** The density profiles of 100% ethanol (A), 100% water (B) and 50-50% (by molecules) ethanol–water mixture (C).

Figure 4 shows the radial distribution functions ( $g(r)$ ) which can provide information about the interaction between Pt surface and liquid molecules. By comparing the structure behaviour of ethanol on Pt surface with that of the water on Pt surface we observe that the water molecules are more ordered on the surface than the ethanol molecules. It is also clear that, the interaction of ethanol with Pt surface is stronger in the mixture rather than of pure liquid; at the

same time the water molecules prefer to strongly interact in pure liquid compared with that in the mixture. These results seem to be in a good agreement with the density profiles discussed before. It is worth to mention that, by the temperature increase the amplitude of radial distribution peaks for pure water will essentially decrease; at the same time in the case of the ethanol one observes an opposite picture indicating that the ethanol desorption energy to be higher than that of water. The similar results were obtained for the ethanol–water mixture as in.<sup>2</sup>

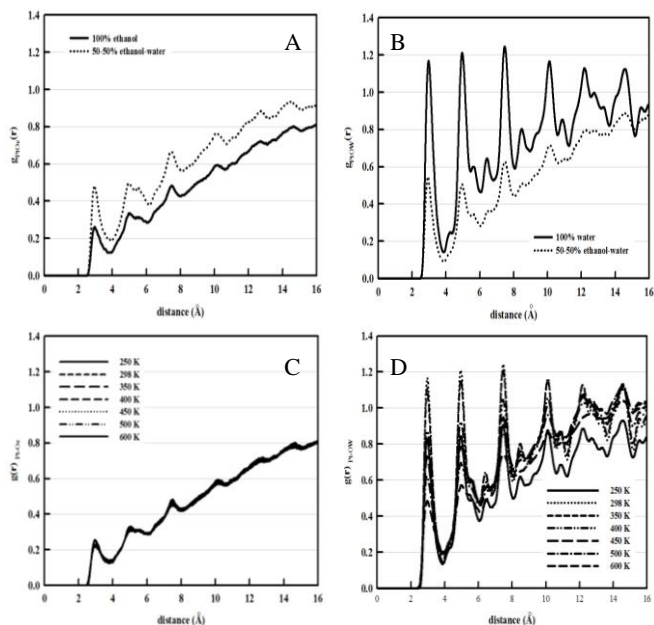


**Figure 4.** The radial distribution functions showing the interaction between Pt surface and liquid molecules. Pt–Oe (A), Pt–OW (B), effect of temperature on Pt–Oe (C) and effect of temperature on Pt–OW (D).

### 3.3. RDF correlation behaviour

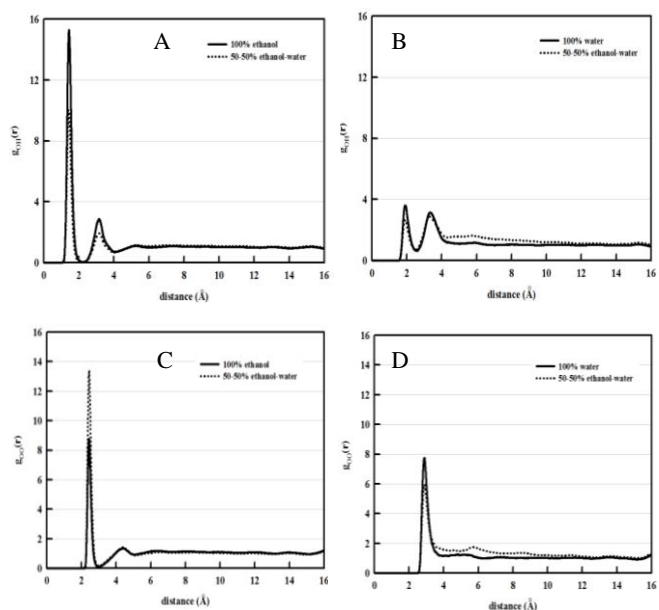


**Figure 5.** The radial distribution functions of Oe–He (A), OW–HW (B), Oe–Oe (C) and OW–OW (D) for pure liquids (solid lines) and in case of mixture (dotted lines).

In studying of the liquid structures the  $g_{OH}(r)$  and  $g_{OO}(r)$  RDFs have to be the most interesting statistical data to compare. The pure liquids, as discussed above, revealed different behaviour compared to the solution, so now one compare the  $g(r)$  behaviour for the pure liquids and the solution mixture. Figure 5 compare the  $g_{OH}(r)$  of pure ethanol with that of the ethanol molecules inside the solution. The first RDF peak is located at the distance less than  $2\text{Å}$ , thereby referring a presence of the strong intermolecular hydrogen bonding between the ethanol molecules. Additionally, the height of the RDF peaks is higher for the 100% ethanol comparing with that of the ethanol–water mixture. This behaviour seems well correlated with the density profiles as shown in Figure 3. Thus the probability of finding two ethanol molecules at very short distances and formation of hydrogen bonds to be higher in the case of pure ethanol in comparison with the ethanol–water mixture one. The phenomena seem to be attributed by the hydration of the ethanol molecules to relatively separate and by the decrease of the probability in forming the intermolecular hydrogen bonds with other ethanol molecules. The similar results were obtained for the 100% water in Figure 5(B), though with a lower probability than that for the ethanol molecules. Regarding the  $g_{OO}(r)$ , it is obvious that the second O–O peak for water molecules is very weak or fully absent as it is shown in Figure 5(D). On the other hand, the first peak amplitude of the RDF  $g_{OO}(r)$  is higher in the case of the ethanol–water mixture comparing with that of 100% ethanol (Figure 5(C)).

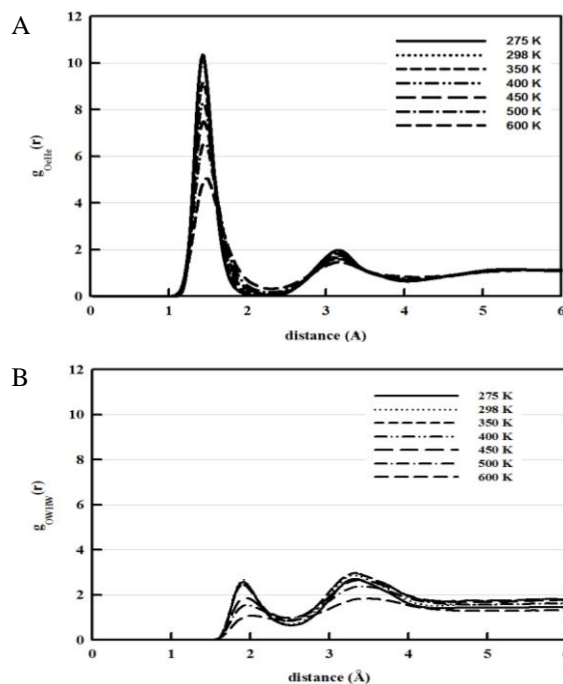


**Figure 6.** The effect of temperature on radial distribution functions of Oe–He (A), OW–HW (B), for pure liquids, insets: the corresponding coordination number as function of the distance.

The phenomena seem to be attributed by the steric hindrance of the methyl group in the ethanol that increases in the pure liquids in comparison with that of the mixture solution. Another probable consequence of the point above, the O–O RDF for pure water displayed in Figure 5(D), it shows maximum reaching almost 8 which is much above what is expected for pure SPC water model (about 3, but without ethanol or surface). Thus, introducing of a Pt

surface into consideration seems to affect the water RDF, so the deviation from "expected" results for SPC (and other) water models is strong, thereby providing further interesting verification or application.

By investigating of the effect of temperature on the RDF we found that for the O–H atomic pair in pure ethanol and pure water the RDF peaks decrease with the temperature increase. This is the result of the atomic ordering decrease in the liquid system. At the same time as shown in Figure 6 the corresponding coordination number also decreases with the temperature. Comparing the coordination number versus distance in pure ethanol and pure water we found that in case of ethanol the flat plateau comparably is well-defined.

### 3.4. The nature of metal surface influence

In order to investigate the effect of changing the type of metallic substrates, we compared our data to those obtained by Wang Yao-Chun et al.<sup>4</sup> who simulate the molecular dynamics of ethanol, water and their mixture inside Au nanotubes. We found noticeable resemblance for the results obtained for pure liquids especially in the shape of the density profiles. On the other hand, the height of the adsorption peaks in this study is much higher than those obtained by Wang et al. This can be attributed to the higher number of both ethanol and water molecules we used than those used by Wang Yao-Chun. But in case of a mixture the situation is completely reversed. Therefore, it could be concluded that Au surface tends to attract water molecules much stronger than ethanol molecules in the mixture. Water molecules will therefore preferentially adsorb to the Au surface prohibiting competitive adsorption of ethanol molecules. This could be noticed from the positive shift in the position of the first peak of ethanol in the mixture – compared to pure ethanol. In fact Au surface appeared to be more hydrophobic in nature than Pt surface while, Pt and Pt-like metals (Rh, Ru and Pd) are supposed to behave as hydrophilic surfaces unlike Au surface that is supposed to behave as a hydrophobic surface.<sup>43</sup> However, some literatures proved that water molecules have a contact angle approaching zero at clean gold surface.<sup>44</sup> From the molecular dynamics simulation point of view Au surface is very pure so we can consider Au surface in this case hydrophilic in nature that explains the high affinity of water to Au surface. All of these results refer to the affinity of ethanol molecules to Pt surface is much higher than to Au surface that is in agreement with the experimental results that consider Pt surface is the best catalyst for dissociative adsorption of ethanol<sup>45</sup> and it is always used as the best catalyst for oxidation of ethanol in fuel cell applications and many other applications.<sup>46</sup> By the same way we can consider that the other Pt-like metals behave as Pt surface in its trend.

### 4. Conclusion

We have simulated the ethanol/Pt and water/Pt systems using DL\_POLY\_2.0 code and the results were correlated with our previous study concerning the molecular dynamics simulations of the 50-50% (by molecules) ethanol–water mixture. The self-diffusion coefficients of both 100% ethanol and 100% water were calculated at room temperature and the analysis showed that the diffusion coefficient of pure ethanol is much lower than that in the

mixture. The diffusion activation energies for both ethanol and water were estimated through the calculation of the self-diffusion coefficients at various temperatures (250–600 K); the energies were found to be 3.411 and 3.718 Kcal mol<sup>-1</sup>, respectively. These values were compared with that of the ethanol–water mixture and it was found that the activation energy of diffusion decreases in case of the mixture. That is due to the decrease in the probability of formation of hydrogen bonds between the similar molecules and the increase in the mobility of molecules toward the metal surface. Our MD simulation results for the Pt surface were compared with other works, where the Pt is replaced with the Au as a metal surface. The comparative analysis reveals that the nature of the metal surface has possess a great influence on the structural and dynamical behaviour of the solution. Also the correlation between RDFs and density profiles is well established. Finally, we conclude that the affinity of the ethanol molecules to the Pt surface is much higher than their affinity to the Au surface. These results seem to be in a good agreement with the experimental data demonstrating that Pt surface has to be the best surface for dissociative adsorption of the ethanol molecules.

### 5. Acknowledgement

This work has been performed in the framework of joint collaborative agreement Arab Republic of Egypt (ARE) – Joint Institute for Nuclear Research (JINR) (project #302). This work was supported in part by the Grant in Aid for the Global Centre of Excellence Program of the Centre for Education and Research of Symbiotic, Safe and Secure System Design from Japan's Ministry of Education, Culture, Sport, and Technology.

### 6. References

- Okkerse, C., van Bekkum, H. *Green Chem.*, **1999**, *1*, 107.
- Kholmurodov, Kh., Dushanov, E., Yasuoka, K., Khalil, H., Galale, A., Ahmed, S., Sweilam, N., Moharram, H. *Chem. Phys.*, **2012**, *402*, 41.
- Shen, S. Y., Zhao, T. S., J. B. Xu, J. B. *Int. J. Hydrogen Energ.*, **2010**, *35*, 12911.
- Chun, W. Y., Chuan, C., Pon, J. S., *Chin. J. Catal.*, **2008**, *29*, 1099.
- Galal, A., Atta, N. F., Khalil, H. K. *Int. J. Electrochem. Sci.*, **2012**, *7*, 768.
- Sachtler, W. M. H., Ichikawa, M. *J. Phys. Chem.*, **1986**, *90*, 4752.
- Kusalik, P. G., Lyubartsev, A. P., Bergman, D. L., Laaksonen, A. *J. Phys. Chem. B.*, **2000**, *104*, 9533.
- Soper, A. K., Finney, J. L. *Phys. Rev. Lett.*, **1993**, *71*, 4346.
- Kholmurodov, Kh., Puzynin, I., Smith, W., Yasuoka, K., Ebisuzaki, T. *Comput. Phys. Commun.*, **2001**, *141*, 1.
- David, C. Y., *Computational Chemistry: A Practical Guide for Applying Techniques to Real-World Problems*, John Wiley & Sons, Inc., New York, **2001**.
- Yang, M.-M., Bao, X.-H., Li, W.-X. *J. Phys. Chem. C*, **2007**, *111*, 7403.
- Cooke, D. J., Gray, R. J. *Langmuir*, **2010**, *26*, 14520.
- Smith, W., Forester, T. R. *J. Mol. Graph.*, **1996**, *14*, 136.

- <sup>14</sup> Smith, W., Forester, T. R., Todorov, I. T. *The DL Poly 2 user manual*, Version 2.19, STFC Daresbury Laboratory, Daresbury, Warrington WA4 4AD Cheshire, UK, 2008.
- <sup>15</sup> WWW-MINCRYST, Crystallographic and Crystallochemical Database for Minerals and their Structural Analogues. <http://database.iem.ac.ru/mincryst/>.
- <sup>16</sup> Brooks, B. R., Brooks III, C. L., Mackerell, A. D., Nilsson, L., Petrella, R. J., Roux, B., Won, Y., Archontis, G., Bartels, C., Boresch, S., Caflisch, A., Caves, L., Cui, Q., Dinner, A. R., Feig, M., Fischer, S., Gao, J., Hodoscek, M., Im, W., Kuczera, K., Lazaridis, T., Ma, J., Ovchinnikov, V., Paci, E., Pastor, R. W., Post, C. B., Pu, J. Z., Schaefer, M., Tidor, B., Venable, R. M., Woodcock, H. L., Wu, X., Yang, W., York, D. M., Karplus, M., *J. Comp. Chem.*, **2009**, *30*, 1545.
- <sup>17</sup> CHARMM c36b1 Documentation. HTML formatting scripts developed by Venable, R. M., NIH/NHLBI/DIR, Lab. of Comput. Bio. <http://www.charmm.org/documentation/c36b1/index.html>.
- <sup>18</sup> Bjelkmar, P., Larsson, P., Cuendet, M. A., Hess, B., Lindahl, E., *J. Chem. Theory Comput.*, **2010**, *6*, 459.
- <sup>19</sup> van der Vegt, N. F. A., van Gunsteren, W. F., *J. Phys. Chem. B*, **2004**, *108*, 1056.
- <sup>20</sup> Schravendijk, P., van der Vegt, N., *J. Chem. Theory Comp.*, **2005**, *1*, 643.
- <sup>21</sup> Patel, S., Brooks, Ch. L., *J. Chem. Phys.*, **2005**, *123*, 164502.
- <sup>22</sup> Glennon, T. M., Zheng, Y.-J., Le Grand, S. M., Shutzberg, B. A., Merz, K. M. Jr., *J. Comput. Chem.*, **1994**, *15*, 1019.
- <sup>23</sup> Cheatham, T. E. III, Crowley, M. F., Fox, T., Kollman, P. A., *Proc. Natl. Acad. Sci.*, **1997**, *94*, 9626.
- <sup>24</sup> Xia, X., Perera, L., Essmann, U., Berkowitz, M. L., *Surf. Sci.*, **1995**, *335*, 401.
- <sup>25</sup> Anisimov, V. M., Vorobyov, I. V., Roux, B., MacKerell A. D. Jr., *J. Chem. Theory Comput.*, **2007**, *3*, 1927.
- <sup>26</sup> Siepmann, J. I., Sprik, M., *J. Chem. Phys.*, **1995**, *102*, 511.
- <sup>27</sup> Sakuma, H., Tsuchiya, T., Kawamura, K., Otsuki, K., *Surf. Sci.*, **2003**, *536*, L396.
- <sup>28</sup> Michaelides, A., Ranea, V. A., de Andres, P. L., King, D. A., *Phys. Rev. Lett.*, **2003**, *90*, 216102.
- <sup>29</sup> Morin, C., Simon, D., Sautet, P., *J. Phys. Chem. B*, **2004**, *108*, 5653.
- <sup>30</sup> Sutton, A. P., Chen, J., *Philos. Mag. Lett.*, **1990**, *61*, 139.
- <sup>31</sup> Xu, J. Z., Zhang, X. P., Zenobi, R., Yoshinobu, J., Xu, Z., Yates. J. T., *Surf. Sci.*, **1991**, *256*, 288.
- <sup>32</sup> Bowker, M., Holroyd, R. P., Sharp, R. G., Corneille, J. S., Francis, S. M., Goodman, D. W., *Surf. Sci.*, **1997**, *370*, 113.
- <sup>33</sup> Holroyd, R. P., Bennett, R. A., Jones, I. Z., Bowker, M., *J. Chem. Phys.*, **1999**, *110*, 8703.
- <sup>34</sup> Shekhar, R., Barteau, M. A., *Catal. Lett.*, **1995**, *31*, 221.
- <sup>35</sup> Carlson, T. A., Agron, P. A., Thomas, T. M., Grimm, F. A., *J. Elec. Spec. Rel. Phenom.*, **1981**, *23*, 13.
- <sup>36</sup> Camplin, J. P., McCash, E. M., *Surf. Sci.*, **1996**, *360*, 229.
- <sup>37</sup> Bowker, M., Madix, R. J., *Surf. Sci.*, **1982**, *116*, 549.
- <sup>38</sup> Sexton, B. A., Rendulic, K. D., Hughes, A. E., *Surf. Sci.*, **1982**, *121*, 181.
- <sup>39</sup> Rajumon, M. K., Roberts, M. W., Wang, F., Wells, P. B., *J. Chem. Soc., Faraday Trans.*, **1998**, *94*, 3699.
- <sup>40</sup> Panja, C., Saliba, N., Koel, B. E., *Surf. Sci.*, **1998**, *395*, 148.
- <sup>41</sup> Cong, Y., van Spaendonk, V., Masel, R. I., *Surf. Sci.*, **1997**, *385*, 246.
- <sup>42</sup> Zhong, L. W., Cong, C., Jian, Y., *Heat Tran. Asian Res.*, **2008**, *37*, 86.
- <sup>43</sup> Meng, S., *J. Chem. Phys.*, **2007**, *127*, 244710.
- <sup>44</sup> Butt, H.-J., Graf, K., Kappl, M., *Physics and Chemistry of Interfaces*, Wiley-VCH Verlag & Co. KGaA, Weinheim, **2003**.
- <sup>45</sup> Wang, M., Guo, D.-J., Li, H.-L., *J. Solid State Chem.*, **2005**, *178*, 1996.
- <sup>46</sup> Zhao, Y., Yang, X., Tian, J., Wang, F., Zhan, L., *Int. J. Hydrogen Energ.*, **2010**, *35*, 3249.

Received: 11.01.2013.

Accepted: 23.01.2013.





# SYNTHESES AND SPECTRAL CHARACTERIZATION OF SOME NOVEL MACROCYCLIC COMPLEXES OF OXOVANADIUM(IV) WITH 1,1'-OXALYLDIIMIDAZOLE

Ashok Kumar Yadava<sup>[a]</sup>, Hardeo Singh Yadav<sup>[a]</sup> and Devendra Pratap Rao<sup>[b]\*</sup>

**Keywords:** oxovanadium(IV), amines, kinetic template, macrocyclic complexes.

A new series of five complexes of oxovanadium(IV) with the general formula [VO(mac)]SO<sub>4</sub> (where mac = tetraazamacrocyclic ligands derived by condensation of 1,1'-oxalyldiimidazole with 1,2-diaminopropane and their reactions with β-diketones) have been prepared using oxometal ion as kinetic template. The prepared complexes have been characterized on the basis of electrical conductance, molecular weight, magnetic moment, elemental analyses, infrared, e.s.r. and electronic spectral data. The probable coordination number of central metal is five (distorted square-pyramid).

\*Corresponding Authors

\*E-mail: [devendraprataprao@yahoo.com](mailto:devendraprataprao@yahoo.com)

[a] Department of Chemistry, North Eastern Regional Institute of Science and Technology (NERIST), Nirjuli-791109, Arunachal Pradesh, India

[b] Department of Chemistry, D.A-V. College, Kanpur 208001, Uttar Pradesh, India

## Introduction

Schiff bases play an important role in chemistry as they easily form stable complexes with most of transition metal ions. Schiff base complexes may serve as models for biologically important species. Vanadium is an essential element for biological systems. Vanadium is reported to participate in some enzymatic reactions such as nitrogen fixation.<sup>1,2</sup> Vanadium is found naturally in soil and water as trace metal. "Accumulated" vanadium in the form ores such as vanadinite or patronite is rare. Vanadium is actually the second most abundant transition metal in sea water, only surpassed by molybdenum as molybdate. Vanadium compounds with oxidation state IV and V exist in the biological systems. The oral administration of vanadate is reported to reduce hyperglycemia in diabetic rats. The chemistry of oxovanadium complexes has attracted due to their insulinomimetic properties in the therapeutics of diabetes.<sup>3-5</sup> 1,1'-oxalyldiimidazole is a versatile chelating agent having two reactive carbonyl groups capable of undergoing Schiff-base condensation with a variety of amines. Studies on the macrocyclic ligands of oxovanadium(IV) incorporating four nitrogen donor atoms have received less attention.<sup>5-7</sup> Oxovanadium(IV) complexes have been commonly utilized as precatalysts for olefin epoxidation and sulfide oxidation when combined with peroxide co-oxidants.<sup>8-10</sup> The 1,2-diaminopropane can form chelate ring using in-situ method of synthesis in presence of metal cation due to kinetic template effect.<sup>11-13</sup>

Considering these facts a new series of oxovanadium(IV) complexes were synthesized using in-situ method of synthesis by condensation of β-diketones viz. acetylacetone, benzoylacetone, thenoyltrifluoroacetone and

dibenzoylmethane with 1,2-diaminopropane in molar ratio 1:2 in the presence of VO<sup>2+</sup> cation as kinetic template using 1,1'-oxalyldiimidazole. These complexes were isolated in solid state. We report here the synthesis of these complexes and their tentative structures on the basis of elemental analyses, molar conductance, magnetic susceptibility measurements and spectral (ir, esr and electronic) data.

## Experimental

### Materials

Oxovanadium(IV) sulfate was purchased from Aldrich. The β-diketones viz. acetylacetone, benzoylacetone, thenoyltrifluoroacetone and dibenzoylmethane were obtained from Sisco Research Laboratories Pvt. Ltd., Mumbai, India. 1,1'-oxalyldiimidazole and 1,2-diaminopropane used were Aldrich products. The solvents were purified before use by standard techniques.

### Analytical and Physical Measurements

Estimation of vanadium was done by gravimetrically as its vanadate, after decomposing the complex with concentrated nitric acid.<sup>14</sup> Sulfur was estimated as BaSO<sub>4</sub> in the laboratory.<sup>15</sup> Melting point (uncorrected) determination of the complexes were done by the standard technique using sulfuric acid bath. Molar conductance were measured using Toshniwal conductivity bridge (Model CL-01-02A, cell constant 0.5 cm<sup>-1</sup>) using 1x10<sup>-3</sup> M solution of the complexes in DMF at room temperature. Carbon, hydrogen and nitrogen microanalyses of the complexes were estimated at CRF, NERIST, Nirjuli-791109, Itanagar, Arunachal Pradesh, India.

Room temperature magnetic susceptibilities of the complexes in powder form were measured by Gouy's balance using mercury tetrathiocyanatocobaltate(II), Hg[Co(NCS)<sub>4</sub>], ( $\chi_g = 16.44 \times 10^{-6}$  c.g.s. unit at 20 °C), as calibrant. The UV-Vis electronic spectra of the complexes were obtained by using Beckmann DU-2 spectrophotometer in the range 2000-185 nm.

**Table 1.** Physical and analytical data of the complexes

Complex	Empirical Formula	T <sub>dec</sub> , °C	Elem. Anal., Calcd./ (Found)					μ <sub>eff.</sub> BM, 300 °K
			C %	H %	N %	V %	S %	
[VO(L)]SO <sub>4</sub>	C <sub>14</sub> H <sub>22</sub> N <sub>8</sub> VSO <sub>5</sub>	221	36.1 (35.8)	4.7 (4.5)	24.0 (23.8)	11.0 (10.9)	6.9 (6.6)	1.75
[VO(mac <sup>1</sup> )]SO <sub>4</sub>	C <sub>19</sub> H <sub>26</sub> N <sub>8</sub> VSO <sub>5</sub>	220	43.1 (42.9)	5.0 (4.9)	21.2 (21.0)	9.6 (9.4)	6.1 (5.9)	1.72
[VO(mac <sup>2</sup> )]SO <sub>4</sub>	C <sub>24</sub> H <sub>28</sub> N <sub>8</sub> VSO <sub>5</sub>	216	48.7 (48.3)	4.8 (4.7)	18.9 (18.7)	8.6 (8.5)	5.4 (5.2)	1.72
[VO(mac <sup>3</sup> )]SO <sub>4</sub>	C <sub>22</sub> H <sub>23</sub> N <sub>8</sub> VSO <sub>5</sub> F <sub>3</sub>	215	40.6 (40.2)	3.6 (3.3)	17.2 (16.9)	7.8 (7.6)	9.8 (9.7)	1.71
[VO(mac <sup>4</sup> )]SO <sub>4</sub>	C <sub>29</sub> H <sub>30</sub> N <sub>8</sub> VSO <sub>5</sub>	220	53.3 (53.0)	4.6 (4.3)	17.1 (16.8)	7.8 (7.6)	4.9 (4.7)	1.74

The room temperature and liquid nitrogen temperature ESR spectra were recorded at RSIC, IIT, Chennai, India. The FTIR spectra of the complexes in the range 4000-200 cm<sup>-1</sup> were measured in KBr pellets on Perkin-Elmer 621. Purity of the complexes was tested by TLC on silica.

### Synthesis of oxovanadium(IV) complexes

The Schiff base ligand (L) was prepared by mixing ethanolic solutions of 1,1'-oxalyldiimidazole (4 mmol, 25 mL) with 1,2-diaminopropane (8 mmol, 50 mL) and refluxing the mixture for about 3 h. After completion of the reaction, green solid product was filtered and washed with ethanol. The purity of compound was checked by TLC. Yield: 60 %, m.p. 255 °C; UV-Vis (CH<sub>3</sub>OH) λ<sub>max</sub>/nm: 242, 265. Vanadyl sulfate (4 mmol) dissolved in ethanol (25 mL) was added to the refluxing solution of ligand and again this mixture was refluxed for 3 h, when the color of the solution is intensified and turned to green. The solid which separated at room temperature was washed with ethanol and dried over P<sub>4</sub>O<sub>10</sub> in vacuo. The purity of complex was checked by TLC. The yield was 65 % (Type I).

The reaction mixture of I suspended in ethanol was further reacted with β-diketones such as acetylacetone or benzoylacetone or thenoyltrifluoroacetone or dibenzoylmethane (1:1) to get macrocyclic complexes (Type II). These macrocyclic complexes were isolated under vacuo.

The ligand L is derived by condensation of 1,1'-oxalyldiimidazole with 1,2-diaminopropane (1:2); Mac<sup>1</sup> = macrocyclic ligand derived by condensation of L<sup>1</sup> with acetylacetone; Mac<sup>2</sup> = macrocyclic ligand derived by condensation of L<sup>1</sup> with benzoylacetone; Mac<sup>3</sup> =

macrocyclic ligand derived by condensation of L<sup>1</sup> with thenoyltrifluoroacetone; Mac<sup>4</sup> = macrocyclic ligand derived by condensation of L<sup>1</sup> with dibenzoylmethane.

### Results and Discussion

The oxovanadium(IV) complexes were synthesized using in-situ method by refluxing the reaction mixture of 1,1'-oxalyldiimidazole with diamines and vanadylsulfate in 1:2:1 molar ratio in aqueous ethanol. The reactions appear to proceed according to the given scheme.

### Infrared spectra

Important infrared spectral bands of the complexes and their tentative assignments are given in Table 2. In all complexes of oxovanadium(IV), the coordination of nitrogen atoms of azomethine groups to the VO<sup>2+</sup> is evidenced by the shift of ν<sub>C=N</sub> to lower frequencies.<sup>16-21</sup> Here >C=N absorption is observed around 1620 - 1615 cm<sup>-1</sup>, which normally appears at 1650 cm<sup>-1</sup> in free ligands. The presence of a band at around 300 cm<sup>-1</sup> may be assigned to ν<sub>V-N</sub> vibration.<sup>22</sup> The appearance of >C=N band and the absence of the >C=O band around 1710 cm<sup>-1</sup> is a conclusive evidence for condensation of the diamines with the two keto group of 1,1'-oxalyldiimidazole.<sup>21</sup> The bands appearing at 3345 and 3175 cm<sup>-1</sup> may be assigned to asymmetrical and symmetrical N-H stretching modes of the coordinated terminal amino group.<sup>23</sup> The oxovanadium(IV) complexes show a band at around 975 - 980 cm<sup>-1</sup>, which is assigned to ν<sub>V=O</sub> vibration.<sup>24-26</sup> The presence of an ionic sulfate group in the complexes is confirmed by the appearance of three bands at ca. 1130-1135 cm<sup>-1</sup> (ν<sub>3</sub>), 945-952 cm<sup>-1</sup> (ν<sub>1</sub>) and 600-604 cm<sup>-1</sup> (ν<sub>4</sub>). The absence of a ν<sub>2</sub> band and non-splitting of ν<sub>3</sub> band confirms that tetrahedral symmetry is retained.<sup>27</sup>

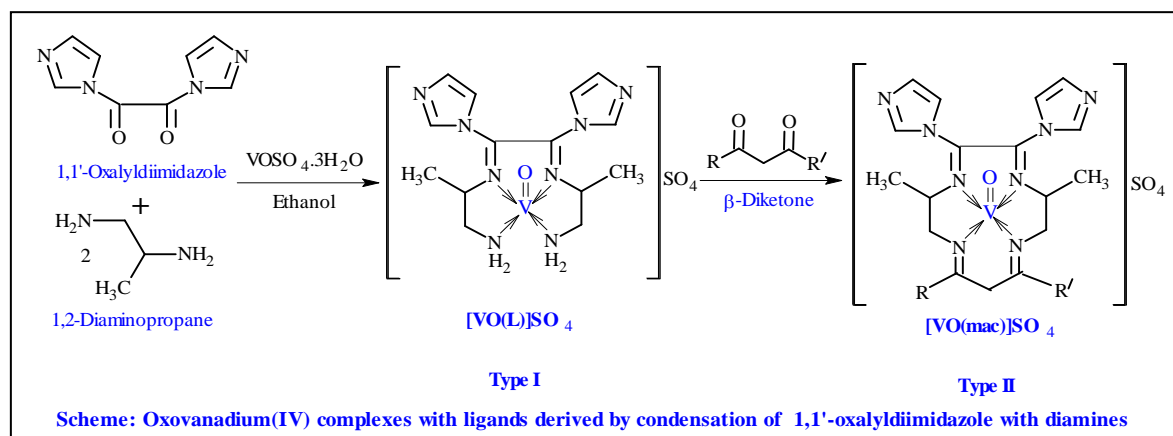


**Table 2.** Infrared spectral bands of complexes

Complex	Bands (cm <sup>-1</sup> )							
	$\nu_{C=N}$	$\nu_{V-N}$	$\nu_{V=O}$	$\nu_3(SO_4^{2-})$	$\nu_1(SO_4^{2-})$	$\nu_4(SO_4^{2-})$	$\nu_{as}(NH)$	$\nu_s(NH)$
[VO(L)]SO <sub>4</sub>	1620	300	975	1130	950	602	3345	3172
[VO(mac <sup>1</sup> )]SO <sub>4</sub>	1615	303	975	1132	952	602	3345	3175
[VO(mac <sup>2</sup> )]SO <sub>4</sub>	1620	300	975	1130	950	604	3348	3180
[VO(mac <sup>3</sup> )]SO <sub>4</sub>	1618	301	980	1135	950	600	3345	3180
[VO(mac <sup>4s</sup> )]SO <sub>4</sub>	1616	302	978	1135	952	602	3345	3178

### Electronic Spectra

The electronic spectra of oxovanadium(IV) complexes were recorded in 10<sup>-3</sup> mol L<sup>-1</sup> DMF solution. The electronic spectra show bands in the regions 11,030 – 11,960 cm<sup>-1</sup>, 15,020 – 15,850 cm<sup>-1</sup> and 21,030 – 22,340 cm<sup>-1</sup>. These spectra are similar to other five coordinate oxovanadium(IV) complexes involving nitrogen donor atoms. These spectral bands are interpreted according to an energy level scheme reported by Tsuchimoto et al. for distorted five coordinate square pyramidal oxovanadium(IV) complexes.<sup>28</sup> Accordingly, the observed bands can be assigned to <sup>2</sup>B<sub>2</sub> → <sup>2</sup>E, <sup>2</sup>B<sub>2</sub> → <sup>2</sup>B<sub>1</sub> and <sup>2</sup>B<sub>2</sub> → <sup>2</sup>A<sub>2</sub> transitions, respectively. One more band is observed in the region 35,150 – 35,680 cm<sup>-1</sup>, which may be due to transition of the azomethine linkages<sup>29,30</sup>.

### Molar conductance measurements

The molar conductivity ( $\Lambda_M$ ) values of all the oxovanadium(IV) complexes were measured in dimethylformamide and the obtained values lie between 90 – 102 ohm<sup>-1</sup> cm<sup>2</sup> mol<sup>-1</sup> indicating their 1:1 electrolytic nature.

### Magnetic moment measurements

Magnetic moments of oxovanadium(IV) complexes were measured at room temperature and effective magnetic moment ( $\mu_{eff}$ ) values are given in Table 1. The magnetic moment values of the vanadyl complexes ranges from 1.71–1.76 B.M which correspond to a single electron of the 3d<sup>1</sup> system of square-pyramidal oxovanadium(IV) complexes.<sup>28</sup>

### ESR spectra

The X-band ESR spectra of an oxovanadium(IV) complex was recorded in DMSO at room temperature and at liquid nitrogen temperature (177 K). ESR spectra of the complexes were analyzed by the method of Mishra, Yadava Sand and Ando et al.<sup>29–32</sup> ESR spectra at room temperature show eight lines, which are due to hyperfine splitting arising from the interaction of the unpaired electron with a <sup>51</sup>V nucleus having the nuclear spin I = 7/2. This confirms the presence of a single oxovanadium(IV) cation as the metallic centre in the complex. The anisotropy is not observed due to rapid tumbling of molecules in solution at room temperature and only g-average values are obtained. The anisotropy is clearly visible in the spectra at liquid nitrogen temperature and eight bands each due to g<sub>||</sub> and g<sub>⊥</sub> are observed separately which are in good agreement for a square pyramidal vanadyl complexes.<sup>33–35</sup>

The g<sub>||</sub>, g<sub>⊥</sub>, A<sub>||</sub> and A<sub>⊥</sub> values are measured from the spectra, which are in good agreement for a square-pyramidal structure. The g<sub>iso</sub> value from mobile solution at room temperature and g<sub>av</sub> from frozen solution at liquid nitrogen temperature do not agree very closely since the g and A tensors are corrected for second-order. Further, g values are all very close to the spin-only value (free electron value) of 2.0023, suggesting little spin-orbit coupling. On the basis of these studies, the tentative structures are proposed for these oxovanadium(IV) complexes of the type (I) and (II).

### Conclusions

The present study demonstrates simple synthetic routes to 5 new oxovanadium(IV) complexes with tetraaza macrocyclic ligands. The obtained spectral data suggest that the 1,1'-oxalyldiimidazole is good chelating agents having two reactive carbonyl groups capable of undergoing Schiff base condensation with a variety of diamine. Schiff bases behave as tetradentate ligands by bonding to the metal ion through the azomethine nitrogen and amino group. The analytical data show the presence of one metal ion per ligand molecule and suggest a mononuclear structure for the VO<sup>2+</sup> complexes. The electrical conductance, magnetic moment values, infrared, e.s.r. and electronic data are in the favour of square pyramidal structure for VO(IV) complexes.

### Acknowledgements

The authors are thankful to the Director, NERIST, Nirjuli, Itanagar, Arunachal Pradesh, India for providing laboratory facilities and department of chemistry for microanalysis of carbon, hydrogen and nitrogen.

### References

- <sup>1</sup>Chisnell, J. R., Premakumar, R., Bishop, P. E., *J. Bact.*, **1988**, 170, 27.
- <sup>2</sup>Rehder, D., *Inorg. Chem. Commun.*, **2003**, 6, 604.
- <sup>3</sup>Butler, A., Walker, J. V., *Chem. Rev.*, **1993**, 93, 1937.
- <sup>4</sup>Thompson, K. H., Orvig, C., *J. Chem. Soc., Dalton Trans.*, **2000**, 17, 2885.
- <sup>5</sup>Gatjens, J., Meier, B., Adachi, Y., Sakurai, H., Rehder, D., *Eurasian J. Inorg. Chem.*, 2006, 3575.
- <sup>6</sup>Koo, B. K., Jang, Y. J., Lee, U., *Bull. Korean Chem. Soc.*, **2003**, 24, 1014.
- <sup>7</sup>Maurya, M. R., *Coord. Chem. Rev.*, 2003, 237, 163.
- <sup>8</sup>Radosevich, A. T., Musich, C., Toste, F. D., *J. Am. Chem. Soc., Commun.*, **2005**, 127, 1090.
- <sup>9</sup>Ligtenberg, A. G. J., Hage, R., Feringa, B. L., *Coord. Chem. Rev.*, **2003**, 237, 89.

- <sup>10</sup>Bolm, C., Bienewald, F., *Angew. Chem. Int. Ed. Engl.*, **1995**, *34*, 2640.
- <sup>11</sup>Cutler, A. R., Alleyne, C. S., Dolphin, D., *Inorg. Chem.*, **1985**, *24*, 2281.
- <sup>12</sup>Malek, A., Fresco J. M., *Can. J. Chem.*, **1973**, *51*, 1981.
- <sup>13</sup>Prasad, R. N., Agrawal, M., Sharma, S., *J. Serb. Chem. Soc.*, **2005**, *70*, 54.
- <sup>14</sup>Vogel, A. I., "Book of quantitative inorganic analysis" 4th ed., Longmans Green Co. Ltd., London, **1978**.
- <sup>15</sup>Vogel, A. I., "Book of Practical Organic Chemistry", 4th ed., Longman, London, **1978**.
- <sup>16</sup>Rana, V. B., Singh, P., Singh, D. P., Teotia, M. P., *Transit. Met. Chem.*, **1982**, *7*, 174.
- <sup>17</sup>Sreeja, P. B., Kurup, M. R. P., *Spectrochim. Acta Part A*, **2005**, *61*, 331.
- <sup>18</sup>Yadava, H. D. S., Sengupta, S. K., Tripathi, S. C., *Inorg. Chim. Acta*, 1987, *128*, 1.
- <sup>19</sup>Serin, S., *Transit. Met. Chem.*, **2001**, *26*, 300.
- <sup>20</sup>Ferraro, J. R., "Low Frequency Vibrations of Inorganic and Coordination Compounds," Plenum Press, New York, NY, USA, **1971**.
- <sup>21</sup>Nakamoto, K., "IR and Raman Spectra of Inorganic and Coordination Compound, part A and B," John Wiley & Sons, New York, NY, USA, **1998**.
- <sup>22</sup>Sakata, K., Kuroda, M., Yanagida, S., Hashimoto, M., *Inorg. Chim. Acta*, **1989**, *156*, 107.
- <sup>23</sup>Nonoyama, M., Tomita, S., Yamasaki, K., *Inorg. Chim. Acta*, **1975**, *12*, 33-37.
- <sup>24</sup>Samanta, S., Ghosh, D., Mukhopadhyay, S., Endo, A., Weakley, T. J. R., Chaudhury, M., *Inorg. Chem.* **2003**, *42*, 1508.
- <sup>25</sup>Muhammad, N., Ali, S., Shahzadi, S, Khan, A. N., *Russian J. Coord. Chem.*, **2008**, *34*, 448.
- <sup>26</sup>Yaul, A. R., Pethe G. B., Aswar, A. S., *Russian J. Coord. Chem.*, **2010**, *36*, 254.
- <sup>27</sup>Sarkara, A., Pal, S., *Inorg. Chim. Acta*, **2008**, *361*, 2296.
- <sup>28</sup>Tsuchimoto, M., Hoshina, G., Yoshioka, N., Inoue, H., Nakajima, K., Kamishima, M., Kojima, M., Ohba S., *J. Solid State Chem.*, **2000**, *153*, 9.
- <sup>29</sup>Mishra, A. P., Pandey, L. R., *Indian J. Chem. A*, **2005**, *44*, 94.
- <sup>30</sup>Yadava, A. K., Yadav, H. S., Singh, S., Yadav, U. S., Rao, D. P., *J. Chem.*, **2013**, article ID 689518, 5 pages.
- <sup>31</sup>Sands, R. H., *Phys. Rev.*, **2005**, *99*, 1222.
- <sup>32</sup>Ando, R., Nagai, M., Yagyū, T., Masunobu, *Inorg. Chim. Acta*, **2003**, *351*, 107.
- <sup>33</sup>Dodwad, S. S., Dhamnaskar, R. S., Prabhu, P. S., *Polyhedron*, **1989**, *8*, 1748-1750.
- <sup>34</sup>Rao, S.N., Mishra D. D., Maurya R. C., Rao, N. N., *Polyhedron*, **1997**, *16*, 1825.
- <sup>35</sup>Boucher, L. J., Yen, T. F., *Inorg. Chem.*, **1969**, *8*, 689.

Received: 14.01.2013.

Accepted: 22.01.2013.



# SOLVATION PARAMETERS FOR SODIUM OXALATE IN MIXED ETHANOL-WATER SOLVENTS AT 301.15 K

Esam A.Gomaa<sup>[a]</sup>

**Keywords:** molar solubility, sodium oxalate, free energies of solvation, water and ethanol

The molar solubility of sodium oxalate ( $\text{Na}_2\text{Ox}$ ) in mixed ethanol (EtOH) – water solvent mixtures were measured at 301.15 K. From the molar solubilities, the activity coefficients, solubility products, free energies of solvation and the transfer free energies for the interaction of ( $\text{Na}_2\text{Ox}$ ) in mixed (EtOH- $\text{H}_2\text{O}$ ) solvents were evaluated.

\*Corresponding Authors

\*E-mail: eahgomaa65@yahoo.com

[a] Chemistry Department, Faculty of Science, Mansoura University, Mansoura, EGYPT

## Introduction

The solubility of solutes in mixed solvents is of great practical importance since many industrial processes as well as laboratory procedures need the use of solvent mixtures.

We know that, the solubility of solutes in mixed solvents depends primarily on the solvation of solutes or their constituent ions by the components of solvent mixture.<sup>1</sup>

Sodium oxalate, like citrate, can be used to remove calcium ions from blood plasma. This salt prevents blood clotting. Sodium oxalate can be responsible for the impairment of brain function, and deposit calcium oxalate in the kidneys.<sup>2</sup> Solvation processes is also important to apply for ( $\text{Na}_2\text{Ox}$ ) to understand its behaviour in solutions.<sup>3</sup>

## Experimental

Sodium oxalate ( $\text{Na}_2\text{Ox}$ ) and ethanol (EtOH) were supplied from Merck Co. Saturated solutions of ( $\text{Na}_2\text{Ox}$ ) were prepared by dissolving different amounts in closed test tubes containing different EtOH- $\text{H}_2\text{O}$  mixtures. These mixtures were then saturated with nitrogen gas as an inert atmosphere. The tubes were placed in a shaking thermostat (Model GEL) for a period of four days till equilibrium reached.

The solubility of ( $\text{Na}_2\text{Ox}$ ) in each mixture was measured conductometrically (three times measurements for each) by using conductometer YSI Model-35 which connected with ultra thermostate of the type Kottermann-4130.

All the measurements were done at 301.15 K with the accuracy of the solubility in the average of the second number after comma as given in previous work.<sup>4</sup>

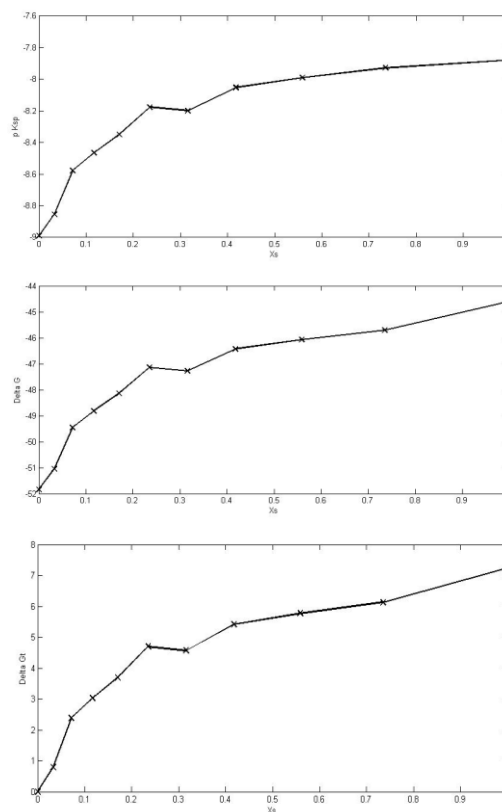


**Figure 1.** Solubility product ( $\text{pK}_{\text{sp}}$ ),  $\Delta G$  (Gibbs free energy) and  $\Delta G_t$  (Gibbs transfer free energy) for  $\text{Na}_2\text{Ox}$  in mixed EtOH- $\text{H}_2\text{O}$  solvents at 301.15K.

## Results and Discussion

The molar solubility ( $S$ ) for ( $\text{Na}_2\text{Ox}$ ) at 301.15 K were measured conductometrically in water, ethanol (EtOH) and their mixtures. The  $S$  values are cited in Table 1. The solubility of ( $\text{Na}_2\text{Ox}$ ) in water agreed well with that in Literature values.<sup>5</sup> The activity coefficients were calculated by the use of Debye-Hückel equation.<sup>6</sup>

$$\log \gamma_{\pm} = -0.5062S^{0.5} \quad (1)$$

**Table 1.** Molar solubilities ( $S$ ), log activity coefficients ( $\gamma_{\pm}$ ), solubility products ( $pK_{sp}$ ) and free energies of solvation ( $\Delta G$  and  $\Delta G_t$ ) for ( $Na_2Ox$ ) in different ethanol-water solvents at 301.15 K.

$X_s$ , mole fraction of ethanol)	$S$ , g.mol <sup>-1</sup>	$\log \gamma_{\pm}$	$pK_{sp}$	$\Delta G$ , kJ mol <sup>-1</sup>	$\Delta G_t$ , kJ mol <sup>-1</sup>
0	7.91	-1.4236	-8.9909	-51.8433	0
0.0330	7.65	-1.4001	-8.8530	-51.0484	0.7949
0.0715	7.16	-1.3535	-8.5780	-49.4624	2.3809
0.1166	6.45	-1.3344	-8.4656	-48.814	3.0297
0.1703	6.750	-1.3151	-8.3503	-48.1495	3.6938
0.2355	6.61	-1.3014	-8.1764	-47.1467	4.6966
0.3159	6.493	-1.2898	-8.1985	-47.274	4.5693
0.4181	6.250	-1.2655	-8.0517	-46.428	5.4153
0.5591	6.150	-1.2553	-7.9898	-46.0707	5.7726
0.7349	6.051	-1.2451	-7.9279	-45.7138	6.1295
1.0	5.97	-1.2368	-7.8771	-44.600	7.243

where  $S$  is the molar solubility. Their data ( $\log \gamma_{\pm}$ ) were tabulated also in Table 1. The solubility product was calculated by the use of equation 2.<sup>3</sup>

$$pK_{sp} = -\lg 4S^3 + 4(\log \gamma_{\pm})^3 \quad (2)$$

$pK_{sp}$  data are given in Table (1). From these solubility products, the Gibbs free energies of solvation and the transfer Gibbs free energies from water to mixed solvent were calculated by using equation (3) and (4). Their values are tabulated also in table (1).

$$\Delta G = 2.303 RT pK_{sp} \quad (3)$$

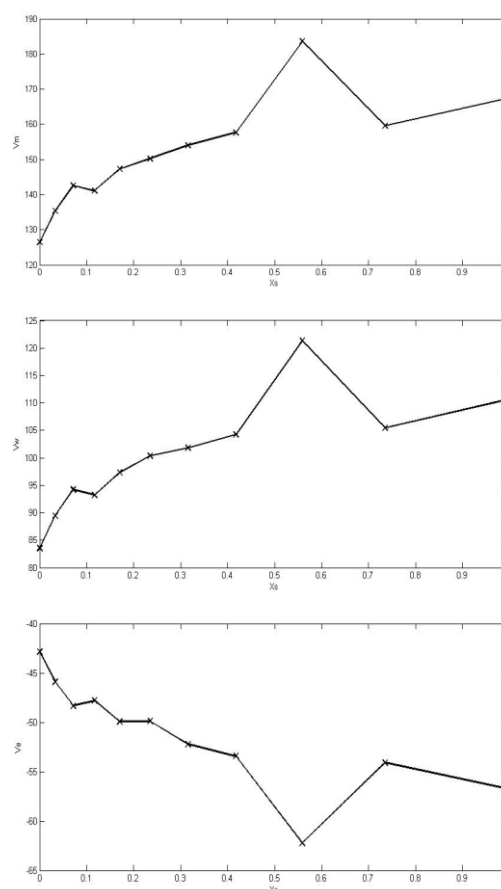
$$\Delta G_t = \Delta G_s - \Delta G_w \quad (4)$$

It was concluded that the Gibbs free energies of transfer  $\Delta G_t$  increase in positivity by increasing the mole fraction of ethanol in the mixtures. This is due to less solvation behaviour in the mixed solvents than that of water.

**Table 2.** Molar ( $V_M$ ), Van der Waals ( $V_W$ ) and electrostriction volumes ( $V_e$ ) for ( $Na_2Ox$ ) in mixed EtOH-H<sub>2</sub>O solvents at 301.15 K (in cm<sup>3</sup> mol<sup>-1</sup>).

$X_s$ , EtOH	$V_M$	$V_W$	$V_e$
0	126.4151	83.5604	-42.8547
0.033	135.3535	89.4686	-45.8848
0.0715	142.5532	94.2276	-48.3255
0.1166	141.0526	93.2358	-47.8168
0.1703	147.2527	97.3340	-49.9186
0.2355	150.2327	100.3340	-49.8986
0.3159	154.0224	101.8091	-52.2138
0.4181	157.6471	104.2047	-53.4423
0.5591	183.5616	121.3342	-62.2274
0.7349	159.5238	105.4452	-54.0786
1.0	167.500	110.7175	-56.7825

The molar volumes ( $V_m$ ) for ( $Na_2Ox$ ) in mixed EtOH-H<sub>2</sub>O were calculated by dividing the molecular weight of ( $Na_2Ox$ ) by the exact solvation densities, the values are given in Table 2.

**Figure 2.** Different volumes, molar ( $V_M$ ), Van der Waals ( $V_W$ ) and electrostriction volumes ( $V_e$ ) for  $Na_2Ox$  saturated solutions in mixed EtOH-H<sub>2</sub>O solvents.

The packing density ( $p$ ) as explained in reference 6, i.e., the relation between Van der Waals volume ( $V_W$ ) and the molar volume ( $V_M$ ) for relatively large molecules ( $M.W. > 40$ ) was found to be constant and equal to 0.661.

$$P = \frac{V_W}{V_M} = 0.661 \pm 0.017 \quad (5)$$

The electrostriction volume ( $V_e$ ) which is the volume compressed by the solvent can be calculated by using equation (6) as follows:

$$V_e = V_w - V_M \quad (6)$$

All the different volumes for ( $\text{Na}_2\text{Ox}$ ) in mixed EtOH- $\text{H}_2\text{O}$  solvents are represented in Table 2. The data in Table 2 indicate that the ( $\text{Na}_2\text{Ox}$ ) volumes increase by adding more ethanol favouring more energy required for solvation, i.e. less solvation process.

## References

- <sup>1</sup>Marcus, Y., *Pure Appl. Chem.*, **1990**, 62, 2069-2076.
- <sup>2</sup>Roazini, M. Z. H., Brimblecombe, P., *J. Chem. Thermodyn.*, **2009**, 41(9), 980-983.
- <sup>3</sup>Gomaa, E. A., *Thermochim. Acta*, **1989**, 156, 91-99.
- <sup>4</sup>Gomaa, E. A., *An. Univ. Bucuresti*, **2010**, 19(1), 45-48.
- <sup>5</sup><http://rruff.geo.arizona.edu/doclib/hom/natroxalate>.
- <sup>6</sup>El-Khouly, A. A., Gomaa, E. A., Abou El-Leef, S., *Bull. Electrochem.*, **2003**, 19(4), 153-164.

Received: 07.01.2013.

Accepted: 13.01.2013.



## RESEARCH AND DEVELOPMENT ADVANCES IN WOOD FUNCTIONAL MODIFICATION IN CHINA

Liu Shu<sup>[a]</sup>

**Keywords:** Wood; functional modification; development trend.

Since China carried out natural forest protection project in 1998, the timber supply in China depends mainly on international market. In order to solve the problem of the supply and demand of wood in China, the fast-growing plantations of aspen wood, eucalyptus, Chinese fir, and masson pine have been explored in China. The functional modification must be performed to make better due to the low quality of these kinds of plants species. The advances in wood functional modification, such as colour processing, softening, size stabilization, strengthening, fire-retardant treatment and preservative treatment in latest 10 years, has been summarized in the present paper.

\*Corresponding Authors

\*E-mail: liuxinlin-yj@163.com

[a] Fax: 86-24-56860869

Liaoning Shihua University, Fushun, Liaoning, P.R. China.

### Introduction

Logs are one kinds of the most important building materials. China is a larger producer of timber and wood products, and is also a huge consumer of wooden articles<sup>1,2</sup>. In the first half of 2012, the timber production of Chinese forestry industry was *ca.*  $3.502.55 \times 10^7$  cubic meters with an output value of *ca.*  $1.4 \times 10^{12}$  yuan. However, China is short of forest reserves. The country had carried out natural forest protection project in 1998, and took measures to reduce cutting of the domestic forest year after year, so a big gap of supply and demand in domestic timber market appeared and thus the timber supply in China is heavily dependent on international market. Wood is one of strategic commodities which play a important role in the sustainable development of China's economy. In order to solve the problem of the supply and demand of wood, the fast-growing plantations of aspen wood, eucalyptus, Chinese fir, and masson pine have caught more attention in China. These tree species usually are low quality, functional modification thus must be performed to make better. The functional modification on wood such as color processing, softening, size stabilization, strengthening, fire-retardant treatment and preservative treatment in recent 10 years, has been summarized in present paper<sup>3-9</sup>.

### Discussion

#### Color processing

Bleaching can removes Blue-stains and splashes on the veneer surface. Hydrogen peroxide (H<sub>2</sub>O<sub>2</sub>) and sodium hypochloride (NaClO<sub>2</sub>) are the most often used bleaching agents. Pretreatment by sodium hydroxide or ammonia will show a better effect of wood bleaching.

Decolourization of the timber is mainly caused by the external factors, such as bacteria, temperature, light, oxygen,

water, and acid and base substances, and ferric like which interact with the wood's components (lignin and extractives, etc.).

The anti-tarnishing process by employing chemical and physical treatments, can preserve the tones and texture of wood, and maintain the value of the furniture. The physical methods use extract agents to leach the extractives of wood, where controlled temperature and humidity contribute to inhibit or even kill the decolourant bacteria. The thin films coating on the wood surface by physical methods can play the role of water and light exclusions. The wood can be coated with ultraviolet absorbents using chemical methods, or the surface can be disposed with anti-oxidizing agent solution or the pH adjusting agent solution, to prevent from decolourization of wood.

The dyeing can improve decorative function and increase the value of the medium or low-rank wood. The dyeing effect depends on physical and chemical properties of the timber species and dyeing conditions. The Chromatic characteristics of dyeing on Chinese fir are associated to the anatomic factor, where the cellulose and hemicellulose are stained quite easier than other timber species. The dyeing rates of poplar, birch and oak species increase with an increased microwave power and longer treating time.

#### Softening treatment

Softening treatment of timbers presently involves cooking, microwave heating moulding at water-saturated state, alkali treatment, and the nitrogen-containing compound treating (liquid ammonia, gaseous ammonia, aqueous ammonia, hydrazine, etc.). The wood can be softened effectively by heating a urea solution with timber impregnated in it.

The expansion ratio increases with the higher abilities of the solutions to form hydrogen bonds with the three major kinds of components in wood. N atom forms a hydrogen bond much more easily than O atom, therefore, wood treating by using nitrogenous compounds generally shows a more obvious softening effect than the cooking method. The heating modes of wood softening also involve microwave heating and high-frequency electric heating.



### Size stabilizing treatment

Wood is hygroscopic *per se*. The change of moisture content in it is the main reason for the shrinkage and the swelling of wood. Heat treatment and waterproof treatment are the physical methods for size stabilization of wood. Silicone oil and paraffin are used as waterproof agents to modify the wood surface. After the timbers of ash, oak wood, camphor and schima superba ect. are treated in a low oxygen atmosphere at 200 °C, the population of hydroxyl group in cell wall decreases, leading to a significant decrease of moisture content, thus the dimension stability of wood can effectively improve. During the chemical treatment, polyethylene glycol, acetic anhydride, phenol formaldehyde resin, or urea formaldehyde resin can be used. These low molecular weight chemicals react with hydrophilic hydroxyl in wood to form thermosetting resin. The dimensional stability of eucalyptus greatly improves by dipping the timber in urea-formaldehyde resin modified by melamine and then heating. Chinese wood industry currently consumes large amounts of phenolic resin and urea formaldehyde resin in dimensional stabilizing process due to the significant improvement on the wood functions.

### Strengthening treatment

Strengthening treatment increases the densities and mechanical strength of low quality wood by using the physical, chemical or mechanical methods. The inner steam pressure of the timbers increases rapidly during hot-press oxidization treatment, where the drying of the timbers is accelerated. The densities of wood and the hardness of surface both increase, which lead to a promotion on the performances and a raise of the value of timbers. The best processing conditions of hot-pressure treatment for thinning wood of Chinese fir is a moisture content of 50% prior to the treatment, a time compression of about 30 min at 180 - 200 °C, where a Compression ratio of 50 % - 60 % is obtained with significant improved physical and mechanical properties.

Dipping treatment is used for medium and low-grade timbers by soaking them in low molecular weight polymers to increase the mechanical strength. Due to more refractory injection of heartwood than sapwood, extraction treatment and vacuum impregnation is often employed simultaneously as the injection to enhance the impregnation ratio and the uniform distribution of the polymers in the timbers.

### Flame retardant treatment

The effect of flame retardant treatment depends on the processing method and fire retardant used. The flame retardant processing mainly includes impregnation, spraying and coating, veneering, hot pressing, complex method, radiation method, ultrasonic method, centrifugal rotation method and high energy jet method and so on. The wood fire retardants usually are classified into phosphorus based, boron based, phenolic, halogenated, nitrogenous, and halogen-phenolic flame-retardants. The phosphorus-nitrogenous-boric composite fire retardants have been recently introduced into China market due to its multiple functions, such as flame retarding, smoke-suppression, anti-corrosion, and no pollution. Aqueous amino resin coating on

wood also has attracted a lot of attention now, because of the extended flame combustion time and the less released burning heat.

### Preservation treatment

Wood decay is mainly caused by wood rot fungi. On using wood preservatives lots of factors should be taken into consideration, such as human health, safety and environmental effects, effective recycling, with broad spectrum sterilization, resistance to erosion, the relatively low cost. Wood preservatives are mainly made down into three types in China, namely water borne preservatives are widely used in China, such as CCA (a solution of copper sulphate 35 %, potassium dichromate 40 % and arsenic pentoxide 25 %), ACQ (ammoniacal copper quaternary types), CA-B (copper azole-type B), ect.

### Research prospects on function modification of wood in China

Along with the change of national forest resources structure and the awareness of ecological environment protection, the functional modification of wood in China has focused in long term on the fast unripe plantation wood. Poplar, Paulownia, pine, eucalyptus, Sugiki are all abundant in china and with shortcomings in the performances. Multi-functional modification takes the trend in improvement of wood processing. Inorganic fillers have advantages of low cost, environmental protection, no volatile harmful gas etc. The poplar wood treated by silicate monomer solution gives a higher dimensional stability and resistance to erosion. Fir wood treated by a solution of aluminium sulphate solution or water glass solution produces significantly increased dimensional stability, the bending strength, bending modulus of elasticity, compression strength, compressive strength parallel to grain, and hardness.

Treating timber by using nanomaterials is highlighted in lumber functionality improvement in China during recently 10 years. The nanometer interstices between the micro fine fibres on the cell wall of the timber can accommodate the nanoparticles which can combine with the reactive groups there. The wood/inorganic nanocomposites can be produced by using the sol-gel method, in situ intercalation synthesis method, injection filling method, leading to a promotion of the performance of wood, even to producing a new performance.

The nano sized SiO<sub>2</sub> aero gels prepared by sol-gel method can be injected into the timber through the vacuum/pressure method to form a wood and nano particles composites of good performance. The wood/nano montmorillonite intercalation composite are produced by introducing montmorillonite into wood in phenolic resin medium. This intercalation composite shows a significantly lower water swelling ratio, an increased strength parallel to grain, a markedly improved thermal stability.

### References

- <sup>1</sup>Lin, J. G., Xu. Y. J., *Acta Agric, Univ, Jiangxiensis*, **2003**, 25(2), 140.

<sup>2</sup>Yang, H. Q., Ying, N., *J. Int. Trade*, **2006**(6), 51.

<sup>3</sup>Wang, Y. H., Gu, L. B., Wang, C. G., Ke, S.-H., Liu, X. E. *China Forestry Sci. Technol*, **2005**, 19(3), 13.

<sup>4</sup>Cui, H., Du, G., *World Forestry Res.*, **2008**, 21(3), 43.

<sup>5</sup>Guan, X., Guo, M., *Furniture*, **2009**, 5(5), 42.

<sup>6</sup>Zhao, Y., Feng, S., Huang, R., *World Forestry Res.*, **2010**(6), 40.

<sup>7</sup>Lin, L. Y., Fu, F., *Wood Process. Machinery*, **2011**, 22 (4), 10.

<sup>8</sup>Chen, X. H., Lin, J. G., *J. Fujian Forestry Sci. and Tech.*, **2011**, 38, 154.

<sup>9</sup>Wang, Y. W., Huang, R.-F., *Forestry Machinery & Woodworking Equipment*, **2011**, 39(8), 13.

Received: 13.12.2012.

Accepted: 25.01.2013.



# POLARIZATION STUDY OF CORROSION INHIBITION BY GLYCINE- Zn<sup>2+</sup> SYSTEM

J. Angelin Thangakani<sup>[a]</sup>, S. Rajendran<sup>[b,c]\*</sup>, J. Sathiyabama<sup>[b]</sup>, J. Lydia Christy<sup>[d]</sup>,  
A. Suriya Prabha<sup>[e]</sup> and M. Pandiarajan<sup>[b]</sup>

**Keywords:** Corrosion inhibition, mild steel, polarization studies, glycine, zinc<sup>2+</sup>

The inhibition efficiency of glycine-Zn<sup>2+</sup> system has been evaluated by weight loss method and polarization study. Glycine alone has some corrosion inhibition efficiency (IE). In presence of Zn<sup>2+</sup>, IE increases. Synergistic effects exist between Zn<sup>2+</sup> and glycine. The formulation consisting of 250 ppm of glycine and 50 ppm of Zn<sup>2+</sup> has 86% IE. Polarization study reveals that this system function as mixed inhibitor system, controlling the anodic reaction and cathodic reaction to an equal extent.

\*Corresponding Authors

\*E-mail: [srmjoany@sify.com](mailto:srmjoany@sify.com)

- [a] CEOA Matriculation Higher Secondary School, A Kosakulam, Madurai, E-mail: [angelinthangakani@gmail.com](mailto:angelinthangakani@gmail.com)  
 [b] Corrosion Research Centre, PG and Research, Department of Chemistry, GTN Arts College, Dindigul- 624005, India. E-mail: [pandiarajan777@gmail.com](mailto:pandiarajan777@gmail.com)  
 [c] Department of Chemistry, Corrosion Research Centre, RVS School of Engineering and Technology, Dindigul 624005, India. E-mail: [srmjoany@sify.com](mailto:srmjoany@sify.com)  
 [d] Department of Chemistry, VSB Engineering College, Karur- 639 111, Tamilnadu, India.  
 [e] Department of Chemistry, Shanmuganathan Engineering College, Arasampatti-622 507, India. E-mail: [suriya31980@gmail.com](mailto:suriya31980@gmail.com)

acids will exist as zwitter ions, having both positive and negative charges. When an electric field is applied these ions will not move towards either the anode or the cathode. Hence these zwitter ions will be in the bulk of the solution. They will not be adsorbed on the metal surface. Hence their corrosion protection efficiency considerably decreases.

The present work is undertaken (i) to evaluate the corrosion inhibition efficiency of glycine in controlling corrosion of mild steel in an aqueous solution containing 60 ppm of Cl<sup>-</sup>, in the absence and presence of Zn<sup>2+</sup> and (ii) to investigate the mechanistic aspects of corrosion inhibition by polarization study

## Introduction

Metals are extracted from their ores by reduction process. When metals come in contact with the environment, especially oxygen and moisture, they deteriorate. This process, we call corrosion. Corrosion is the expression of desire of pure metals to go back to their original state of ores. Corrosion is a natural, spontaneous and thermodynamically stable process. The process of corrosion can be controlled but it cannot be prevented. There are many methods by which corrosion can be controlled.

One such method is the use of inhibitors. These inhibitors when added in small quantity, decrease the rate of corrosion. Corrosion inhibitors usually contain polar groups with atoms such as nitrogen, sulphur and oxygen. Correspondingly inhibitors include a wide list of organic and inorganic compounds containing the functional groups such as amines<sup>1,2</sup> nitrocompounds<sup>3,4</sup>, amides,<sup>5,6</sup> aldehydes,<sup>7,8</sup> ketones,<sup>9,10</sup> ester,<sup>11,12</sup> carboxylic acids,<sup>13,14</sup> thiocompounds,<sup>15,16</sup> phosphates,<sup>17,18</sup> phosphonates<sup>19,20</sup> and amino acids.<sup>21-25</sup>

Amino acids contain both carboxyl group and amino group. There are several amino acids. The simplest amino acid is glycine. Several amino acids such as valine,<sup>26</sup> glutamic acid,<sup>27</sup> phenyl alanine,<sup>30</sup> tyrosine,<sup>31</sup> and tryptophan<sup>32</sup> have been used as corrosion inhibitors. These corrosion inhibition efficiency is very much influenced by pH value of the medium since, under high pH value the carboxyl group will be in ionized form and under low pH value the carboxyl group will be in unionized form; but the amino group will be in protonated form. Interestingly, at isoelectric point amino

## MATERIALS AND METHODS

### Metal specimens

Mild steel specimen was used in the present study. (Composition (wt %): 0.026 S, 0.06 P, 0.4 Mn, 0.1 C and balance iron. The dimension of the specimen was 1 x 4 x 0.2 cm

### Weight-loss method:

Mild steel specimens in triplicate were immersed in 100 ml of aqueous solution containing 60 ppm of Cl<sup>-</sup> in the presence and absence of Zn<sup>2+</sup> and glycine for one day. The weight of the specimens before and after immersion was determined using a Shimadzu balance, model AY62. The corrosion products were cleansed with Clarke's solution<sup>33</sup>. The inhibition efficiency (IE) was then calculated using the

$$IE = 100 \frac{W_2}{W_1} \% \quad (1)$$

equation:

where

W<sub>1</sub> = corrosion rate in the absence of the inhibitor.

W<sub>2</sub> = corrosion rate in the presence of the inhibitor.

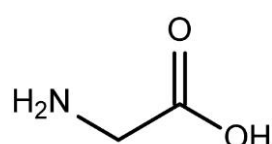
## Potentiodynamic polarization

Polarization studies were carried out in a CHI – Electrochemical workstation with impedance, Model 660A. A three-electrode cell assembly was used. The working electrode was mild steel. A saturated calomel electrode (SCE) was the reference electrode and platinum was the counter electrode. From the polarization study, corrosion parameters such as corrosion potential ( $E_{\text{corr}}$ ), corrosion current ( $I_{\text{corr}}$ ) and Tafel slopes (anodic =  $b_a$  and cathodic =  $b_c$ ) and Linear polarization resistance ( $LPR$ ) were calculated.

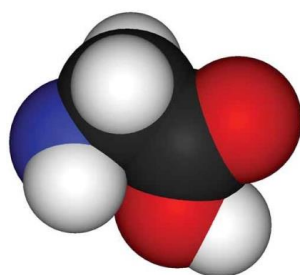
## Results and Discussion

### Analysis of weight loss method

The inhibition efficiency of glycine (Schemes 1 and 2) in controlling corrosion of mild steel immersed in an aqueous solution containing 60 ppm of Cl<sup>-</sup> at pH 7.6 has been evaluated by weight loss method and polarization study, in the absence of and presence of Zn<sup>2+</sup> ion.



**Scheme 1.** Molecular structure of glycine



**Scheme 2.** Space filling model of glycine

Corrosion rates of mild steel immersed in an aqueous solution containing 60 ppm of Cl<sup>-</sup>, in the absence and presence of Zn<sup>2+</sup> are given in Table 1. The inhibition efficiencies are also given in this Table.

**Table 1.** Corrosion rates (CR) of mild steel immersed in an aqueous solution containing 60 ppm of Cl<sup>-</sup> and the inhibition efficiency (IE) obtained by weight loss method

Glycine concentration, ppm	Zn <sup>2+</sup> concentration, ppm					
	0 ppm		25 ppm		50 ppm	
	CR	IE%	CR	IE%	CR	IE%
0	36	-	30.60	15	28.80	20
50	31.68	12	27.00	25	12.60	65
100	30.60	15	25.2	30	10.80	70
150	28.80	20	22.32	38	5.40	85
200	27.00	25	21.60	40	5.04	86
250	23.04	36	19.80	45	5.02	86

Immersion period: One Day; CR – Corrosion Rate (mdd), IE- Inhibition Efficiency

It is observed that glycine alone has some inhibition efficiency. As the concentration of glycine increases, IE also increases. 50 ppm of glycine has 12% IE and 250 ppm Glycine has 36% IE.

## Influence of Zn<sup>2+</sup> on inhibition efficiency of glycine

When Zn<sup>2+</sup> (as ZnSO<sub>4</sub>·7H<sub>2</sub>O) is added to glycine system, the IE of glycine increases. This suggests that a synergistic effect exists between Zn<sup>2+</sup> and glycine. Similar synergistic effect existing between Zn<sup>2+</sup> and inhibitors has been reported by several researchers.<sup>34-38</sup>

The synergistic effect existing between Zn<sup>2+</sup> and glycine can be explained as follows. When glycine and Zn<sup>2+</sup> are mixed, Zn<sup>2+</sup>-glycine complex is formed. It is transported towards the metal surface. On the metal surface, Zn<sup>2+</sup>-glycine complex is broken. The released glycine combines with Fe<sup>2+</sup> (formed on the metal surface due to corrosion process) resulting in the formation of Fe<sup>2+</sup>-glycine complex. Fe<sup>2+</sup>-glycine complex is more stable than Zn<sup>2+</sup>-glycine complex.<sup>39-43</sup>

## Potentiodynamic polarization study

Corrosion is a problem facing us every day and in almost every activity. Corrosion wastes material and energy, and could prevent objects from doing the job they were made to do, possibly with dangerous consequences.

The rate at which corrosion occurs depends on the kinetics of the reactions taking place and so the **electrical double layer** is important.

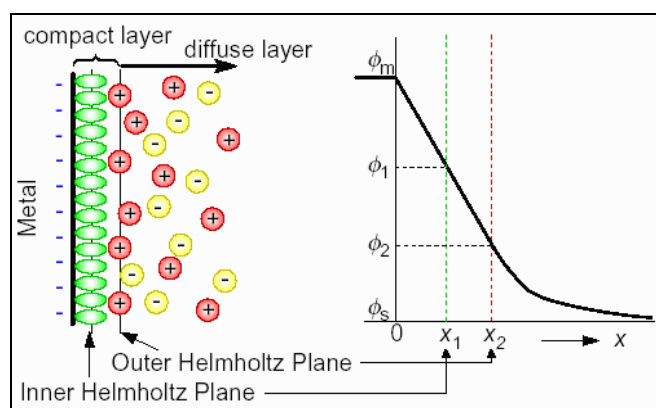
An electrical double layer is the name given to any region between two different phases when charge is separated across the interface between them.

In aqueous corrosion, this is the region between a corroding metal and the bulk of the aqueous environment (“free solution”). In the double layer, the water molecules of the solution align themselves with the electric field generated by applying a potential to the metal. In the Helmholtz model, there is a layer of aligned molecules (or ions), which is one particle thick and then immediately next to that, free solution. In later models (proposed by Louis Georges Gouy, David Leonard Chapman and Otto Stern) the layer is not well defined, and the orientation becomes gradually less noticeable further from the metal surface. However, for the purposes of determining the rate of corrosion, the Helmholtz model will suffice. To corrode, an ion in the metallic lattice must pass through the double layer and enter free solution. The double layer presents a potential barrier to the passage of ions and so has an acute effect on corrosion kinetics.

## Helmholtz Double Layer

This theory is a simplest approximation that the surface charge is neutralized by opposite sign counter ions placed at an increment of  $d$  away from the surface.

The surface charge potential is linearly dissipated from the surface to the counterions satisfying the charge. The distance,  $d$ , will be that to the center of the counterions, i.e. their radius. The Helmholtz theoretical treatment does not adequately explain all the features, since it hypothesizes rigid layers of opposite charges. This does not occur in nature.



**Scheme 3.** Helmholtz Double Layer

If an electrode is at its equilibrium potential, both forwards and backwards reactions occur at the same rate, so no net reaction will occur. Net reactions only occur when the potential is moved away from equilibrium.

### Kinetics of Corrosion - the Tafel Equation

Armed with the new Arrhenius expression and the generalized reaction:



where M is a metal that forms M<sup>z+</sup> ions in solution, we can now derive an equation describing corrosion kinetics.

Consider the rate of the anodic (oxidation, corrosion) reaction,  $k_a$

$$k_a = k_a' \exp\left(\frac{\Delta G^0}{RT}\right) \quad (3)$$

Since the reaction involves the release of electrons, its progress can be expressed as a current density,  $i$  (current per unit area).

The **exchange** current density,  $i_0$  is defined as the current flowing in both directions per unit area when an electrode reaction is at equilibrium (and, hence, at its equilibrium potential).

If  $i_0$  is small, then little current flows and the reactions at dynamic equilibrium are generally slow. Likewise, a high  $i_0$  gives a fast reaction. The metal itself affects the value of  $i_0$ , even if the reaction does not involve the metal directly.

$$i_0 = zFk_a = zFk_a' \exp\left(\frac{-\Delta G^0}{RT}\right) \quad (4)$$

If over potential is applied, the activation energy is changed.

$$i_a = i_0 \exp\left(\frac{\alpha zF\eta}{RT}\right) \quad (5)$$

This is one form of the **Tafel equation**. The Tafel equation can also be written in several equivalent ways. The quantity

$$\frac{2.303RT}{\alpha zF}$$

is given the symbol  $b_a$  and is known as the anodic Tafel slope. It has units of volts per decade of current.

Similarly, if the cathodic reaction were to be considered, the quantity would be

$$\frac{2.303RT}{(1-\alpha)zF}$$

since  $(1-\alpha)$  is applicable instead of  $\alpha$  and  $E - E_e$  is negative. This quantity is the cathodic Tafel slope,  $b_c$ .

The usual form of Tafel's equation is

$$\eta = a + b_a \lg i_a \quad (6)$$

where

$$a = -\frac{2.303RT}{\alpha zF} \lg i_0 \quad (7)$$

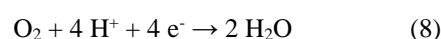
Through consideration of the reaction as both a chemical and electrical process and manipulation of algebra, it has been found that the applied potential is proportional to the log of the resulting corrosion current. This is certainly different to Ohmic behaviour where applied potential is directly proportional to the resulting current.

Corrosion occurs when two electrodes with different equilibrium potentials are in both electronic and electrolytic contact. Tafel plots can be used to predict corrosion rates.

### Diffusion Limited Corrosion

So far all reactions have been assumed to proceed (if they are thermodynamically possible) at the rate predicted by the Tafel analysis. In reality, reactions are often limited by other factors and don't achieve this maximum rate. One such factor is the availability of oxygen in solution.

In aqueous solutions that contain dissolved oxygen, an important cathodic reaction is the oxygen reduction reaction:



The reaction takes place at the surface of the metal and so oxygen must be present at that site. If the reaction occurs quickly enough, the concentration of oxygen at the surface cannot be maintained at the same level as that in the bulk of the solution. In this case the rate of oxygen diffusion may become a limiting factor. With less oxygen available, the cathodic reaction slows down and so must the anodic reaction to conserve electrons (electrons can only be used up at the same rate as they are released as charge must always

be conserved). Fick's first law can be used to find the maximum rate of oxygen diffusion. Since each oxygen molecule consumes 4 electrons, according to the reaction above, this maximum rate of diffusion corresponds to a maximum current density that the oxygen reduction reaction can sustain and, hence, a maximum corrosion rate for the anode (since electrons must be used at the cathode at the same rate as they are released at the anode).

Since the corrosion current is limited, the cathodic arm of the Tafel plot is flattened:

Oxygen reduction is not the only process that deviates from the Tafel analysis. The hydrogen evolution reaction can be limited by the rate at which molecules desorb from the cathode surface. This is usually the rate-determining factor for hydrogen evolution on iron, copper, platinum and other metals. Relatively few metals behave as predicted by the Tafel analysis, examples being cadmium, mercury and lead.

### Passivation

Another effect that limits the rate of corrosion is **passivation**. If the potential of an electrode is raised above some **passivation potential**, a passive product may become favorable forming a layer on the surface of the anode. In this case, the rate of corrosion can be much reduced. This is characterized by the value of  $\log(i)$  peaking at a **critical current density**, before falling to some lower value.

In other words, the anodic arm of the Tafel plot reaches a peak and falls away to a roughly horizontal region:

### Predicting Corrosion Rates

Armed with the Tafel equation and Tafel plots, it is now possible to predict whether a particular setup will result in corrosion and if so how fast the corrosion will be.

In order for corrosion to occur, there must be a suitable anodic reaction and an appropriate cathodic reaction. This is manifested as an intersection of a cathodic branch and an anodic branch on a Tafel plot. The point of intersection gives the corrosion potential and the corrosion current (or, more accurately the log of the corrosion current density).

The rate of corrosion is governed by all the factors discussed previously. When all the effects are taken into account, Tafel plots get quite complicated and some interesting effects occur:

Faraday's law allows the current density to be expressed as the mass of material lost per unit time.

The calculation involves a few simple steps. For a corrosion reaction:

The current is converted into a rate of electron consumption using the electronic charge constant. The number of electrons is divided by the stoichiometric number of electrons in the corrosion reaction, giving the number of metal atoms lost per unit time.

This answer is then divided by Avogadro's number to give the number of moles of metal atoms lost per unit time.

The number of moles is then converted to mass lost per unit time, using the molar mass.

The mass is then converted to a volume using the density.

The volume is then converted to a thickness lost per unit time by dividing by the area that the current passes over. If a current density was given, this step has already been done.

Overall, the thickness of metal lost per unit time is given by the formula:

$$t = \frac{im_M}{\rho ezN_A} \quad (9)$$

where

- t thickness (m),
- i current density (A m<sup>-2</sup>),
- m<sub>M</sub> molar mass (kg mol<sup>-1</sup>),
- e electronic charge (C),
- z stoichiometric number of electrons in oxidation reaction,
- N<sub>A</sub> Avogadro's number.

It is also possible to have a situation where corrosion does not occur for thermodynamic reasons, for example if there was a driving force for the reverse of the corrosion reaction to occur due to an applied potential. This would result in deposition (electroplating) if there were metal ions in solution available to be reduced. If deposition is being carried out commercially, for example to electroplate silver onto stainless steel cutlery, the rate must be maximized to make production as cost effective as possible. However, care must be taken to avoid the hydrogen evolution reaction starting at the cathode in addition to the metal ion deposition.

Applying an over potential to an electrode drives the reaction in one direction and away from equilibrium. Tafel's law governs the new rate and as long as the reaction kinetics are activation controlled, the over potential is proportional to the log of the corrosion current.

Other factors may limit the maximum rate of corrosion, with oxygen depletion limiting the speed of the cathodic reaction to the rate at which oxygen can be supplied from the bulk. The anodic reaction may be limited by passivation, if a sufficiently large over potential is applied to form a passive layer. Passive layers separate the metal from the electrolyte and slow the corrosion reaction.

Faraday's law can give meaningful results from the predicted corrosion current, i.e. giving the mass loss per unit time.

Corrosion can be slowed by either adding an inhibitor to remove hydrogen ions and move to a passivating region of the Pourbaix diagram, by adding an inhibitor to form a passive layer on the anode, or by adding an inert barrier to the surface of the anode

### Linear polarization resistance (LPR)

LPR is most effective in aqueous solutions, and has proven to be a rapid response technique. Electrical conductivity (the reciprocal of resistance) of a fluid can be related to its corrosiveness. The polarization resistance is the ratio of the applied potential and the resulting current level. The measured resistance is inversely related to the corrosion rate. The electrical resistance of any conductor is given by:

$$R = \frac{V}{I} \quad (10)$$

where

- R = Effective instantaneous resistance
- V = Applied voltage
- I = Instantaneous current between electrodes.

If the electrodes are corroding at a high rate with the metal ions passing easily into solution, a small potential applied between the electrodes will produce a high current, and therefore a low polarization Resistance. This corresponds to a high corrosion rate.

Polarization study has been used to investigate the passive film formed on metal surface during corrosion process in presence of inhibitors.<sup>44-48</sup> The corrosion parameters of mild steel immersed in an aqueous solution in the absence and presence of inhibitor system are given in Table 2. The corrosion parameters include corrosion potential ( $E_{\text{corr}}$ ), Tafel slopes ( $b_c$ = cathodic;  $b_a$ =anodic), Linear polarization resistance (LPR) and corrosion current ( $I_{\text{corr}}$ ).

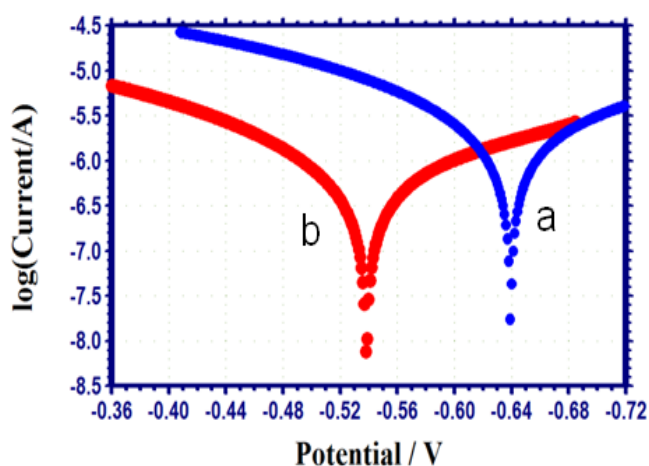


**Figure 1.** Polarization curve of mild steel immersed in various test solution a) Cl<sup>-</sup> 60 ppm b) Cl<sup>-</sup> 60 ppm + glycine 250 ppm + Zn<sup>2+</sup> 50 ppm

The polarization curves are shown in Figures 1 to 3. When mild steel is immersed in the environment (aqueous solution containing 60 ppm Cl<sup>-</sup>), the corrosion potential is -639 mV vs SCE. The LPR value is 17180 ohmcm<sup>2</sup> and the corrosion current is 2.241x10<sup>-6</sup>A cm<sup>-2</sup>. When inhibitor system (glycine 250 ppm + Zn<sup>2+</sup> 50 ppm) is introduced in the environment; the corrosion potential is shifted to the anodic side that is noble side. This indicates that a passive film is formed on

the metal surface in presence of inhibitor. The shifting of corrosion potential towards anodic side in presence of inhibitors has been reported by several researchers.<sup>49-56</sup>

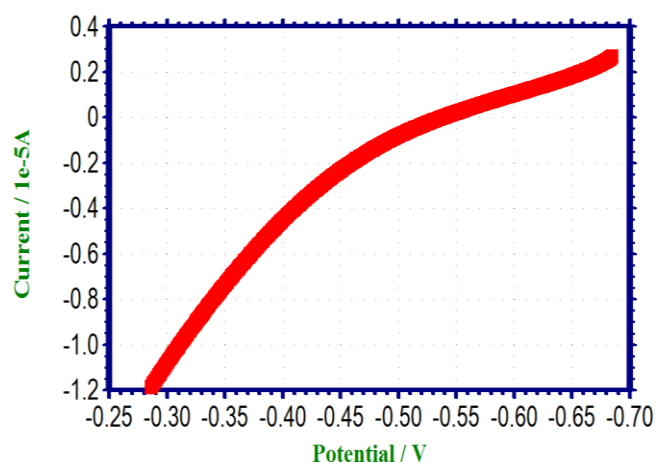


**Figure 2.** Polarization curve of mild steel immersed in an aqueous solution containing 60 ppm Cl<sup>-</sup>

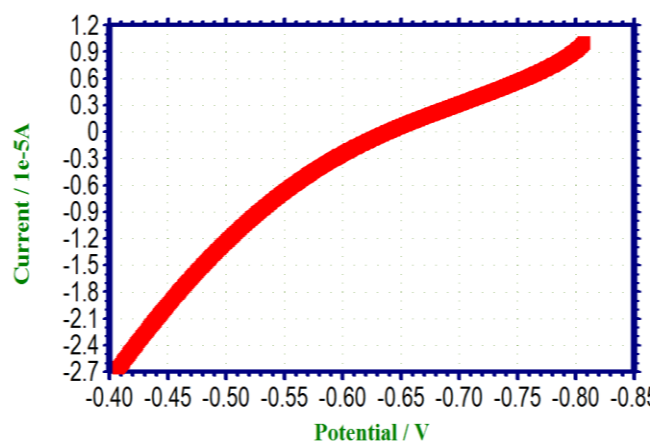


**Figure 3.** Polarization curve of mild steel immersed in an aqueous solution containing 60 ppm Cl<sup>-</sup> + glycine 250 ppm + Zn<sup>2+</sup> 50ppm

**Table 2.** Corrosion parameters of mild steel immersed in an aqueous solution containing 60 ppm of Cl<sup>-</sup> obtained from polarization study

System	$E_{\text{corr}}$ , mV*	$b_a$ , mV**	$b_c$ , mV**	LPR, ohm cm <sup>2</sup>	$I_{\text{corr}}$ , A cm <sup>-2</sup>
Cl <sup>-</sup> 60 ppm	-639	202	158	17180	2.241x10 <sup>-6</sup>
Cl <sup>-</sup> 60 ppm+A	-538	202	158	53494	6.920x10 <sup>-7</sup>

A = glycine 250 ppm + Zn<sup>2+</sup> 50 ppm, \*mV vs SCE; \*\*mV in one decade

It is also observed that, when inhibitor system is introduced in to the environment, LPR value increases and corrosion current decreases. When a passive film formed on mild steel surface, in presence of inhibitor system, the electron transfer from the metal surface towards the bulk of the solution is difficult and prevented. So rate of corrosion decreases and hence corrosion current decreases in presence of inhibitor system.

It is observed from Table 2 that the Tafel slope values are not changed much in the presence of inhibitor system, when compared to the blank system. This suggests that the glycine-Zn<sup>2+</sup> system, controls the anodic reaction



and the cathodic reaction



to an equal system. The anodic reaction is controlled by formation of Fe<sup>2+</sup>-glycine complex on the anodic site of the metal surface. The cathodic reaction is controlled by deposition of Zn(OH)<sub>2</sub> on the cathodic sites of the metal surface. Thus anodic reaction and cathodic reaction are controlled effectively. This accounts for the synergistic effect of Zn<sup>2+</sup>- glycine system.<sup>57, 58</sup>

The variation of current with potential, when mild steel is immersed in blank system and inhibitor system is shown in Figures 3 and 4. It is observed that the rate of change of current with potential is less in presence of inhibitor system than in its absence.

## Conclusion

The inhibition efficiency of glycine-Zn<sup>2+</sup> system has been evaluated by weight loss method and polarization study. Glycine alone has some corrosion inhibition efficiency (IE). In presence of Zn<sup>2+</sup>, IE increases. Synergistic effect exists between Zn<sup>2+</sup> and glycine. The formulation consisting of 250 ppm of glycine and 50 ppm of Zn<sup>2+</sup> has 86% IE. Polarization study reveals that this system function as mixed inhibitor system, controlling the anodic reaction and cathodic reaction to an equal extent.

## Acknowledgement

The authors are thankful to their Managements and St. Joseph's Research and Community Development Trust, Dindigul, India for their help and encouragement.

## References

- <sup>1</sup>Li, P., Wu, G., Xu, R., Wang, W., Wu, S., Yeung, K. W. K., Chu, P.K., *Mater. Lett.*, **2012**, 89, 51.
- <sup>2</sup>Goudarzi, N., Peikari, M., Reza Zahiri, M., Reza Mousavi, H., *Arch Metallurg Mater.*, **2012**, 57(3), 845.
- <sup>3</sup>Baghaei Ravari, F., Dadgarinezhad, A., Gazi., *Univ. J. Sci.*, **2012**, 25(4), 835.
- <sup>4</sup>Hosseini, S. M. A., Salari, M., Jamalizadeh, E., Jafari, A. H., *Corros.*, **2012**, 68(7), 600.
- <sup>5</sup>Zhou, M., Zhao, J., Hu, X., *J. Surfactants and Deter.*, **2012**, 15(3), 309.
- <sup>6</sup>Zou, C., Tang, Q., Tan, N., Xiao, P., Hu, X., *Starch/Staerke.*, **2012**, 64(4), 281.
- <sup>7</sup>Li, J.-l., Bai, F.-l., Lu, Y.-b., Lai, D.-m., *Corros. Prot.*, **2012**, 33(9), 787.
- <sup>8</sup>Elmalah, N. M., Elhaliem, S. A., Ahmed, A. M., Ghozy, S. M. *Int. J. Electrochem. Sci.*, **2012**, 7(8), 7720.
- <sup>9</sup>Fragoza-Mar, L., Olivares-Xometl, O., Domínguez-Aguilar, M. A., Flores, E. A., Arellanes-Lozada, P., Jiménez-Cruz, F., *Corros. Sci.*, **2012**, 61, 171.
- <sup>10</sup>Caliskan, N., Akbas, E., *Mat. Chem Phys.*, **2011**, 126(3), 983.
- <sup>11</sup>Zarrouk, A., Hammouti, B., Dafali, A., Zarrok, H., *Der Pharma Chemica.*, **2011**, 3(4), 266.
- <sup>12</sup>Abdurrahman, J., Wahyuningrum, D., Achmad, S., Bundjali, B., *Sains Malays.*, **2011**, 40(9), 973.
- <sup>13</sup>Eddy, N. O., Ebenso, E. E., *J. Mole. Model.*, **2010**, 16(7), 1291.
- <sup>14</sup>Pate, N. S., Jauhari, S., Mehta, G. N., *Acta Chim. Slov.*, **2010**, 57(2), 297.
- <sup>15</sup>Caliskan, N., Akbas, E., *Mater. Chem Phys.*, **2011**, 126(3), 983.
- <sup>16</sup>Elayyachy, M., El Idrissi, A., Hammouti, B., *Corros. Sci.*, **2006**, 48(9), 2470.
- <sup>17</sup>Harish Kumar, Vishal Saini, Dheeraj Kumar, and Chaudhary, R.S., *Indian. J. chem Technol.*, **2009**, 16, 401.
- <sup>18</sup>Zhang, J., Gong, X. L., Yu, H. H., Du, M., *Corros. Sci.*, **2011**, 53(10), 3324
- <sup>19</sup>Appa Rao, B.V., Srinivasa Rao, S., *Mater Corros.*, **2010**, 61(4), 285.
- <sup>20</sup>Dufek, E. J., Buttry, D. A., *J. Electrochem. Soc.*, **2009**, 156(9), C322.
- <sup>21</sup>Deng, Q., Ding, N.-N., Wei, X.-L., Cai, L., He, X.-P., Long, Y.-T., Chen, G.-R., Chen, K., *Corros. Sci.*, **2012**, 64, 64.
- <sup>22</sup>Ghazoui, A., Saddik, R., Benchat, N., Hammouti, B., Guenbour, M., Zarrouk, A., Ramdani, M. *Der Pharma Chemica.*, **2012**, 4(1), 352.
- <sup>23</sup>Liu, P., Gao, L., Zhang, D., *J. Chinese Soc. Corros Prot.*, **2012**, 32(2), 163.
- <sup>24</sup>Hamed, E., Abd El-Rehim, S.S., El-Shahat, M. F., Shaltot, A.M., *Mater. Sci Eng B Solid State Mater Adv. Technol.*, **2012**, 177(5), 441.
- <sup>25</sup>Gomma, G. K., Wahdan, M.H., *Mater Chem Phys.*, **1994**, 39(2), 142.
- <sup>26</sup>Wilson Sahayaraj, J., Susai Rajendran, Muthu mekala, T.S., John amalraj, A., *Zastit. Mater.*, **2010**, 51(4), 232.
- <sup>27</sup>Gowri, S., sathiyabama, J., Rajendran, S., Robert Kennedy, Z., Agila Devi, S., *Chem. Sci Trans.*, **2013**, 2(1), 275.
- <sup>28</sup>Quan, Z.-L., Zhang, D.-M., Hou, W.-G., *Corros. Sci Prot. Tech.*, **2011**, 23(2), 151.
- <sup>29</sup>Fouda, A, S., Ahamed sbdel Nazeer, E. A., Ashour, *Zastit. Mater.*, **2011**, 52(1), 23.
- <sup>30</sup>Sahaya Raja, A., Rajendran, S., Satyabama, P., *J. Chem., Hindawi publications.*, **2012**, 2013, 1.
- <sup>31</sup>Abdel-Fatah, H. T. M., *Anti-Corros Methods.Mater.*, **2012**, 59(1), 23.
- <sup>32</sup>Gowri, S., Sathiyabama, J., Rajendran, S., Angelin Thangakani, J., *J. Chem. Bio. Phy. Sci.*, **2012**, 2(4), 2223.
- <sup>33</sup>Wranglen, G., *Introduction to Corrosion and Protection of Metals.:Chapman & Hall, London.*, **1985**, 236.
- <sup>34</sup>Rajendran, S., John Amalraj, A., Joice, M. J., Anthony, N., Trivedi, D. C., Sundara vadivelu, N., *Corros. Rev.*, **2004**, 22, 23.
- <sup>35</sup>Yesu Thangam, Y., Kalanithi, M., Mary Anbarasi, C., Rajendran, S., *The Arab. J. sci. eng.*, **2009**, 34(2c), 49.
- <sup>36</sup>Rajendran, S., Peter, B.R.E., Regis, P. P., John Amal Raj, A., Sundara vadivelu, N., *Trans. SAEST.*, **2003**, 38, 115.
- <sup>37</sup>Agnesia Kanimozhi, S., Rajendran, S., *The Arab. J. sci. eng.*, **2009**, 34(2c), 37.
- <sup>38</sup>Rajendran, S., Vaibhavi, S., Anthony, N., *Corros.*, **2003**, 59, 529.



- <sup>39</sup>Sahayaraja, A., Rajendran, S., Sathiyabama, J., Muthu Megala, T.S., Krishnaveni, A., Palaniswamy, N., Prabhakar, P., *Zastit. Mater.*, **2011**, 52(2), 101.
- <sup>40</sup>Anu Radha, K., Vimala, R., Narayanasamy, B., Arockia selvi, J., Rajendran, S., *Chem. Eng. Comm.*, **2008**, 195, 352.
- <sup>41</sup>Arockia selvi, J., Rajendran, S., John Amalraj, A., *Indian. J. Chem. Technol.*, **2007**, 14(4), 382.
- <sup>42</sup>Rajendran, S., Apparao, B.V., Palanisamy, N., *Anti-Corros. Methods. Mater.*, **2000**, 47, 83.
- <sup>43</sup>Leema Rose, A., Peter pascal Regis, A., Susai Rajendran, Krishnaveni, A., Felicia Rajammal Selvarani., *Arab. J. Sci. Eng.*, **2012**, 37(5), 1313.
- <sup>44</sup>Kavipriya, K., Sathiyabama, J., Rajendran, S., Krishnaveni, A., *Int. J. Adv. Eng. Sci. Technol.*, (IJAEST), **2012**, 2(2), 106.
- <sup>45</sup>Sahayaraja, A., Rajendran, S. *J. Electrochem. Sci. Eng.*, **2012**, 2, 91.
- <sup>46</sup>Sribharathy, V., Rajendran, S., *Int. J. Adv. Eng. Sci. Technol.*, (IJAEST), **2011**, 1(1), 77.
- <sup>47</sup>Anbarasi, M.C., Rajendran, S., Vijaya, N., Manivannan, M., Shanthi, T., *The Open Corros. J.*, **2011**, 4, 40.
- <sup>48</sup>Johnsirani, V., Rajendran, S., Sathiyabama, J., Muthumegala, T. S., Krishnaveni, A., Hajarabeevi, N., *Bulg. Chem. Commun.* **2012**, 44 (1), 41.
- <sup>49</sup>Manimaran, N., Rajendran, S., Manivannan, M., John mary, S., *Res. J. Chem. Sci.*, **2012**, 2(3), 52.
- <sup>50</sup>Arockia selvi, J., Susai Rajendran, John Amalraj, A., Narayanasamy, B., *Port. Elecrotchim. Acta.*, **2009**, 27(1), 1.
- <sup>51</sup>Shyamala Devi, B., and Rajendran, S., *Eur. Chem. Bull.*, **2012**, 1(5), 150.
- <sup>52</sup>Nagalakshmi, R., Rajendran, S., Sathiyabama, J., Pandiarajan, M., and Lydia Christy, J., *Eur. Chem. Bull.*, **2013**, 2(4), 150.
- <sup>53</sup>SahayaRaja, A., Rajendran, S., Nagalakshmi, R., Angelin Thangakani, J., and Pandiarajan, M., *Eur. Chem. Bull.*, **2012**, 1(3), 130.
- <sup>54</sup>AgilaDevi, S., Rajendran, S., Jeyasundari, J., and Pandiarajan, M., *Eur. Chem. Bull.*, **2013**, 2(2), 84.
- <sup>55</sup>Rajendran, S., AnuRadha, K., Kavipriya, K., Krishnaveni, A., and Angelin Thangakani, J., *Eur. Chem. Bull.*, **2012**, 1(12), 503.
- <sup>56</sup>Pandiarajan, M., Prabhakar, P., and Rajendran, S., *Eur. Chem. Bull.*, **2012**, 1(7), 238.
- <sup>57</sup>Rajendran, S., Shanmugapriya, S., Rajalakshmi, T., and Amalraj, A., *Corrosion*, **2005**, 61, 685.
- <sup>58</sup>Vijayagopal Sribharathy and Susai Rajendran *J. Electrochem. Sci. Eng.*, **2012**, 2, 121.

Received: 20.12.2012.

Accepted: 26.01.2013.



# AN OVERVIEW ON SYNTHETIC METHODS OF BENZYL ACETATE

Lu Hongjie<sup>[a]</sup> and Linda Zhang<sup>[b]</sup>

**Keywords:** overview; synthetic methods; benzyl acetate; catalysts

Synthetic methods of benzyl acetate using different catalysts such as strong acid cation exchange resins, inorganic salts (the weight ratio of FeCl<sub>3</sub> to carbon (46 %) and Fe<sub>2</sub>(SO<sub>4</sub>)<sub>3</sub>), inorganic acids (H<sub>2</sub>SO<sub>4</sub>) heteropoly compounds ((NH<sub>4</sub>)<sub>6</sub>[MnMo<sub>9</sub>O<sub>32</sub>]·8H<sub>2</sub>O), heteropolyacids (phosphotungstic acid), solid superacids (S<sub>2</sub>O<sub>8</sub><sup>2-</sup> - Fe<sub>2</sub>O<sub>3</sub> - ZnO, S<sub>2</sub>O<sub>8</sub><sup>2-</sup> - Fe<sub>2</sub>O<sub>3</sub> - CoO, S<sub>2</sub>O<sub>8</sub><sup>2-</sup> - ZrO<sub>2</sub> - Al<sub>2</sub>O<sub>3</sub>, SO<sub>4</sub><sup>2-</sup> - Al<sub>2</sub>O<sub>3</sub>, SO<sub>4</sub><sup>2-</sup> - ZrO<sub>2</sub> - Nd<sub>2</sub>O<sub>3</sub> and SO<sub>4</sub><sup>2-</sup> - MoO<sub>3</sub> - TiO<sub>2</sub>), organic salts (tris(trimethylsilylmethyl)tin chloride) and ionic liquids (N-methylpyrrolidone hydrosulfate and 1-methyl-3-(3-sulfopropyl)imidazolium tungstophosphate) have been reviewed. The above mentioned catalysts improved the yield of benzyl acetate. These methods have the advantage of simple process and low investment costs.

\* Corresponding Author

Fax: 86-24-56860869

E-Mail: lindazhang362@hotmail.com

[a] Liaoning Shihua University, Fushun, Liaoning, P.R. China.

[b] SAIT Polytechnic, Calgary AB, Canada.

## Introduction

Benzyl acetate is a naturally occurring colourless oily liquid found in many flowers such as jasmine, ylang-ylang and tobira. Its molecular formula, melting point, boiling point, relative density (16 °C), refractive index  $n_D^{20}$  and flash point are C<sub>9</sub>H<sub>10</sub>O<sub>2</sub>, 50 °C, 213 °C, 1.057, 1.5232 and 102 °C, respectively. Benzyl acetate is hard to dissolve in water, but dissolves in organic solvents. <sup>1</sup> Due to floral fragrance and low price, it is widely used in different areas such as soaps, essences and other industrial essences, etc. <sup>2</sup> Benzyl alcohol, with concentrated sulphuric acid as a catalyst, reacts with acetic acid to synthesise benzyl acetate. Concentrated sulphuric acid has a lot of disadvantages such as long reaction time, low yield and purity of benzyl acetate. Large amount of waste water is discharged to cause the problem of environmental pollution and equipments are seriously corroded at the same time. <sup>3</sup>

In the present paper, different catalysts such as strong acid cation exchange resins, inorganic salts (the weight ratio of FeCl<sub>3</sub> to carbon (46 %) and Fe<sub>2</sub>(SO<sub>4</sub>)<sub>3</sub>), inorganic acids (H<sub>2</sub>SO<sub>4</sub>) heteropoly compounds ((NH<sub>4</sub>)<sub>6</sub>[MnMo<sub>9</sub>O<sub>32</sub>]·8H<sub>2</sub>O), heteropolyacids (phosphotungstic acid), solid superacids (S<sub>2</sub>O<sub>8</sub><sup>2-</sup> - Fe<sub>2</sub>O<sub>3</sub> - ZnO, S<sub>2</sub>O<sub>8</sub><sup>2-</sup> - Fe<sub>2</sub>O<sub>3</sub> - CoO, S<sub>2</sub>O<sub>8</sub><sup>2-</sup> - ZrO<sub>2</sub> - Al<sub>2</sub>O<sub>3</sub>, SO<sub>4</sub><sup>2-</sup> - Al<sub>2</sub>O<sub>3</sub>, SO<sub>4</sub><sup>2-</sup> - ZrO<sub>2</sub> - Nd<sub>2</sub>O<sub>3</sub> and SO<sub>4</sub><sup>2-</sup> - MoO<sub>3</sub> - TiO<sub>2</sub>), organic salts (tris(trimethylsilylmethyl)tin chloride) and ionic liquids (N-methylpyrrolidone hydrosulfate) and 1-methyl-3-(3-sulfopropyl)imidazolium tungstophosphate) are discussed.

## DISCUSSION

### Strong acid cation exchange resin as a catalyst

Lan Ping<sup>4</sup> used strong acid cation exchange resin as a catalyst to synthesise benzyl acetate from acetic acid and benzyl alcohol. The optimal conditions were the molar ratio of acetic acid and

benzyl alcohol (4.0 : 5.0), the reaction time (10 hours), the reaction temperature (100 °C) and the weight ratio of strong acid cation exchange resin to acetic acid (25 %) respectively. The maximum yield of benzyl acetate was 84.23 %. The performance of the catalyst was very good when it was reused. For example, the yield of benzyl acetate was 83.88 % even after it had been used 10 times.

### Inorganic salts as catalysts

Yu Junfeng<sup>5</sup> described a similar synthesis using the weight ratio of FeCl<sub>3</sub> to carbon (46 %) as a catalyst. The optimal conditions were the reaction time (2.0 hours), the molar ratio of acetic acid to benzyl alcohol (1.0 : 1.8) and the weight ratio of FeCl<sub>3</sub>/carbon to acetic acid 33.33 %. The maximum yield was 89.10 %. FeCl<sub>3</sub>/carbon had good catalytic performance.

Li Xiaoli<sup>2</sup> used Fe<sub>2</sub>(SO<sub>4</sub>)<sub>3</sub> as a catalyst. The optimal reaction time (2 hr), the molar ratio of acetic acid to benzyl alcohol (1.0 : 2.5) and the weight ratio of Fe<sub>2</sub>(SO<sub>4</sub>)<sub>3</sub> to acetic acid, 33.33 % were described. The maximum yield of benzyl acetate was 67.1 %.

### H<sub>2</sub>SO<sub>4</sub> as a catalyst

Chen Xi<sup>6</sup> used H<sub>2</sub>SO<sub>4</sub> as the catalyst and explained the reasons for its use. The reaction conditions were: ultrasonic frequency (10 k Hz), ultrasonic intensity (1.0 W cm<sup>-2</sup>) and the air velocity (0.3 L min<sup>-1</sup>). The maximum yield of benzyl acetate was 65.8 %.

### (NH<sub>4</sub>)<sub>6</sub>[MnMo<sub>9</sub>O<sub>32</sub>]·8H<sub>2</sub>O as a catalyst

Liu Shuheng<sup>7</sup> described the synthesis of (NH<sub>4</sub>)<sub>6</sub>[MnMo<sub>9</sub>O<sub>32</sub>]·8H<sub>2</sub>O and benzyl acetate. The optimal conditions were: reaction time (1.5 hr), the molar ratio of acetic acid to benzyl alcohol (2.0:1.0) and the weight ratio of (NH<sub>4</sub>)<sub>6</sub>[MnMo<sub>9</sub>O<sub>32</sub>]·8H<sub>2</sub>O to acetic acid (15 %). The maximum yield of benzyl acetate was 80.4 %.

The maximum yield of benzyl acetate was 69.3 % after the catalyst had been used 5 times

### Phosphotungstic acid as a catalyst

Huang Haiyan<sup>8</sup> described the synthesis of benzyl acetate by using phosphotungstic acid as the catalyst. The optimal reaction conditions were: reaction time (2 hr), the molar ratio of acetic acid to benzyl alcohol (2.5:1.0) and the weight ratio of phosphotungstic acid to total reactant (2.54 %). The maximum yield of benzyl acetate was 90.0 %.

### Solid superacids as catalysts

Table 3 showed that different solid superacids with different load had an effect on the yield of benzyl acetate. It is to be noted that Fe<sub>2</sub>O<sub>3</sub> - CoO was the best loads because acid was evenly distributed on its surface, so the yield of benzyl acetate was very high.

### Tri(trimethylsilyl - methylene) tin chloride as a catalyst

Chen Fushan<sup>15</sup> described the use of tris(trimethylsilyl methyl)tin chloride as the catalyst. The optimal reaction time (3.5 hr), the molar ratio of acetic acid to benzyl alcohol (3.5 : 1.0) and the

weight ratio of tris(trimethylsilylmethyl)tin chloride to acetic acid (0.015 : 1.0) on yields of benzyl acetate were mentioned. The maximum yield of benzyl acetate was 91.5 %.

### Ionic liquids as catalysts to generate benzyl acetate

Zhou Beilei<sup>16</sup> described the use of N-methylpyrrolidone hydrosulfate as the catalyst. The reaction conditions such as the reaction time (1 hr), the reaction temperature (110 °C), the molar ratio of acetic acid to benzyl alcohol (1.4:1.0), the weight ratio of N-methylpyrrolidone hydrosulfate to benzyl alcohol (1 %). The maximum yield of benzyl acetate was 98.6 %. The yield of benzyl acetate still reached 97.6 % on the use of the catalyst after it had been used 6 times.

Yang Min<sup>17</sup> used 1-methyl-3-(3-sulfopropyl)imidazolium tungstophosphate as a catalyst in place of concentrated sulfuric acid. The optimal reaction time (5 hr), the reaction temperature (110 °C), the molar ratio of acetic acid to benzyl alcohol (2.0 : 1.0), the molar ratio of 1-methyl-3-(3-sulfopropyl)imidazolium tungstophosphate to benzyl alcohol (0.2 %) were described. The maximum yield of benzyl acetate was 95.52 %, and it was 84.15 % after the catalyst had been used 5 times.

**Table 1.** effect of different t solid superacids on yields of benzyl acetate

Catalyst	Acetic acid to benzyl alcohol ratio	Weight ratio of the catalyst to total reactant (%)	Reaction time, h	Yield of benzyl acetate, %	Reference
S <sub>2</sub> O <sub>8</sub> <sup>2-</sup> - Fe <sub>2</sub> O <sub>3</sub> - CoO	1.0:1.3	1.49	2.5	98.2	9
S <sub>2</sub> O <sub>8</sub> <sup>2-</sup> - ZrO <sub>2</sub> - Al <sub>2</sub> O <sub>3</sub>	1.0:1.3	1.98	2.5	98.0	10
S <sub>2</sub> O <sub>8</sub> <sup>2-</sup> - Fe <sub>2</sub> O <sub>3</sub> - ZnO	1.7:1.0	0.83	2.5	85.2	11
SO <sub>4</sub> <sup>2-</sup> - ZrO <sub>2</sub> - Nd <sub>2</sub> O <sub>3</sub>	2.0:1.0	2.83	5.0	92.0	12
SO <sub>4</sub> <sup>2-</sup> - MoO <sub>3</sub> - TiO <sub>2</sub>	1.3:1.0	0.41	2.0	87.2	13
SO <sub>4</sub> <sup>2-</sup> - Al <sub>2</sub> O <sub>3</sub>	2.0:1.0	3.5	6.0	76.0	14

## CONCLUSION

Based on the above discussion and review, N-methyl pyrrolidone hydrosulfate is one of the best catalysts for the highest yield of benzyl acetate (98.6 %). However, due to high cost, N-methyl pyrrolidone hydrosulfate is not considered as the good choice for catalyst. S<sub>2</sub>O<sub>8</sub><sup>2-</sup> - Fe<sub>2</sub>O<sub>3</sub> - CoO is equally a good catalyst considering the yield of benzyl acetate (98.2 %) which is almost similar to that of N-methyl pyrrolidone hydrosulfate. H<sub>2</sub>SO<sub>4</sub> is the worst of the catalysts since the maximum yield of benzyl acetate was only 65.8 %.

## REFERENCES

- Wang, G. X., *Appl. Sci. Technol.*, **2000**, 11, 22.
- Li, X. L. and Zhang, K., *J. Changchun Normal Univer.*, **2008**, 27(5), 22.
- Sun, D. G. and Wei, M., *Shandong Chem. Ind.*, **2006**, 35(6), 24-25.
- Lan, P., Lan, L. H., Yan, R. Y., Wu, R. C., Li, M. and Liao, A. P., *Sci. Technol. Food Ind.*, **2005**, 26(5), 128-132.
- Yu, J. F. and Zhu, L., *Sci. Technol. Food Ind.*, **2005**, 26(1), 162-163.
- Chen, X., Wang, J., Lu, X. P. and Han, P. F., *J. Nanjing Univer. Technol.*, **2011**, 33(3), 49-52.
- Liu, S. H., Wang, L. X., Yuan, H. and Yang, F. Z., *J. Cangzhou Normal Univer.*, **2012**, 28(1), 9-11,27.
- Huang, H. Y., Xie, F. H. and Tang, P. W., *Appl. Chem. Ind.*, **2007**, 36(3), 279-282.
- Zhang, Y. J., Li, H. P., Cheng, H. J. and Zhang, C. X., *J. Henan Normal Univer.*, **2006**, 34(2), 89-93.
- Jin, H. F. and Li, W. G., *Chemistry World*, **2008**, 3, 133-138.
- Zhang, Y. J., Wang, J. L. and Yang, H., *J. Zhengzhou Univer. Light Ind.* **2005**, 20(3), 26-28.
- Yang, Y. W., Li, L. and Chen, H. Z., *Chem. Agents*, **2006**, 28(11), 665-667.
- Sun, T., *Zhengjiang Chem. Ind.*, **2005**, 36(7), 15-16.
- Wang, M. Y. and Qiu, L. G., *Chemistry and Adhesion*, **2007**, 29(1), 27-29.
- Chen, F. S., Xu, J. P., Gao, E. L., Zhang, L. M. and Lin, S., *Speciality Petrochemicals*, **2011**, 28(6), 37-39.

<sup>16</sup>Zhou, B. L., Fang, Y. X., Zhai, Z. C., Deng, Y. Q., Huang, B. H. and Lao, X. L., *ACTA Scientiarum Naturalium Universitatis Sunyatseni*, **2009**, 48(4), 66-69.

<sup>17</sup>Yang, M., Xiong, Y., Peng, Q. R., Hu, J. P., Shi, X. Y. and Liu, Z. X., *China Food Additives*, **2010**, 5, 149-153.

Received: 29. 01. 2013.

Accepted: 20. 01. 2013.



# ROLE OF $Zn^{2+}$ IN ENHANCING THE INHIBITION EFFICIENCY OF TRISODIUM CITRATE

N.Vijaya<sup>[a]</sup>, A. Peter Pascal Regis<sup>[b]</sup>, S. Rajendran<sup>[c,d]\*</sup>, M. Pandiarajan<sup>[c]\*</sup>, and R. Nagalakshmi<sup>[e]</sup>

**Keywords:** Corrosion inhibitors, well water, synergistic effect, trisodium citrate

The inhibition efficiency (IE) of trisodium citrate (TSC)- $Zn^{2+}$  system in controlling corrosion of mild steel in well water has been evaluated by weight loss method. A synergistic effect exists between TSC and  $Zn^{2+}$ . The formulation consisting of 50 ppm of TSC and 25 ppm of  $Zn^{2+}$  provides 87% of IE. FTIR spectra reveal that the protective film consists of  $Fe^{2+}$ -TSC complex and  $Zn(OH)_2$ . Polarization of study confirms the formation of a protective film on the metal surface. The inhibitor system controls the cathodic reaction predominantly.

Corresponding Authors\*

E-mail: [pandiarajan777@gmail.com](mailto:pandiarajan777@gmail.com),

- [a] Department of Chemistry, Vellalar College for Women, Thindal, Erode, India, E-mail: [chemvijaya68@gmail.com](mailto:chemvijaya68@gmail.com)  
 [b] Department of Chemistry, St. Joseph's College, Tiruchirappaili  
 [c] Corrosion Research Centre, PG and Research, Department of Chemistry, GTN Arts College, Dindigul- 624005, E-mail: [pandiarajan777@gmail.com](mailto:pandiarajan777@gmail.com)  
 [d] Department of Chemistry, Corrosion Research centre, RVS School of Engineering and Technology, Dindigul 624005, India. E-mail: [srmjoany@sify.com](mailto:srmjoany@sify.com)  
 [e] Department of chemistry, Aarupadai Veedu Institute of technology, Chennai-603110, Tamilnadu, India. Email:nagalakshmirajan@gmail.com

## Introduction

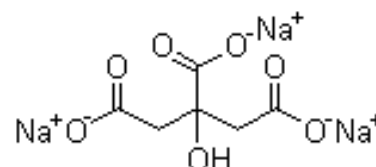
Metals are extracted from their ores by reduction process. When metals come in contact with the environment, especially oxygen and moisture, they deteriorate. This process, we call, corrosion. Corrosion is the desire of pure metals to go back to its original state of ores. Corrosion is a natural, spontaneous and thermodynamically stable process. The process of corrosion can be controlled but it cannot be prevented. There are many methods by which corrosion can be controlled one such method is the use of inhibitors. These inhibitors when added in small quantity, decrease the rate of corrosion. Corrosion inhibitors usually contain polar groups with atoms such as nitrogen, sulphur and oxygen. Correspondingly inhibitors include a wide list of organic and inorganic compounds<sup>1</sup> containing the functional groups such as aldehydes,<sup>2</sup> amines,<sup>3,4</sup> amino acids,<sup>5,6</sup> nitrocompounds,<sup>7,8</sup> amides,<sup>9,10</sup> ester,<sup>11,12</sup> thio compounds,<sup>13,14</sup> phosphates,<sup>15,16</sup> phosphonates,<sup>17,18</sup> ketones,<sup>19,20</sup> and carboxylic acids<sup>21-23</sup>. Trisodium citrate has carboxyl groups and hydroxyl groups. Such compounds are expected to have good inhibition efficiency.

The present work is undertaken (i) to evaluate the inhibition efficiency of trisodium citrate (TSC)-  $Zn^{2+}$  system in controlling corrosion of mild steel in well water, (ii) to analyse the protective film by FTIR spectroscopy and (iii) to study the mechanistic aspects of corrosion inhibition by polarization study.

## MATERIALS AND METHODS

### Metal specimens

Mild steel specimen was used in the present study. (Composition (wt %): 0.026 S, 0.06 P, 0.4 Mn, 0.1 C and balance iron). The dimension of the specimen was 1 x 4 x 0.2 cm. The molecular structure of trisodium citrate is shown in scheme 1.



**Scheme 1.** Structure of trisodium citrate

The inhibition efficiency of TSC- $Zn^{2+}$  system in controlling corrosion of mild steel in well water (Table 1) has been evaluated.

**Table 1.** Parameters of well water

Parameters	Value
pH	8.38
Conductivity	3110 $\mu\Omega^{-1} \text{ cm}^{-1}$
Chloride	665 ppm
Sulphate	14 ppm
TDS	2013 ppm
Total hardness	1100 ppm

### Weight –Loss Method

Mild steel specimens in triplicate were immersed in 100 ml of well water containing various concentration of TSC in the presence and absence of  $Zn^{2+}$  for three days. The weight of the specimens before and after immersion was determined using a Shimadzu balance, model AY62. The corrosion products were cleansed with Clarke's solution<sup>24</sup>.

The inhibition efficiency (IE, %) was then calculated using the equation:

$$IE = 100 * \left[ 1 - \frac{W_2}{W_1} \right] \quad (1)$$

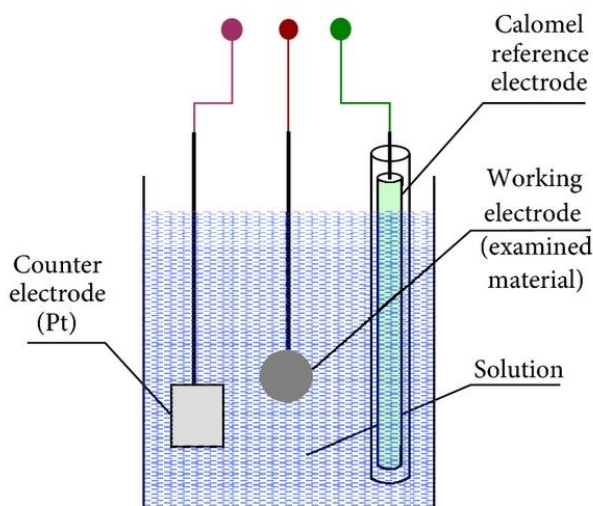
where

W<sub>1</sub> - corrosion rate in the absence of the inhibitor,

W<sub>2</sub> - corrosion rate in the presence of the inhibitor.

### Potentiodynamic polarization

Polarization studies were carried out in a CHI – Electrochemical workstation with impedance, Model 660A. A three-electrode cell assembly was used. The three-electrode assembly is shown in Scheme 2. The working electrode was mild steel. A saturated calomel electrode (SCE) was the reference electrode and platinum was the counter electrode. From the polarization study, corrosion parameters such as corrosion potential ( $E_{corr}$ ), corrosion current ( $I_{corr}$ ) and Tafel slopes (anodic =  $b_a$  and cathodic =  $b_c$ ) and Linear polarization resistance (LPR) were calculated.



Scheme 2. Circuit diagram of three-electrode cell assembly.

### FTIR Spectra

FTIR spectra were recorded in a Perkin – Elmer 1600 spectrophotometer. The film was carefully removed, mixed thoroughly with KBr made into pellets and FTIR spectra were recorded.

## Result and Discussion

### Analysis of Results of Weight-loss method

Corrosion rates of mild steel immersed in well water in the absence and presence of tri sodium citrate (TSC) and Zn<sup>2+</sup> are given in Table 2. It is observed that TSC alone has some inhibition efficiency. As the concentration of TSC increases inhibition efficiency also increases. 50 ppm of TSC has 13% inhibition efficiency and 250 ppm of TSC has 30%.

Table 2. Corrosion rates (CR) of mild steel immersed in well water and the inhibition efficiency obtained by weight loss method.

TSC ppm	Zn <sup>2+</sup>					
	0 ppm		25 ppm		50 ppm	
	CR	IE%	CR	IE%	CR	IE%
0	1a24.67	-	22.20	10	20.97	15
50	2a21.46	2b13	3.20	87	9.87	60
100	3a19.74	3b20	4.93	80	11.84	52
150	4a18.50	4b25	9.87	60	14.30	42
200	5a18.25	5b26	11.10	55	16.03	35
250	6a17.27	6b30	12.33	50	17.26	30

Immersion period: 3 Days; CR =Corrosion Rate; IE =Inhibition Efficiency

### Influence of Zn<sup>2+</sup> on the inhibition efficiency of TSC

When Zn<sup>2+</sup> is added to TSC the corrosion inhibition efficiency TSC to a great extent. This suggests that a synergistic effect exists between Zn<sup>2+</sup> and the inhibitor namely TSC. Similar synergistic effect existing between Zn<sup>2+</sup> and inhibitors has been reported by several researchers.<sup>25-29</sup> The synergistic effect between Zn<sup>2+</sup> and TSC can be explained as follows. When TSC and Zn<sup>2+</sup> are mixed, Zn<sup>2+</sup>-TSC complex is formed. It is transported towards the metal surface. On the metal surface, Zn<sup>2+</sup>-TSC complex is broken. The released TSC combines with Fe<sup>2+</sup> (formed on the metal surface due to corrosion process) resulting in the formation of Fe<sup>2+</sup>-TSC complex. Fe<sup>2+</sup>-TSC is more stable than Zn<sup>2+</sup>-TSC.

The released Zn<sup>2+</sup> combines with OH<sup>-</sup> formed by cathodic reaction and Zn(OH)<sub>2</sub> is precipitated on the cathodic site of the metal surface. The Zn<sup>2+</sup>-TSC bond is strong enough to carry the complex towards the metal surface and it is weak enough to break in presence of Fe<sup>2+</sup>. This accounts for the breaking of Zn<sup>2+</sup>-TSC complex and formation of Fe<sup>2+</sup>-TSC complex.<sup>30-33</sup>

### Analysis of polarization curve

Polarization study has been used to know if a protective film is found on the metal surface. If a protective film is formed on the metal surface, the linear polarization resistance (LPR) increases and corrosion current decreases.<sup>34-38</sup>

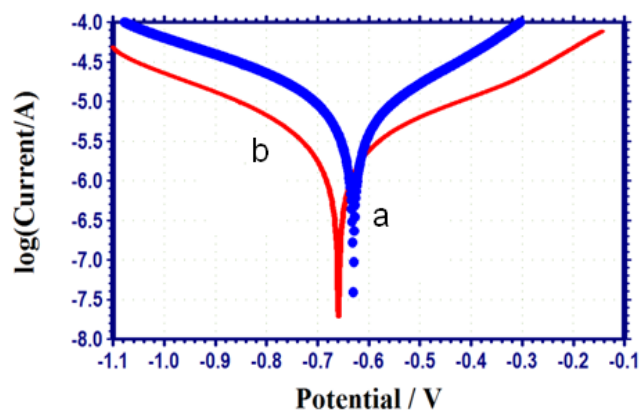


Figure 1. Polarization curve of mild steel immersed in various test solutions: a) well water b) well water + TSC 50 ppm+ Zn<sup>2+</sup> 25 ppm

Table 3. Corrosion parameters of mild steel is immersed in well water in the absence and presence of inhibitor obtained by polarization method.

System	$E_{corr}$ , mV*	$b_a$ , mV**	$b_c$ , mV**	LPR, ohm $cm^2$	$I_{corr}$ , A $cm^{-2}$
well water	-630	202	194	7799.9	$5.537 \times 10^{-6}$
well water+A	-659	186	208	23589.8	$1.810 \times 10^{-6}$

A = TSC 50ppm +  $Zn^{2+}$  25 ppm, \*mV vs SCE; \*\*mV in one decade

The potentiodynamic polarization curves of mild steel immersed in various test solutions are shown in fig 1. The corrosion parameters, namely, corrosion potential ( $E_{corr}$ ), Tafel slopes ( $b_c$  = cathodic  $b_a$  = anodic), linear polarization resistance (LPR) and corrosion current ( $I_{corr}$ ) are given in Table 3.

When mild steel is immersed in well water the corrosion potential is -630 mV vs SCE. The LPR value is 7799.9 ohm  $cm^2$ . The corrosion current is  $5.537 \times 10^{-6}$  A  $cm^{-2}$ . When inhibitors (TSC 50 ppm +  $Zn^{2+}$  50 ppm) are introduced into the system, the LPR value, increases tremendously from 7799.9 to 23589.8 ohm  $cm^2$ . Increases in LPR value is an indication of formation protective film formed on the metal surface.<sup>39-43</sup> This is also supported that by the fact that there is a sharp decrease in the corrosion current value; the corrosion current decreases from  $5.537 \times 10^{-6}$  to  $1.810 \times 10^{-6}$  A  $cm^{-2}$ . It is observed that the corrosion potential has shifted to the cathodic side (-630 to -659 mV vs SCE), in presence of inhibitors. This suggests that the cathodic reaction is controlled predominantly in presence of inhibitor system. When 2.5 ml of Zn is added to TSC solution 87% IE is obtained for 50 ppm of TSC. However as the concentration of TSC increases the inhibition efficiency decreases.

This is due to the fact that, as the concentration of TSC, the  $Zn^{2+}$ -TSC complex becomes more stable and bond is not broken in presence of  $Fe^{2+}$ . This accounts for the decreases in the IE in presence of higher concentration of TSC. Similar reason can be given for the decrease in IE of 50 ppm  $Zn^{2+}$ -TSC system. It is observed that 50 ppm  $Zn^{2+}$ -50 ppm TSC system has 60 %IE. However the IE decreases as the concentration of TSC increases.

### Analysis of FTIR spectra

FTIR spectroscopy has been used to analyse the protective film formed on the metal surface.<sup>44</sup> The FTIR spectrum of pure TSC is shown in Fig 2(a). The  $>C=O$  stretching frequency of the carboxyl group appears that  $1647 cm^{-1}$ . The -OH stretching frequency appears that  $3432 cm^{-1}$ . The FTIR spectrum of the film formed on mild steel surface after immersion in the solution containing 50 ppm of TSC and 25 ppm of Zinc is shown in Fig 2(b). It is observed that the  $>C=O$  stretching frequency has shifted from  $1647 cm^{-1}$  to  $1608 cm^{-1}$ . The -OH stretching frequency shifted from  $3432 cm^{-1}$  to  $3417 cm^{-1}$ . This indicates that the oxygen atoms of the carboxyl group and -OH have coordinate with  $Fe^{2+}$  resulting in the formation of  $Fe^{2+}$ -TSC complex formed on the anodic sites of the metal surface. The peaks at  $1274.92 cm^{-1}$  and  $612.17 cm^{-1}$  are due to Zn-O bond. The -OH stretching frequency appears at  $3417 cm^{-1}$ . These observations suggest that  $Zn(OH)_2$  is formed on the cathodic sites of the metal surface.<sup>45-48</sup>

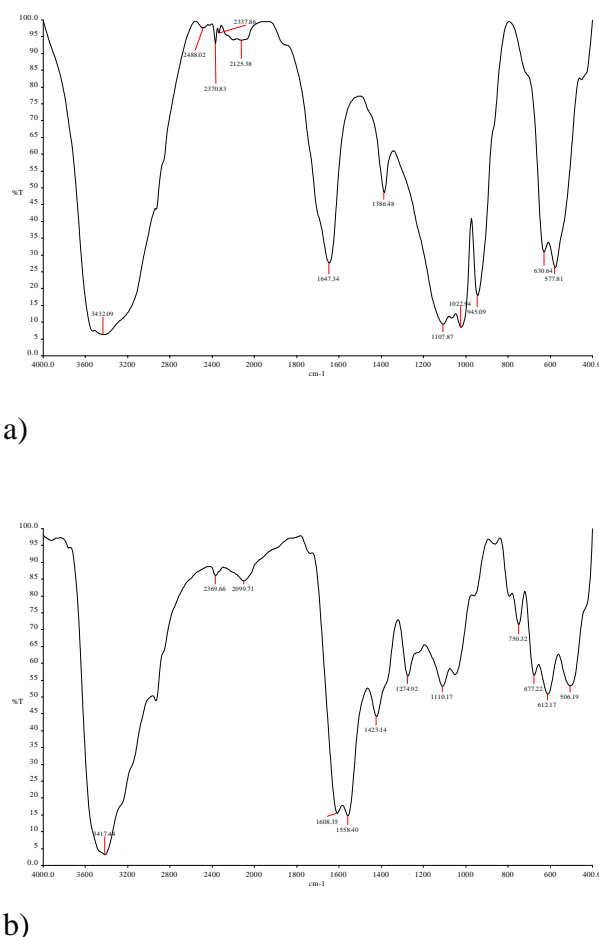


Figure 2. IR spectra of pure TSC (a) and film formed on TSC after immersion in containing 50 ppm of TSC and 15 ppm of  $Zn^{2+}$  (b)

### Conclusion

The inhibition efficiency (IE) of trisodium citrate (TSC)- $Zn^{2+}$  system is controlling corrosion of mild steel in well water has been evaluated by weight loss method.

A synergistic effect exists between TSC and  $Zn^{2+}$ . The formulation consisting of 50 ppm of TSC and 50 ppm of  $Zn^{2+}$  provides 87% IE. FTIR spectra reveal that the protective film consists of  $Fe^{2+}$ -TSC complex and  $Zn(OH)_2$ . Polarization study confirms the formation of protective film on the metal surface. The inhibitor system controls the cathodic reaction predominantly.

## Acknowledgement

The authors are thankful to their Managements and St. Joseph's Research and Community Development Trust, Dindigul, India for their help and encouragement.

## References

- <sup>1</sup>Manivannan, M., Rajendran, S., and Suriya Prabha, A., *Eur. Chem. Bull.* **2012**, 1(8), 317-29; Pandiarajan, M., Rajendran, S., Sathiyabama, J., Lydia Christy, J., Jeyasundari, J., Prabhakar, P., *Eur. Chem. Bull.* **2013**, 2(1), 1-8; Saranya, R., Rajendran, S., Krishnaveni, A., Pandiarajan, M., and Nagalakshmi, R., *Eur. Chem. Bull.*, **2013**, 2(4), 163-170; Nagalakshmi, R., Rajendran, S., Sathiyabama, J., Pandiarajan, M., and Lydia Christy, J., *Eur. Chem. Bull.*, **2013**, 2(4), 171-179; Mary Anbarasi, C., Rajendran, S., Pandiarajan, M., and Krishnaveni, A., *Eur. Chem. Bull.*, **2013**, 2(4), 197-207.
- <sup>2</sup>Abdallah, M., Zaafarany, I., Fouda, A. S., *J. Mater. Eng. Perform.*, **2012**, 21(6), 995; Feng, Y., Qi, X., Jian, H.-L., Sun, R.-C., Jiang, J.-X., *Bio Resources.*, **2012**, 7(3), 3755.
- <sup>3</sup>Kashkovskiy, R.V., Kuznetsov, Y., Kazansky, L. P., *Corros. Sci.*, **2012**, 64, 126.
- <sup>4</sup>Hosseini, S. M. A., Salari, M., Jamalizadeh, E., Jafari, A. H., *Corros.*, **2012**, 68(7), 600.
- <sup>5</sup>Gomma, G. K., Wahdan, M. H., *Mater Chem Phys.*, **1994**, 39(2), 142; Gowri, S., Sathiyabama, J., Rajendran, S., and Angelin Thangakani, J., *Eur. Chem. Bull.*, **2013**, 2(4), 214-219.
- <sup>6</sup>Liu, P., Gao, L., Zhang, D., *J. Chin. Soc. Corros. Prot.*, **2012**, 32(2), 163; Gowri, S., Sathiyabama, J., Rajendran, S., *Eur. Chem. Bull.*, **2012**, 1(11), 470-476.
- <sup>7</sup>Jayateertha, N.S., Hayavadana, N., *Res. J. Pharm. Biol. Chem. Sci.*, **2012**, 3(2), 614.
- <sup>8</sup>Fernando, I. R., Daskalakis, N., Demadis, K. D., Mezei, G., *New. J. Chem.*, **2010**, 34(2), 221.
- <sup>9</sup>Sliwa, A., Dive, G., Marchand-Brynaert, J., *Chemistry - Asian J.*, **2012**, 7(2), 425.
- <sup>10</sup>Gopiraman, M., Selvakumar, N., Kesavan, D., Karvembu, R., *Progress Org. Coatings.*, **2012**, 73(1), 104.
- <sup>11</sup>Baek, S.-Y., Kim, Y.-W., Chung, K.-W., Yoo, S.-H., *Appl. Chem. Engg.*, **2011**, 22(4), 367.
- <sup>12</sup>Kalendová, A., Veselý, D., Sapurina, I., Stejskal, J., *Progress Org. Coat.*, **2008**, 63(2), 228.
- <sup>13</sup>Bouklah, M., Ouassini, A., Hammouti, B., El Idrissi, A., *Appl. Surf. Sci.*, **2006**, 252(6), 2178.
- <sup>14</sup>Musa, A.Y., Mohamad, A. B., Kadhum, A. A. H., Takriff, M.S., Ahmoda, W. *J. Ind. Eng. Chem.*, **2012**, 18(1), 551.
- <sup>15</sup>Michael, J., Franklin, David C., White, Hugh, S., Isaacs, *Corros. Sci.*, **1992**, 33(2), 251.
- <sup>16</sup>Suman lata., and Chaudhary R. S., *Indian. J. Chem. Technol.*, **2008**, 15, 364.
- <sup>17</sup>Papadaki, M., Demadis, K. D., *Comments Inorg. Chem.*, **2009**, 30(3-4), 89; Kavipriya, K., Rajendran, S., Sathiyabama, J., and Suriya Prabha, A., *Eur. Chem. Bull.*, **2012**, 1(9), 366-374.
- <sup>18</sup>Benabdellah, M., Dafali, A., Hammouti, B., Aouniti, A., Rhomari, M., Raada, A., Senhaji, O., Robin, J. J., *Chem. Eng. Commun.*, **2007**, 194(10), 1328.
- <sup>19</sup>Ateş, E., Kizilcan, N., *Pigment Resin Technol.*, **2012**, 41(4), 210.
- <sup>20</sup>Sherif, E. M., Park, S.-M., *Electrochim. Acta.*, **2006**, 51(7), 1313.
- <sup>21</sup>Herrag, L., Chetouani, A., Elkadiri, S., Hammouti, B., Aouniti, A., *Port. Electrochim. Acta.*, **2008**, 26(2), 211.
- <sup>22</sup>Quartarone, G., Battilana, M., Bonaldo, L., Tortato, T., *Corros. Sci.*, **2008**, 50(12), 3467.
- <sup>23</sup>Eddy, N.O., Abasiekong, B.O., *J. Corros. Sci Engg.*, **2006**, 10
- <sup>24</sup>Wranglen, G., *Introduction to Corrosion and Protection of Metals.: Chapman & Hall, London*, **1985**, 236.
- <sup>25</sup>Rajendran, S., John Amalraj, A., Joice, M. J., Anthony, N., Trivedi, D., and Sundaravadevelu, M., *Corros. Rev.*, **2004**, 22, 23.
- <sup>26</sup>Yesu Thangam, Y., Kalanithi, M., Mary Anbarasi, C., and Rajendran, S., *Arab. J. Sci. Eng.*, **2009**, 34(2c), 49.
- <sup>27</sup>Rajendran, S., Peter, B. R. E., Regis, P.P., John Amalraj, A., Sundaravadevelu, M., *Trans. SAEEST*, **2003**, 38, 115.
- <sup>28</sup>Agnesia Kanimozhi, S., Rajendran, S., *Arab. J. Sci. Eng.*, **2009**, 34(2c), 37.
- <sup>29</sup>Rajendran, S., Vaibhavi, S., and Anthony, N., *Corros.*, **2003**, 59, 529.
- <sup>30</sup>Rajendran, S., Apparao, B. V., and Palaniswamy, N., *Bull. Electrochem.*, **1996**, 12, 15.
- <sup>31</sup>Sekine, I., and Hirakawa, V., *Corros.*, **1986**, 42, 276.
- <sup>32</sup>Rajendran, S., Apparao, B. V., and Palaniswamy, N., *Proc. 8<sup>th</sup> Eur. Symp. Corros. Inhibitors, Ferrara, Italy*, **1995**, 1, 465.
- <sup>33</sup>Gowri, S., Sathiyabama, J., Rajendran, S., Robert Kennedy, Z., and Agiladevi, S., *Chem. Sci. Trans.*, **2013**, 2(1), 275.
- <sup>34</sup>Mary Anbarasi, C., Susai Rajendran, S., *J. Electrochem. Sci. Eng.*, **2011**, 2(1), 1.
- <sup>35</sup>Pandiarajan, M., Prabhakar, P., Rajendran, S., *Eur. Chem. Bull.*, **2012**, 1(7), 238.
- <sup>36</sup>Manimaran, N., Rajendran, S., Manivannan, M., Johnmary, S., *Res. J. Chem., Sci.*, **2012**, 2(3), 52.
- <sup>37</sup>Arockia Selvi, J., Susai Rajendran and John Amalraj, A., Narayanasamy, B., *Port. Electrochim. Acta.*, **2009**, 27(1), 1.
- <sup>38</sup>Agila Devi, S., Susai Rajendran, Jeyasundari, J., Pandiarajan, M., *Eur. Chem. Bull.*, **2013**, 2(2), 84.
- <sup>39</sup>Rajendran, S., Anuradha, K., Kavipriya, K., Krishnaveni, A., and Angelin Thangakani, J., *Eur. Chem. Bull.*, **2012**, 1(12), 503.
- <sup>40</sup>Shyamaladevi, B., Rajendran, S., *Eur. Chem. Bull.*, **2012**, 1(5), 150.
- <sup>41</sup>Agnesia Kanimozhi, S., Rajendran, S., *Arab. J. sci. Eng.*, **2009**, 34(2c), 37.
- <sup>42</sup>Mary anbarasi, C., Susai Rajendran., Vijaya, N., Manivannan, M., Shanthi, T., *The open corros.j.*, **2012**, 5, 1.
- <sup>43</sup>Manimaran, N., Rajendran, S., Manivannan, M., John mary, S., *Res. J. chem. Sci.*, **2012**, 2(3), 52.
- <sup>44</sup>Ruba Helen Florence, G., Noreen Anthony, A., Wilson Sahayaraja, J., John Amalraj, A., Susai Rajendran., *Indian. J. Chem. Technol.*, **2005**, 12, 472.
- <sup>45</sup>Umamathi, T., Arockia Selvi, J., Agnesia Kanimolizhi, S., Susai Rajendran., John Amalraj, A., *Indian J. Chem. Technol.*, **2008**, 15, 560.
- <sup>46</sup>Sathiyabama, J., SusaiRajendran., Arockia Selvi, J., John Amalraj, A., *Indian. J. Chem. Technol.*, **2008**, 15, 462.
- <sup>47</sup>Mary Anbarasi, C., Susai Rajendran., Narayanasamy, B., Krishnaveni, A., *Asian J. Chem.*, **2012**, 24(11), 5029.
- <sup>48</sup>Sangeetha, M., Rajendran, S., Sathiyabama, J., Prabhakar, P., *J. Nat. Prod. Plant. Resour.*, **2012**, 2(5), 601.

Received: 31.12.2012.

Accepted: 29.01.2012.





# SILICA-SUPPORTED 2,4,6-TRICHLORO-1,3,5-TRIAZINE (SILICA-TCT): ENVIRONMENTALLY BENIGN, MILD AND EFFICIENT CATALYST FOR THE SYNTHESIS OF 1,4-DIHYDROPYRIDINES UNDER SOLVENT-FREE CONDITIONS

Rajesh H. Tale<sup>a</sup>, Ramprasad U. Siraskar<sup>\*a</sup> and Sainath B. Zangade<sup>b</sup>

**Keywords:** 1,4-dihydropyridines, silica-TCT, ethyl acetoacetate, substituted benzaldehyde, solvent-free

A convenient and environmentally benign silica-supported 2,4,6-trichloro-1,3,5-triazine (Silica-TCT) catalyzed Hantzsch multicomponent reaction has been shown between aldehydes, 1,3-dicarbonyl compounds and ammonium acetate in combination with stirring at room temperature under solvent-free condition to yield 1,4-dihydropyridines. Use of Silica-TCT catalyst gives several advantages in terms of simple reaction procedure, no need of organic solvent, mild reaction conditions giving quantitative yield of desired product.

\*Corresponding Authors

E-mail: [siraskarru@gmail.com](mailto:siraskarru@gmail.com)

- [a] School of Chemical Science, Swami Ramanand Teerth Marathwada University, Nanded-431602 (M.S).  
[b] Department of Chemistry, Madhavrao Patil Mahavidyalaya, Palam, Dist. Parbhani-431720 (M.S).

## Introduction

Solvent-free reaction has captured great current interest towards the development of synthetic organic chemistry.<sup>1-3</sup> In views of these observations in recent years environmentally benign synthetic procedure received considerable attention and some solvent-free protocol have been developed.<sup>4-5</sup> Solid-state reactions have been reported for some well known reactions such as Grignard reactions,<sup>6</sup> Reformatsky reactions,<sup>4</sup> Aldol condensations,<sup>7</sup> Dieckmann condensations,<sup>5</sup> Knoevenagel condensations,<sup>8</sup> reductions<sup>9</sup> and others.<sup>10</sup> Most of these reactions are carried out at room temperature in absence of solvent-free environment.

Arthur Hantzsch was the first to discover and utilize 1,3-dicarbonyl derivatives as potential multi-component substrate for the synthesis of dihydropyridines and pyridines with symmetrical substitution patterns.<sup>11</sup> Hantzsch one-pot three component condensation reactions provides certainly the most efficient access to 1,4-dihydropyridines (DHP) derivatives due to its atom economy feature and the availability and diversity of the building blocks engaged in this reaction. 1,4-Dihydropyridines are class of nitrogen containing heterocycles having a 6-membered ring. 1,4-DHPs, which are the most potent calcium antagonists or calcium channel blockers, have received much attention due to their wide range of pharmaceutical and biological properties such as inhibition of human cytochrome P450 enzyme,<sup>12</sup> angiotensin-converting enzyme inhibition, and blood pressure control on chronic, nondiabetic nephropathies.<sup>13</sup> The classical Hantzsch reaction involves the cyclocondensation of  $\beta$ -keto esters, an aldehyde with

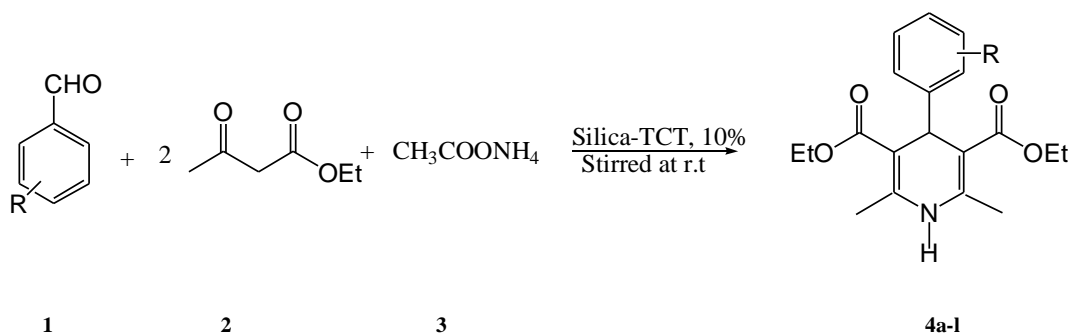
ammonia to give 1,4-dihydropyridines. There are many modification and verification of the Hantzsch synthesis have been made which include use of molecular sieves and pyridine,<sup>14</sup> Yb(OTf)<sub>3</sub>,<sup>15</sup> Me<sub>3</sub>SiI,<sup>16</sup> p-TSA,<sup>17</sup> TBAHS,<sup>18</sup> ionic liquid<sup>19</sup> and microwave technique.<sup>20</sup> The combination of solvents, costly chemicals/expensive reagents, stoichiometric amount of catalyst, strongly acidic conditions and high temperature makes these methods environmentally hazardous. Therefore, there is scope for further work towards mild conditions, increased variation of the substituent in the product and better yields. In views of these observations it was thought worthily to synthesize 1,4-dihydropyridines by the condensation of aldehydes, 1,3-dicarbonyl compounds with ammonium acetate in combination with stirring at room temperature under solvent-free condition using environmentally benign silica-supported 2,4,6-trichloro-1,3,5-triazine (Silica-TCT).

## Materials and Methods

Melting points were determined in an open capillary tube and are uncorrected. IR spectra were recorded in KBr on a Perkin-Elmer spectrometer. <sup>1</sup>H NMR spectra were recorded on a Gemini 400-MHZ instrument in CDCl<sub>3</sub> as solvent and TMS as an internal standard. The mass spectra were recorded on EISHIMADZU-GC-MS spectrometer.

## General procedure for the synthesis of 1,4-dihydropyrazolines

To a mixture of different substituted aromatic aldehydes (5 mmol), ethyl acetoacetate (10 mmol), ammonium acetate (5.5 mmol) was added. To this silica supported 2,4,6-trichloro-1,3,5-triazine (Silica-TCT) (250 mg, 10 mol% equivalent). The resulting reaction mixture was stirred at room temperature for 2-2.5 hr. The progress of the reaction mixture was monitored by TLC. After completion of



Scheme 1

reaction as on TLC, reaction mixture was poured into crushed ice and the solid product was filtered and crystallized from ethanol to give pure yellow crystalline 1,4-dihydropyridines derivatives **4a-l**.

### Preparation and determination of Silica-TCT catalyst

The desired silica supported 2,4,6-trichloro-1,3,5-triazine (Silica-TCT) was prepared in our laboratory by simple approach. The mixture of silica and TCT in appropriate ratio was mixed together and heated in dry dichloromethane (dry DCM) followed by filtration, washing with cold dry DCM drying in air. The exact loading of the TCT in terms of free chloride groups was determined by titrating the HCl generated from supported TCT on silica against standard NaOH using phenolphthalein indicator. The loading of chlorine equivalent was found to be 2.75 mmol/gm of silica which is correspond to 1.0 mmol of TCT. The catalyst so prepared was then used for further catalytic study.

### Spectral analysis of 1,4-dihydropyridines derivatives 4a-l.

**4a: 2,6-Dimethyl-4-phenyl-1,4-dihydro-pyridine-3,5-dicarboxylic acid diethyl ester:** Yellow colored crystalline solid, IR (KBr,  $\text{cm}^{-1}$ ): 3423, 3026, 2983, 1735, 1685, 1556, 1234, 1043, 862, 754, 700.  $^1\text{H}$ NMR ( $\text{CDCl}_3$ ,  $\delta$  ppm): 1.21 (t,  $J = 7.08$  Hz, 6H, two  $\text{CH}_3$ ), 2.32 (s, 6H, two  $\text{CH}_3$ ), 4.08 (q,  $J = 7.04$  Hz, 4H, two  $\text{OCH}_2$ ), 4.98 (s, 1H, broad NH), 7.09-7.13 (m, 1H, Ar-H), 7.20 (t,  $J = 8.52$  Hz, 2H, ArH), 7.26-7.28 (m, 2H, ArH). MS  $m/z$ : 328 ( $\text{M}^+$ ). Anal. Calcd for  $\text{C}_{19}\text{H}_{22}\text{O}_4\text{N}$ : C, 69.15; H, 6.70. Found: C, 69.28; H, 6.63.

**4b: 4-(4-Methoxy-phenyl)-2,6-dimethyl-1,4-dihydro-pyridine-3,5-dicarboxylic acid diethyl ester:** Yellow colored crystalline solid, IR (KBr,  $\text{cm}^{-1}$ ): 3420, 2986, 1732, 1670, 1548, 1230, 1051, 853, 750, 700.  $^1\text{H}$ NMR ( $\text{CDCl}_3$ ,  $\delta$  ppm): 1.23 (t,  $J = 7.10$  Hz, 6H, two  $\text{CH}_3$ ), 2.28 (s, 6H, two  $\text{CH}_3$ ), 3.72 (s, 3H,  $\text{OCH}_3$ ), 4.12 (q,  $J = 7.06$  Hz, 4H, two  $\text{OCH}_2$ ), 4.95 (s, 1H, broad NH), 7.20 (d,  $J = 8.50$  Hz, 2H, ArH), 7.18 (d,  $J = 8.50$  Hz, 2H, ArH). MS  $m/z$ : 358 ( $\text{M}^+$ ). Anal. Calcd for  $\text{C}_{20}\text{H}_{24}\text{O}_5\text{N}$ : C, 67.03; H, 6.70. Found: C, 67.18; H, 6.67.

**4c: 4-(3,4-Dimethoxy-phenyl)-2,6-dimethyl-1,4-dihydro-pyridine-3,5-dicarboxylic acid diethyl ester:** Yellow colored crystalline solid, IR (KBr,  $\text{cm}^{-1}$ ): 3428, 2974, 1730, 1655, 1553, 1233, 1051, 850, 755, 730.  $^1\text{H}$ NMR ( $\text{CDCl}_3$ ,  $\delta$  ppm): 1.27 (t,  $J = 7.13$  Hz, 6H, two  $\text{CH}_3$ ), 2.26 (s, 6H, two  $\text{CH}_3$ ), 3.75 (s, 6H, two  $\text{OCH}_3$ ), 4.14 (q,  $J = 7.10$  Hz, 4H, two

$\text{OCH}_2$ ), 4.92 (s, 1H, broad NH), 6.80 (s, 1H, ArH), 6.72 (d,  $J = 8.28$  Hz, 1H, ArH), 6.79 (d,  $J = 8.28$  Hz, 1H, ArH). MS  $m/z$ : 388 ( $\text{M}^+$ ). Anal. Calcd for  $\text{C}_{21}\text{H}_{26}\text{O}_6\text{N}$ : C, 67.27; H, 6.93. Found: C, 67.35; H, 6.88.

**4d: 4-(4-Hydroxy-phenyl)-2,6-dimethyl-1,4-dihydro-pyridine-3,5-dicarboxylic acid diethyl ester:** Yellow colored crystalline solid, IR (KBr,  $\text{cm}^{-1}$ ): 3436, 2970, 1732, 1662, 1580, 1226, 1047, 855, 750.  $^1\text{H}$ NMR ( $\text{CDCl}_3$ ,  $\delta$  ppm): 1.26 (t,  $J = 7.13$  Hz, 6H, two  $\text{CH}_3$ ), 2.26 (s, 6H, two  $\text{CH}_3$ ), 4.13 (q,  $J = 7.10$  Hz, 4H, two  $\text{OCH}_2$ ), 4.94 (s, 1H, broad NH), 5.72 (s, 1H, OH), 7.18 (d,  $J = 8.48$  Hz, 2H, ArH), 7.20 (d,  $J = 8.48$  Hz, 2H, ArH). MS  $m/z$ : 388 ( $\text{M}^+$ ). Anal. Calcd for  $\text{C}_{21}\text{H}_{26}\text{O}_6\text{N}$ : C, 64.94; H, 6.70. Found: C, 64.83; H, 6.74.

**4e: 4-(4-Hydroxy-3-methoxy-phenyl)-2,6-dimethyl-1,4-dihydro-pyridine-3,5-dicarboxylic acid diethyl ester:** Yellow colored crystalline solid, IR (KBr,  $\text{cm}^{-1}$ ): 3432, 2978, 1736, 1680, 1575, 1220, 1043, 852, 758.  $^1\text{H}$ NMR ( $\text{CDCl}_3$ ,  $\delta$  ppm): 1.26 (t,  $J = 7.12$  Hz, 6H, two  $\text{CH}_3$ ), 2.26 (s, 6H, two  $\text{CH}_3$ ), 3.71 (s, 3H,  $\text{OCH}_3$ ), 4.15 (q,  $J = 7.11$  Hz, 4H, two  $\text{OCH}_2$ ), 4.90 (s, 1H, broad NH), 5.78 (s, 1H, OH), 6.83 (s, 1H, ArH), 6.75 (d,  $J = 8.30$  Hz, 1H, ArH), 6.82 (d,  $J = 8.30$  Hz, 1H, ArH). MS  $m/z$ : 374 ( $\text{M}^+$ ). Anal. Calcd for  $\text{C}_{20}\text{H}_{24}\text{O}_6\text{N}$ : C, 64.17; H, 6.41. Found: C, 64.28; H, 6.45.

**4f: 4-(4-Dimethylamino-phenyl)-2,6-dimethyl-1,4-dihydro-pyridine-3,5-dicarboxylic acid diethyl ester:** Yellow colored crystalline solid, IR (KBr,  $\text{cm}^{-1}$ ): 3435, 2972, 1732, 1689, 1572, 1217, 1047, 858, 751.  $^1\text{H}$ NMR ( $\text{CDCl}_3$ ,  $\delta$  ppm): 1.24 (t,  $J = 7.12$  Hz, 6H, two  $\text{CH}_3$ ), 2.28 (s, 6H, two  $\text{CH}_3$ ), 2.85 (s, 6H,  $\text{N}(\text{CH}_3)_2$ ), 4.13 (q,  $J = 7.10$  Hz, 4H, two  $\text{OCH}_2$ ), 4.93 (s, 1H, broad NH), 7.24 (d,  $J = 8.51$  Hz, 2H, ArH), 7.18 (d,  $J = 8.51$  Hz, 2H, ArH). MS  $m/z$ : 370 ( $\text{M}^+$ ). Anal. Calcd for  $\text{C}_{21}\text{H}_{27}\text{O}_4\text{N}_2$ : C, 68.10; H, 7.29. Found: C, 68.17; H, 7.36.

**4g: 4-(4-Chloro-phenyl)-2,6-dimethyl-1,4-dihydro-pyridine-3,5-dicarboxylic acid diethyl ester:** Yellow colored crystalline solid, IR (KBr,  $\text{cm}^{-1}$ ): 3432, 2958, 1726, 1680, 1535, 1224, 1038, 852, 746.  $^1\text{H}$ NMR ( $\text{CDCl}_3$ ,  $\delta$  ppm): 1.28 (t,  $J = 7.14$  Hz, 6H, two  $\text{CH}_3$ ), 2.29 (s, 6H, two  $\text{CH}_3$ ), 4.15 (q,  $J = 7.12$  Hz, 4H, two  $\text{OCH}_2$ ), 4.91 (s, 1H, broad NH), 7.16 (d,  $J = 8.48$  Hz, 2H, ArH), 7.21 (d,  $J = 8.48$  Hz, 2H, ArH). MS  $m/z$ : 362 ( $\text{M}^+$ ). Anal. Calcd for  $\text{C}_{19}\text{H}_{21}\text{O}_4\text{NCl}$ : C, 62.98; H, 5.80; Cl, 10.23. Found: C, 63.08; H, 5.83; 9.74.

**4h: 4-(4-Bromo-phenyl)-2,6-dimethyl-1,4-dihydro-pyridine-3,5-dicarboxylic acid diethyl ester:** Yellow colored crystalline solid, IR (KBr,  $\text{cm}^{-1}$ ): 3436, 2952, 1730,

1683, 1531, 1218, 1042, 848, 755. <sup>1</sup>HNMR (CDCl<sub>3</sub>, δ ppm): 1.27 (t, *J* = 7.14 Hz, 6H, two CH<sub>3</sub>), 2.26 (s, 6H, two CH<sub>3</sub>), 4.12 (q, *J* = 7.11 Hz, 4H, two OCH<sub>2</sub>), 4.90 (s, 1H, broad NH), 7.18 (d, *J* = 8.48 Hz, 2H, ArH), 7.20 (d, *J* = 8.48 Hz, 2H, ArH). MS *m/z*: 407 (M<sup>+</sup>). Anal. Calcd for C<sub>19</sub>H<sub>21</sub>O<sub>4</sub>NBr: C, 56.01; H, 5.15; Br, 19.65. Found: C, 56.13; H, 5.19; Br, 19.74.

**4i: 2,6-Dimethyl-4-p-tolyl-1,4-dihydro-pyridine-3,5-dicarboxylic acid diethyl ester:** Yellow colored crystalline solid, IR (KBr, cm<sup>-1</sup>): 3430, 2963, 1734, 1683, 1546, 1224, 1040, 842, 747. <sup>1</sup>HNMR (CDCl<sub>3</sub>, δ ppm): 1.28 (t, *J* = 7.15 Hz, 6H, two CH<sub>3</sub>), 2.23 (s, 3H, ArCH<sub>3</sub>), 2.29 (s, 6H, two CH<sub>3</sub>), 4.14 (q, *J* = 7.13 Hz, 4H, two OCH<sub>2</sub>), 4.92 (s, 1H, broad NH), 7.23 (d, *J* = 8.51 Hz, 2H, ArH), 7.20 (d, *J* = 8.51 Hz, 2H, ArH). MS *m/z*: 342 (M<sup>+</sup>). Anal. Calcd for C<sub>20</sub>H<sub>24</sub>O<sub>4</sub>N: C, 70.17; H, 7.01. Found: C, 70.25; H, 7.13.

**4j: 2,6-Dimethyl-4-(4-nitro-phenyl)-1,4-dihydro-pyridine-3,5-dicarboxylic acid diethyl ester:** Yellow colored crystalline solid, IR (KBr, cm<sup>-1</sup>): 3435, 2972, 1729, 1672, 1538, 1229, 1022, 846, 742. <sup>1</sup>HNMR (CDCl<sub>3</sub>, δ ppm): 1.26 (t, *J* = 7.14 Hz, 6H, two CH<sub>3</sub>), 2.27 (s, 6H, two CH<sub>3</sub>), 4.15 (q, *J* = 7.13 Hz, 4H, two OCH<sub>2</sub>), 4.94 (s, 1H, broad NH), 7.18 (d, *J* = 8.48 Hz, 2H, ArH), 7.20 (d, *J* = 8.48 Hz, 2H, ArH). MS *m/z*: 372 (M<sup>+</sup>). Anal. Calcd for C<sub>19</sub>H<sub>21</sub>O<sub>6</sub>N<sub>2</sub>: C, 61.29; H, 5.64. Found: C, 61.34; H, 5.71.

**4k: 2,6-Dimethyl-4-(3-nitro-phenyl)-1,4-dihydro-pyridine-3,5-dicarboxylic acid diethyl ester:** Yellow colored crystalline solid, IR (KBr, cm<sup>-1</sup>): 3435, 3084, 2985, 1734, 1601, 1558, 1215, 1082, 916, 860, 792. <sup>1</sup>HNMR (CDCl<sub>3</sub>, δ ppm): 1.22 (t, *J* = 7.08 Hz, 6H, two CH<sub>3</sub>), 2.36 (s, 6H, two CH<sub>3</sub>), 4.10 (q, *J* = 7.12 Hz, 4H, two OCH<sub>2</sub>), 4.97 (s, 1H, broad NH), 7.37 (t, *J* = 7.92 Hz, 1H, ArH), 7.64 (d, *J* = 8.96 Hz, 1H, ArH), 8.01 (d, *J* = 9.4 Hz, 1H, ArH), 8.12 (s, 1H, ArH). MS *m/z*: 372 (M<sup>+</sup>). Anal. Calcd for C<sub>19</sub>H<sub>21</sub>O<sub>6</sub>N<sub>2</sub>: C, 61.29; H, 5.64. Found: C, 61.24; H, 5.70.

**4l: 2,6-Dimethyl-4-(2-nitro-phenyl)-1,4-dihydro-pyridine-3,5-dicarboxylic acid diethyl ester:** Yellow colored crystalline solid, IR (KBr, cm<sup>-1</sup>): 3438, 3089, 2970, 1732, 1606, 1552, 1217, 1087, 912, 858, 790. <sup>1</sup>HNMR (CDCl<sub>3</sub>, δ ppm): 1.23 (t, *J* = 7.08 Hz, 6H, two CH<sub>3</sub>), 2.36 (s, 6H, two CH<sub>3</sub>), 4.11 (q, *J* = 7.12 Hz, 4H, two OCH<sub>2</sub>), 4.95 (s, 1H, broad NH), 7.37-8.15 (m, 4H, ArH). MS *m/z*: 372 (M<sup>+</sup>). Anal. Calcd for C<sub>19</sub>H<sub>21</sub>O<sub>6</sub>N<sub>2</sub>: C, 61.29; H, 5.64. Found: C, 61.27; H, 5.71.

## Results and Discussion

With increasing economical concerns and regulatory faced by pharmaceutical and chemical industries, development of environmentally benign organic reactions has become the crucial and demanding area in modern organic chemical research. Therefore, in present work we decided to look closely at the reactivity of various aromatic aldehydes towards Hantzsch condensation reaction in the presence of Silica-TCT as catalyst. In typical experimental procedure, a mixture of ethyl acetoacetate (**4** mmol), benzaldehydes (**2** mmol) and ammonium acetate (**3** mmol) using varying amount of Silica-TCT was stirred at room temperature (Scheme 1). The reaction was much sluggish in the absence of catalyst and gave unacceptable yields of product. In order to optimize the use of Silica-TCT catalyst, the 3-

nitrobenzaldehyde, ethyl acetate and ammonium acetate was subjected to stirred at room temperature using 2.5 mol %, 5 mol %, 7.5 mol % and 10 mol % of catalyst, the reaction resulted in the formation of 2,6-Dimethyl-4-(3-nitro-phenyl)-1,4-dihydro-pyridine-3,5-dicarboxylic acid diethyl ester **4k** in 45, 59, 77 and 84 % yields respectively (Table 1). Promoted by these results, various aromatic aldehydes were subjected to Hantzsch condensation with ethyl acetoacetate and ammonium acetate using our optimized reaction conditions to yield 1,4-dihydropyridine derivatives (Scheme 1). The product was isolated in high purity by simple aqueous work-up followed by recrystallisation from ethanol. The structures of the products were confirmed on the basis of physical constant and spectroscopic data<sup>21</sup>. It follows from Table 2 that the yields of all the products are good to excellent and a variety of functionalities such as nitro, halide, alkoxy and hydroxyl, etc. can be accommodated in 1,4-dihydropyridine derivatives. Aromatic aldehydes carrying electron withdrawing substituent reacted in shorter reaction time to give excellent yields of corresponding 1,4-dihydropyridine compared to electron releasing substituent.

**Table 1.** 2,6-Dimethyl-4-(3-nitro-phenyl)-1,4-dihydro-pyridine-3,5-dicarboxylic acid diethyl ester.

Entry	Silica-TCT, mol %	Time, min <sup>a</sup>	Yield, % <sup>b</sup>
1	2.5	85	45
2	5	70	59
3	7.5	58	77
4	10	28	88

<sup>a</sup>Time required to convert reactant into product; <sup>b</sup>Isolated yields

**Table 2.** Silica-TCT catalyzed synthesis of 1,4-dihydropyridines derivatives through Hantzsch reaction under solvent-free condition

Compound	Ar	Time, min	Yield, %	M.P., °C
<b>4a</b>	C <sub>6</sub> H <sub>5</sub>	55	84	156-157
<b>4b</b>	4-MeOC <sub>6</sub> H <sub>4</sub>	47	77	80-82
<b>4c</b>	3,4-(MeO) <sub>2</sub> C <sub>6</sub> H <sub>3</sub>	46	71	85-87
<b>4d</b>	4-OHC <sub>6</sub> H <sub>4</sub>	53	79	120-122
<b>4e</b>	4-OH-3-MeOC <sub>6</sub> H <sub>3</sub>	45	81	134-136
<b>4f</b>	4-Me <sub>2</sub> NC <sub>6</sub> H <sub>4</sub>	48	84	95-97
<b>4g</b>	4-ClC <sub>6</sub> H <sub>4</sub>	39	70	144-146
<b>4h</b>	4-BrC <sub>6</sub> H <sub>4</sub>	40	83	112-115
<b>4i</b>	4-CH <sub>3</sub> C <sub>6</sub> H <sub>4</sub>	42	78	127-129
<b>4j</b>	4-NO <sub>2</sub> C <sub>6</sub> H <sub>4</sub>	34	80	150-152
<b>4k</b>	3-NO <sub>2</sub> C <sub>6</sub> H <sub>4</sub>	28	88	162-164
<b>4l</b>	2-NO <sub>2</sub> C <sub>6</sub> H <sub>4</sub>	37	81	155-157

## Conclusion

In summary we have successfully exploited the Silica-TCT as an inexpensive and readily available catalyst for synthesis of 1,4-dihydropyridines. The present protocol has several advantages including simple reaction procedure, shorter reaction time compared to classical Hantzsch condensation reaction, solvent-free conditions and high yields of product.

## References

- <sup>1</sup>Lancaster, M. In: *Handbook of Green Chemistry and Technology*; Clark TH, Macquarrie DJ, Eds.; Blackwell: Abingdon, **2002**.
- <sup>2</sup>Sanchez, L. M., Sathicq, A. G., Jios, J. L., Baronetti, G. T., Thomas, H. J. *Tetrahedron Lett.*, **2011**, *52*, 4412-4416.
- <sup>3</sup>Rothenberg, G., Dowine, A. P., Raston, C. L., Scott, J. L. *J. Am. Chem. Soc.* **2001**, *123*, 8701-8708.
- <sup>4</sup>Tanaka, K., Kishigami, S., Toda, F. *J. Org. Chem.* **1991**, *56*, 4333-4334.
- <sup>5</sup>Zangade, S. B., Mokle, S. S., Shinde, A. T., Vibhute, Y. B., *Green Chem. Lett. Rev.* **2013**, *6*, 123-127.
- <sup>6</sup>Toda, F., Suzuki, T., Higa, S. *J. Chem. Soc. Perkin Trans I.* **1998**, *1*, 3521-3522.
- <sup>7</sup>Miles, W.H., Rivera, S. L., Rosario, J. D. *Tetrahedron Lett.* **1992**, *33*, 305-308.
- <sup>8</sup>Toda, F., Tanaka, K., Hamai, K. *J. Chem. Soc. Perkin Trans I.* **1990**, *1*, 3207-3209.
- <sup>9</sup>Ren, Z., Cao, W., Tong, W. *Synth. Commun.* **2002**, *32*, 3475-3479.
- <sup>10</sup>Toda, F., Kiyoshige, K., Yagi, M., *Angew. Chem., Int. Ed. Engl.* **1989**, *28*, 320-321.
- <sup>11</sup>Zangade S, Mokle S, Vibhute Y, Vibhute, Y., *Chem. Sci. J.*, **2011**, Article ID:CSJ-13, 1-6.
- <sup>11</sup>Hantzsch, A., *Lieb. Ann. Chem.* **1882**, *215*, 1.
- <sup>12</sup>Katoh, M., Nakajima, M., Shimada, N., Yamazaki, H., Yokoi, T. *Eur. J. Clin. Pharmacol.* **2000**, *55*, 843-852.
- <sup>13</sup>Ruggenenti, P., Perna, A., Benini, R., Remuzzi, G., *J. Am. Soc. Nephrol.* **1998**, *9*, 2096-2101.
- <sup>14</sup>Gordeev, M. F., Patel, D. V., Gordan, E. M., *J. Org. Chem.* **1996**, *61*, 924-928.
- <sup>15</sup>Wang, L. M., Sheng, J., Zhang, J. W., Han, J. W., Fan, Z. Y., Yian, H., Qian, C. T., *Tetrahedron* **2005**, *61*, 1539-1543.
- <sup>16</sup>Sabitha, G., Kiran kumar Reddy, G. S., Reddy, C. S., Yadav, J. S., *Tetrahedron Lett.* **2003**, *44*, 4129-4131.
- <sup>17</sup>Cherkupally, S. R., Mekala, R., *Chem. Pharm. Bull.* **2008**, *56*, 1002-1004.
- <sup>18</sup>Tewari, N., Namrata, D., Tripathi, R. P., *Tetrahedron Lett.* **2004**, *45*, 9011-9014.
- <sup>19</sup>Sridhar, R., Perumal, P. T., *Tetrahedron*, **2005**, *61*, 2465-2470.
- <sup>20</sup>Yadav, J. S., Subba Reddy, B. V., Nagaraju, A., Sarma, J. A. R. P., *Synth. Commun.*, **2002**, *32*, 893-896.
- <sup>21</sup>Cotterill, I. C., Usyatinsky, A. Y., Arnold, J. M., Clark, D. S., Dordick, J. S., *Tetrahedron Lett.*, **1998**, *39*, 1117-1120.

Received: 14. 01.2013.

Accepted: 26. 01. 2013.



# APPLICATION OF SPENT TEA LEAVES AS AN EFFICIENT LOW COST BIOSORBENT FOR REMOVAL OF ANIONIC SURFACTANTS FROM AQUEOUS SOLUTIONS

Reza Ansari<sup>[a]\*</sup>, Peyman Hossainzadeh Khanesar<sup>[a]</sup>

**Keywords:** removal of anionic surfactants, spent tea leaves, thermodynamic, kinetic, isotherms

In this research, biomaterial wastes such as spent black tea leaves (SBTL) spent green tea leaves (SGTL) as well as sawdust (SD) obtained from Narra wood were used to remove sodium dodecyl sulfate (SDS) from aqueous solutions. The effect of pH, temperature, amount of adsorbent and initial concentration of SDS has been examined. The result indicated that the SDS can be significantly adsorbed by the used biosorbents at their natural pH values. Equilibrium and kinetics studies were carried out for the adsorbents to assess the adsorption equilibrium model that they followed. The correlation coefficients were determined by linear regression analysis, and compared. The removal efficiency, maximum adsorption capacity and cost were the prime parameters for the selection of the adsorbents in this study. Among the examined adsorbents and considering all parameters, SBTL showed the higher performance for SDS removal.

Corresponding Authors

E-Mail: [ransari@guilan.ac.ir](mailto:ransari@guilan.ac.ir)

Phone: +98-1313243630-4 (Ext. 226)

Fax: +98-131-3233262

[a] Chemistry Department, Faculty of Science, University of Guilan, Rasht, Iran, POB: 41635-19141

## Introduction

Surfactants are one of the major components in the formulation of various industrial and household products. There are four classes (cationic, anionic, amphoteric and non-ionic) based on the ionic charge (if present) of the hydrophilic portion of the surfactant in an aqueous solution<sup>1</sup>. Many industrial effluents such as cosmetic and detergent industries, laundry and car washing services contain mixtures of surfactants.<sup>2-5</sup>

These applications of the surfactant, increasing its discharge in the wastewater, produce foam and enter into the underground water resources and constituting an ecological risk for aquatic organism. They also create many health hazards like dermatitis and harmful for the aquatic flora and fauna.<sup>6-8</sup> According to the Council of European Surfactants Producers Statistics the total quantity of surfactants (without soaps) consumed in Western Europe in 2002 was more than 2.5 million tons.<sup>9</sup> Nowadays, the role of surfactants and surfactant detergents a factor of surface and ground-water pollution is comparable to that of oil pollution of the world oceans<sup>10</sup>. So, the water treatment process is necessary in order to remove surfactant from industrial and domestic wastes to reduce its concentration. Some processes have already been employed for this purpose, such as aerobic and anaerobic degradation, biodegradation and sorption technique.<sup>11-19</sup>

Adsorption of anionic surfactant has been examined onto numerous adsorbent like activated carbon, silica gel, clay, soil, kaolinite, sand stone, granite sand, ozonation, TiO<sub>2</sub> photocatalytic treatment, Fenton oxidation, wet air oxidation and electrochemical treatment.<sup>20-35</sup> Among the various treatments for surfactant degradation, ozonation and

photocatalytic methods are the most costly methods and adsorption seems to be the most efficient and cost effective.<sup>10</sup> In this study, we have selected three low cost, environmental friendly waste materials such as spent green tea leaves (SGTL), spent black tea leaves (SBTL) and wood sawdust (SD) as adsorbent for removal of SDS surfactant. Several experiments have been carried out to optimize the adsorption process.

## Experimental

### Materials and method

SDS ( $M=288.38 \text{ g mol}^{-1}$ ) surfactant solutions were prepared with deionized water. All chemical reagents used were analytical grade. Chemical structure of sodium dodecyl sulfate was shown in Figure 1.

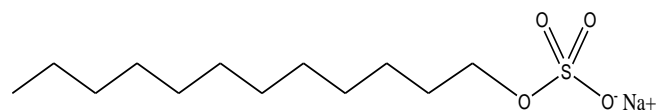


**Figure 1.** Molecular structure of SDS

Sawdust obtained from Narra wood (SD), spent green tea leaves (SGTL) and spent black tea leaves (SBTL) were collected from local carpentry and tea shop. The sawdust was first sieved to 35-50 mesh and washed with tap water and then washed with distilled water. SBTL and SGTL the same sawdust washed first with tap water and then with distilled water to avoid the presence of any foreigner materials. The washed materials thereafter were dried at 50 °C for 12 h and kept at room temperature. SDS (85% purity) was purchased from Merck company, and used as purchased. All the reagents *viz.*, methylene blue (MB), chloroform, NaOH, HCl, and borax were of AR grade. Stock solution of SDS ( $100 \text{ mg L}^{-1}$ ) was prepared in distilled water. SDS test and standard solutions with required concentrations

were prepared by diluting the stock solution appropriately. A high precision electronic balance (Sartorius) was used for weighing purpose. A pH meter (Metrohm, model 827) with a combined double junction glass electrode was utilized for pH measurement.

### Measurement procedures

SDS determination was carried out using methylene blue as per standard method.<sup>36</sup> It forms a complex pair ion with cationic dye of MB. The complex after its formation was extracted into chloroform. The complex was formed anionic part of SDS and cationic part of MB. The color intensity of the chloroform layer gave a measure of the SDS concentration and analysed spectrophotometrically ( $\lambda_{\text{max}}=620$  nm).

A calibration curve (graph of absorbance vs. concentration, known as Lambert-Beer's Law plot) was used to quantify unadsorbed SDS (Fig. 2).

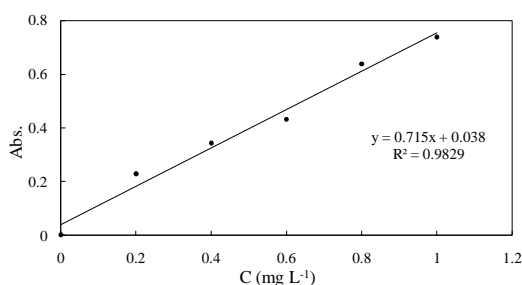


**Figure 2.** Calibration curve prepared for analysis of SDS

A spectrophotometer (Perkin Elmer Junior) was used for all absorbance measurements. The following equations were utilized to calculate the percentage of adsorption and the amount of adsorbed SDS ( $\phi$ , in %), respectively:<sup>37</sup>

$$\phi = \left( \frac{C_0 - C_e}{C} \right) \times 100 \quad (1)$$

$$q = V \left( \frac{C_0 - C_e}{m} \right) \quad (2)$$

where  $C_0$  is initial SDS concentration ( $\text{mg L}^{-1}$ ),  $C_t$  is the left out SDS concentration in bulk solution at time  $t$  ( $\text{mg L}^{-1}$ ),  $V$  is the volume of SDS solution (L),  $m$  is adsorbent mass (g), and  $q$  is the amount of SDS adsorbed onto unit amount of the adsorbent ( $\text{mg g}^{-1}$ ) at equilibrium.

## Results and discussion

### Effect of pH

In this investigation, fixed volumes of SDS solutions (50 mL) with initial concentration of  $10 \text{ mg L}^{-1}$  were mixed with constant amount of selected adsorbents (0.50 g). The mixtures were shaken in a mechanical shaker with 170 rpm

speed at room temperature for duration of 2 h at different pHs (2-12). The results obtained have been shown in Figure 3.

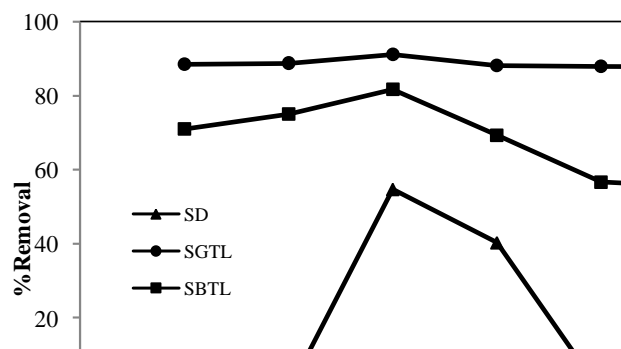


**Figure 3.** The effect of initial pH SDS solution on adsorption efficiency

As the results show, maximum sorption is occurred at the natural pH of selected adsorbents ( $\text{pH}=6-7$ ). Among the used adsorbents, SD showed highest sensitivity to pH for SDS uptake. It seems alkaline pH media is unfavorable for adsorption of SDS. It might be due to the presence of excess  $\text{OH}^-$  ions on the surface of adsorbents that compete with the anionic surfactant (SDS) for adsorption sites. At low pH might also destroy the active sites on the surface of adsorbents which resulted to decrease in SDS removal.

### Effect of dosage

In this study different weights of adsorbents (0.10-0.50 g) were contacted with 50 mL SDS solutions with known concentration ( $10 \text{ mg L}^{-1}$ ). The results obtained have been shown in Figure 4.

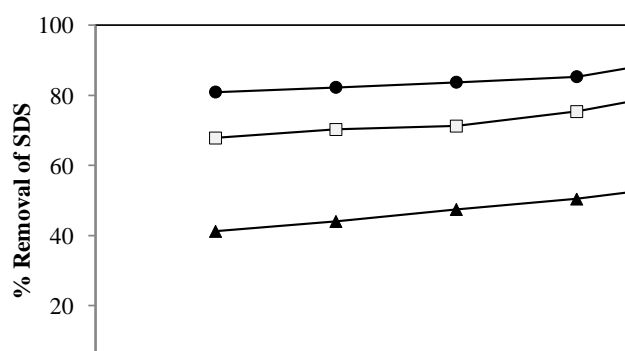


**Figure 4.** Effect of adsorbent dosage on removal of SDS

According to our results the percentage removal of increased with the increase in weight of adsorbents. This may be due to the increase in availability of surface active sites resulting from the increased weight of the adsorbent. However, SGTL indicated higher sorption capacity than the SD and SBTL biosorbents.

### Effect of initial concentration

For performing this experiment 0.50 g of adsorbents were contacted with 50 mL of SDS solution with various concentrations ( $10-100 \text{ mg L}^{-1}$ ) at pH 6-7 for 2 h shaking at

room temperature. The results obtained are shown in Figure 5. As the results indicate, SGTL showed the superior adsorptive behaviour compared to SD and SBTL and SD showed the least sorption capacity. However, with increasing the initial SDS concentration, removal percentages are decreased for all of the used adsorbents.

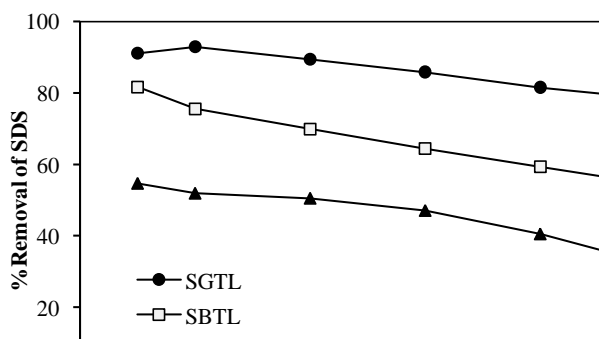


**Figure 5.** Effect of initial concentration of SDS on sorption by SD, SGTL and SBTL adsorbents.

#### Effect of contact time

In this investigation fixed amounts of adsorbents (0.50 g) were contacted with 50 mL of 10 mg L<sup>-1</sup> SDS solution at natural pH values for different exposure times (15-150 minutes) accompanied by shaking at room temperature. The results obtained are shown in Figure 6. As the results exhibit, with increasing contact time up to 120 min, removal percentages of SDS were increased for three adsorbents and the equilibrium of adsorption was reached after 2 h. After 2 hours, some decrease due to desorption was observed.

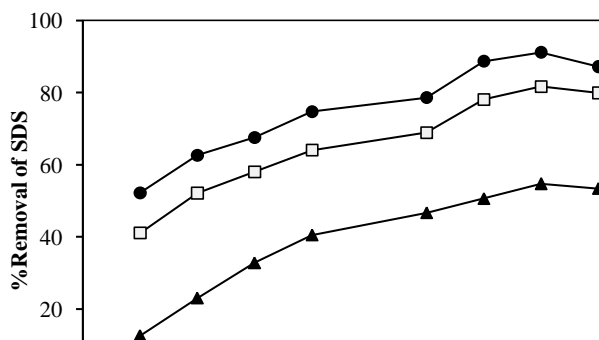


**Figure 6.** Effect of contact time on removal of SDS using SD, SGTL and SBTL adsorbents

#### Adsorption kinetic

Kinetics of adsorption is one of the important characteristics in explaining the efficiency of an adsorption process and potential application of an adsorbent. In order to inspect the mechanism of solute adsorption onto the selected adsorbents, pseudo-first and second order reaction kinetic models were applied and a comparison of the best fit adsorption mechanism was prepared. The pseudo-first order Lagergren rate equation is the one most widely utilized for the adsorption of a solute from a liquid solution and is represented as:<sup>38</sup>

$$\lg(q_e - q_t) = \lg q_e - \frac{K_1}{2.303} \times t \quad (3)$$

where;  $q_t$  and  $q_e$  (mg.g<sup>-1</sup>) are the amount of SDS adsorbed per unit mass of adsorbent at time  $t$  and at equilibrium respectively, and  $K_1$  is equilibrium rate constant of pseudo-first-order adsorption. Therefore a linear trace is carried out between  $\log(q_e - q_t)$  and  $t$ , provided the adsorption follows first order kinetics. For determining of reaction mechanism and potential application of an adsorbent, kinetic study is very useful. The equilibrium kinetic data were further analysed employing pseudo-second-order kinetic model suggested by McKay et al.<sup>39</sup> The differential equation is the following:

$$\frac{dq_t}{dt} = K_2(q_e - q_t)^2 \quad (4)$$

where  $k_2$  is rate constant for pseudo-second-order adsorption (g mg<sup>-1</sup> min<sup>-1</sup>). For the boundary conditions  $t=0$  to  $t=1$  &  $q_t=0$ ,  $q_t=q_t$  integrated form of equation is as follows:

$$\frac{1}{(q_e - q_t)} = \frac{1}{q_e} + K_2 t \quad (5)$$

The linear form of equation can be expressed as follows:

$$\frac{t}{q_t} = \frac{1}{K_2 q_e^2} + \frac{1}{q_e} t \quad (6)$$

The plots of  $t/q_t$  versus  $t$  should give straight lines where slopes and intercepts are  $1/q_e$  and  $1/K_2 q_e^2$ , respectively. The values of the rate constant  $K_2$  and adsorption capacity  $q_e$  are calculated from these parameters and are summarised in Table 1. Based on regression analysis ( $R^2 > 0.95$ ) it could be concluded that adsorption of SDS onto SD, SGTL and SBTL followed the pseudo-second-order kinetics model which suggesting a chemisorption mechanism.<sup>40</sup>

#### Adsorption isotherms

Isotherms provide an estimate of adsorption capacity and also useful information about applicability of a candidate adsorbent for adsorption of an undesired contaminant. In this work Langmuir and Freundlich models were employed for treatment of equilibrium adsorption data. Langmuir model is represented by the following equation:

$$\frac{1}{q_e} = \frac{1}{q_m} + \frac{1}{q_m K_L C_e} \quad (7)$$

where  $C_e$  is the equilibrium concentration of SDS solution (mg L<sup>-1</sup>),  $q$  is the amount adsorbed by adsorbent (mg g<sup>-1</sup>),  $q_m$  is the maximum amount adsorbed,  $K_L$  a Langmuir's constant signifying energy of adsorption.

**Table 1** Adsorption kinetic parameters of SDS onto SD, SGTL and SBTL adsorbents

Adsorbent	Pseudo first order			Pseudo second order			
	$K_1$ ( $\text{min}^{-1}$ )	$q_e$ ( $\text{mg}\cdot\text{g}^{-1}$ )	$R^2$	$K_2$ ( $\text{g}\cdot\text{mg}^{-1}\cdot\text{min}^{-1}$ )	$q_e$ ( $\text{mg}\cdot\text{g}^{-1}$ )	$R^2$	$q_{\text{exp}}$ ( $\text{mg}\cdot\text{g}^{-1}$ )
SD	0.022	0.579	0.8946	0.017	0.816	0.9553	0.546
SGTL	0.016	0.432	0.6830	0.068	0.960	0.9870	0.911
SBTL	0.025	0.721	0.9306	0.049	0.909	0.9868	0.816

**Table 2** Adsorption isotherm constants for the adsorption of SDS onto SD, SGTL and SBTL adsorbents

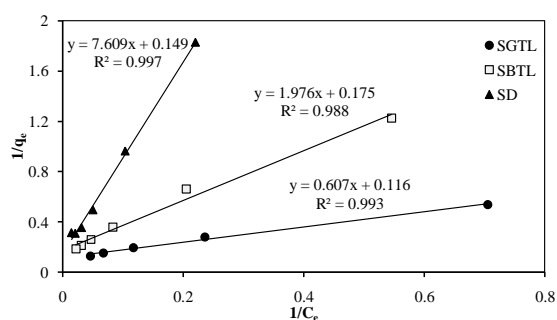
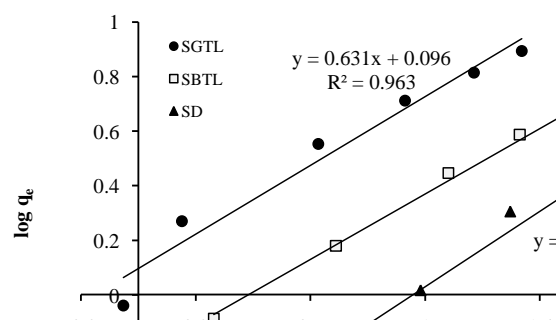
Adsorbent	Freundlich isotherm parameters			Langmuir isotherm parameters			
	$n$	$K_F$	$R^2$	$K_L$ ( $\text{L}\cdot\text{mg}^{-1}$ )	$q_m$ ( $\text{mg}\cdot\text{g}^{-1}$ )	$R^2$	$R_L$
SD	1.44	0.21	0.9511	0.019	6.71	0.9967	0.344
SGTL	1.58	1.24	0.9629	0.191	8.62	0.9930	0.049
SBTL	1.66	0.58	0.9953	0.088	5.71	0.9881	0.102

The values of  $K_L$  and  $q_m$  were calculated from the slope and intercept of the linear plot. The Langmuir model deals with monolayer adsorption and constant adsorption energy. The widely used empirical Freundlich equation based on adsorption on a heterogeneous surface is represented by the following equations:

$$q_e = K_F C_e^{1/n} \quad (8)$$

$$\lg q_e = \lg K_F + \frac{1}{n} \lg C_e \quad (9)$$

where,  $q_e$  is equilibrium adsorption capacity ( $\text{mg}\cdot\text{L}^{-1}$ ),  $C_e$  is the equilibrium or residual concentration ( $\text{mg}\cdot\text{L}^{-1}$ ) of SDS dye in solution, and  $K_F$  and  $1/n$  are empirical parameters indicating adsorption capacity of adsorbent and intensity as

**Figure 7.** Langmuir isotherm obtained for adsorption of SDS**Figure 8.** Freundlich isotherm obtained for adsorption of SDS

well as expression of favorable or unfavorable adsorption process, respectively.  $1/n$  is a dimensionless constant. Its values for a linear, favorable and unfavorable adsorption are 1,  $1/n < 1$  and  $1/n > 1$ , respectively. The values of Freundlich parameters are easily calculated from the slope and intercept of the linear plot of  $\log q_e$  against  $\log C_e$ . The Freundlich equation deals with physicochemical adsorption on heterogeneous surfaces. For a good adsorbent  $n$  is usually between 1 and 10. The adsorption isotherms using both Langmuir and Freundlich equations (linear forms) obtained for removal of SDS have been shown in Figs. 7 and 8, respectively.

The calculated results of the Langmuir and Freundlich isotherm parameters are summarised in Table 2. In the case of SBTL, the correlation coefficient value  $R^2$  obtained shows that the equilibrium data fitted better with the Freundlich model as compared to Langmuir equation under the concentration range studied.

According to the results, the equilibrium data fitted better with the Langmuir model as compared to Freundlich equation under the concentration range studied for SD and SGTL. The essential characteristics of the Langmuir isotherm and the favorable nature of adsorption can also be expressed in terms of a dimensionless constant separation factor ( $R_L$ ), which is defined by the following equation: <sup>41</sup>

$$R_L = \frac{1}{1 + K_L C_0} \quad (10)$$

where;  $K_L$  ( $\text{L}\cdot\text{mg}^{-1}$ ) is the Langmuir constant and  $C_0$  is the highest SDS concentration in solution ( $\text{mg}\cdot\text{L}^{-1}$ ). The values of  $R_L$  indicates the type of isotherm to be irreversible ( $R_L=0$ ), favorable ( $0 < R_L < 1$ ), linear ( $R_L=1$ ) or unfavourable ( $R_L > 1$ ).

#### Effect of temperature and thermodynamic study

The effect of temperature on the adsorption of SDS on SD, SGTL and SBTL was investigated at four temperatures: 298, 308, 323 and 343 K. The adsorption efficiency had a little increase by raising the temperature. This is due to the fact that at high temperature, the diffusion rate of the SDS molecules and their kinetic energy increases through the external boundary layer and internal sites of the adsorbent.



The data obtained at different temperatures can be used to evaluate the thermodynamic parameters. The standard Gibbs free energy change ( $\Delta G^\circ$ ) is the fundamental parameter of spontaneity of a process and can be expressed as:

$$\Delta G^\circ = -RT \ln K_c \quad (11)$$

where  $K_c$  is the adsorption distribution coefficient,  $R$  is the universal gas constant ( $8.314 \text{ J mol}^{-1} \text{ K}^{-1}$ ) and  $T$  is the absolute temperature (K). The standard enthalpy change ( $\Delta H^\circ$ ) and the standard entropy change ( $\Delta S^\circ$ ) were computed from *van't Hoff* equation (Eq. 12).

A plot of  $\ln K_c$  versus  $1/T$  should be straight line. The slope and intercept of the plot gives the values of  $\Delta H^\circ$  and  $\Delta S^\circ$  while  $\Delta G^\circ$  was calculated using fundamental free Gibbs energy equation.<sup>42</sup>

$$\ln K_c = \frac{\Delta S^\circ}{R} - \frac{\Delta H^\circ}{RT} \quad (12)$$

The values associated with the thermodynamic parameters are listed in Table 3. The negative values obtained for  $\Delta G^\circ$  at all investigated temperatures clearly indicate the feasibility of the process and spontaneous nature of the adsorption. Positive values of  $\Delta H^\circ$  indicate the endothermic nature of the process. As the results shown, the positive values of  $\Delta S^\circ$  for all adsorbents confirms the favourable condition for adsorption of anionic surfactant from aqueous solution.

**Table 3** Thermodynamic parameters for adsorption of SDS on SD, SGTL and SBTL

Adsorbent	T (K)	$\Delta G^\circ$ , $\text{kJ mol}^{-1}$	$\Delta H^\circ$ , $\text{kJ mol}^{-1}$	$\Delta S^\circ$ , $\text{J mol}^{-1} \text{ K}^{-1}$
SD	288	-0.1		
	298	-0.4		
	308	-0.7	11.77	41.12
	318	-1.3		
SGTL	288	-4.5		
	298	-5.8		
	308	-7.2	35.17	137.67
	318	-8.7		
SBTL	288	-3.2		
	298	-3.7		
	308	-4.5	19.24	77.43
	318	-5.5		

#### Column study (Breakthrough curves)

Sorption isotherms which are obtained from batch study do not give accurate scale-up data for industrial treatment systems since sorption in a column is not normally in a state of equilibrium.

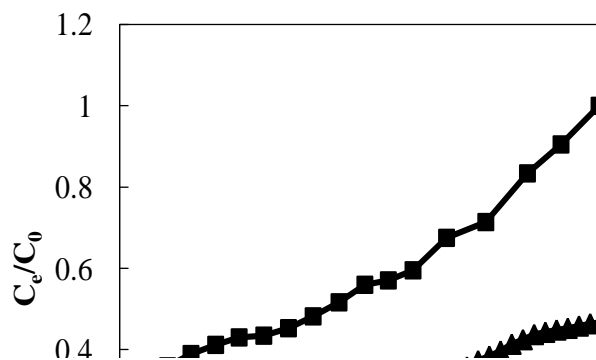


**Figure 9.** Breakthrough curve obtained for removal of SDS using SGTL and SBTL

Consequently, there is a need to perform flow tests using columns to evaluate the performance of adsorbent. The design of packed bed adsorbent in continuous systems, concentration vs. time or volume of solution usually yields as S-shaped curve, at which the solute concentration reaches its maximum allowable value referred to as a breakthrough curve. The point where the effluent solute concentration reaches 95% of its influent value is usually called the point of column exhaustion. For performing this experiment, 1.0 g of adsorbent was packed in a glass column (bed depth=5 cm), and then SDS solution with inlet concentration of  $10 \text{ mg L}^{-1}$  passed through the column with constant flow rate ( $2 \text{ mL min}^{-1}$ ) at  $\text{pH}=6$ . The outlet solution was analyzed for unadsorbed SDS solution. The breakthrough curves obtained for the SGTL and SBTL used for sorption of SDS a column system are shown in Figure 9. As the results show, SGTL was found to be a better adsorbent for SDS removal when used in column system.

To study the influence of flow rate, the SDS solutions were allowed to flow through the adsorbent bed at different flow rates such as 1, 2 and  $5 \text{ mL min}^{-1}$ . The eluents from the column were collected and analyzed for the respective residual SDS concentration. The breakthrough plot of SDS obtained for SGTL at different flow rates is shown in Figure 10. As the results show, with increasing flow rate, the service time and the volume treated were shortened.

The breakthrough analysis was also conducted in the presence of various salts in order to find out the effect of salt on performance of adsorbents toward SDS removal. In this investigation, the breakthrough curves were obtained in the presence of  $\text{AgNO}_3$ ,  $\text{CuSO}_4$  and  $\text{CaCl}_2$  salts with concentration of 0.01 M. The other conditions were the same as described for Figure 9. As the results indicate, among the salts used, SDS removal has been affected by the presence of silver ion considerably (Figure 11). The other salts had not any important effect on the performance of the spent tea leaves for SDS removal.

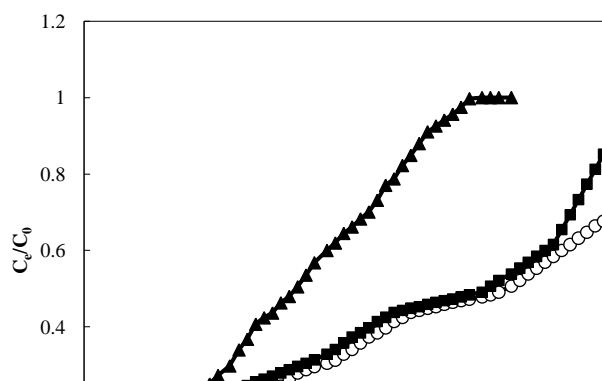


**Figure 10.** Breakthrough curves for the adsorption of SDS onto SGTL at different flow rates

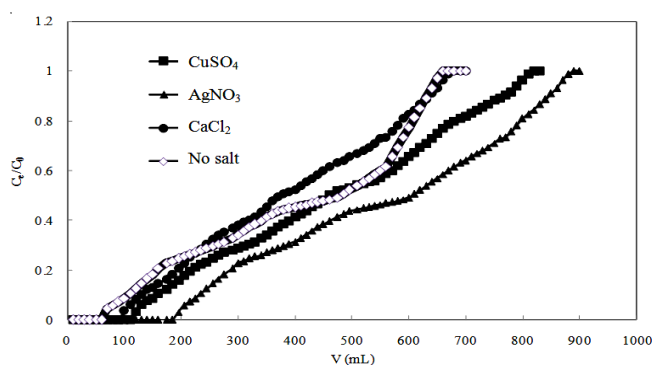


**Figure 11.** Breakthrough curves for the adsorption of SDS onto SGTL at different salt solution

## Conclusion

Three adsorbents sawdust, spent green tea leaves and spent black tea leaves were used for SDS removal. Among the examined adsorbents in this study, SGTL showed maximum removal efficiency. Both Langmuir and Freundlich isotherms for all adsorbents depicted and  $q_m$  values were compared. In batch study the optimum adsorbent dose and equilibrium time were found to be 0.50 g and 2 h, respectively. Under optimized conditions 93.6%, 75.4% and 53% SDS could be removed from wastewater with SGTL, SBTL and SD, respectively. According to results spent green tea leaves (SBTL) showed the highest performance for SDS removal from aqueous solutions. However, in column system, SGTL was found to be more efficient. Spent tea leaves seem to be efficient and very cost effective adsorbents for removal of SDS from aqueous solutions.

## Acknowledgment

Partial support of this study by the Research Council of University of Guilan is acknowledged.

## References

<sup>1</sup>Levine, L. H., Garland J. L., Johnson J. V., *J. Chromatogr. A*, **2005**, 1062, 217.  
<sup>2</sup>Dhouib, A., Hdiji, N., Hassairi, I., Sayadi, S., *Process. Biochem.*, **2005**, 40, 2715.

<sup>3</sup>Cullum, D. C., *Introduction to Surfactant Analysis*, Blackie Academic & Professional, **1994**.  
<sup>4</sup>Porter, M. R., *Handbook of Surfactants*, Blackie Academic & Professional, **1991**.  
<sup>5</sup> Amat, A. M., Arques, A., Miranda, M. A., Sequi, S., *Solar Energy*, **2004**, 77, 559.  
<sup>6</sup> Lewis, M. A., *Water Res.*, **1992**, 26, 1013.  
<sup>7</sup>Mathur, A. K., Gupta, B. M., *Ind. J. Environ. Prot.*, **1998**, 18, 90.  
<sup>8</sup>Whiting V. K., Cripe G. M., Lepo J. E., *Arch. Environ. Contam. Toxicol.*, **1996**, 31, 293.  
<sup>9</sup>Gonza, ilez .S, Petrovic, M., Barcelo, D., *Chemosphere*, **2007**, 67, 335.  
<sup>10</sup> Yüksel, E., Ayhan, Ş. İ., Özacar, M., *J. Chem. Eng.*, **2009**, 152, 347.  
<sup>11</sup>Mezzanotte, V., Castiglioni, F., Todeschini, R., Pavan, M., *Bioresour. Technol.*, **2003**, 87, 87.  
<sup>12</sup>Garcia, M. T., Ribosa, I, Guindulain, T., Sanchez, L. J., *J. Environ. Pollut.* **2001**, 111, 169.  
<sup>13</sup>Scott, M. J., Jones, M. N., *Biochem. Biophys. Acta*, **2000**, 1508, 235.  
<sup>14</sup>Dhouib, A., Hamad, N., Hassairi, I., Sayadi, S., *Process Biochem.*, **2003**, 38, 1245.  
<sup>15</sup>Somasundaran, P., Huang, L., *J. Adv. Colloid Interface Sci*, **2000**, 88, 179.  
<sup>16</sup>Musselman, S. W., Chander, S., *J. Colloid Interface Sci.*, **2002**, 256, 91.  
<sup>17</sup>Li, F., Rosen, M. J., *J. Colloid Interface Sci*, **2000**, 224, 265.  
<sup>18</sup>Adak, A., Bandyopadhyay, M., pal, A., *J. Colloids surfaces A: Physicochem. Eng. Aspects*, **2005**, 254, 165.  
<sup>19</sup>Adak A., Bandyopadhyay M., Pal A., *J. Environ. Sci. Health. A. Tox. Hazard. Subst. Environ. Eng*, **2005**, 40, 167.  
<sup>20</sup>Gonzalez-Garcia, C. M., Gonzalez-Martin, M. L., Denoyel, R., Gallardo-Moreno, A. M., *J. Colloid Interface Sci*, **2004**, 278, 257.  
<sup>21</sup>Chiming, M., Chenglong, L., *J. Colloid Interface Sci*, **1989**, 131, 485.  
<sup>22</sup>Wenzhi, H., Haddad, P. R., *Anal. Commun*, **1998**, 35, 191.  
<sup>23</sup>Basar, C. A., Karagunduz, A., Cakici, A., Keskinler, B., *Water Research*, **2004**, 38, 2117.  
<sup>24</sup>Kuei, C., Yeh, J., *J. Environ. Sci. Health (Part A)* **2003**, 38, 1145.  
<sup>25</sup>Atia, A. A., Radwan, A. A., *Adsorption Sci. Technol*, **1997**, 15, 619.  
<sup>26</sup>Lunkenheimer, K., Fruhner, H., Theil F., *Colloids Surf.*, **1993 A**, 76, 289.  
<sup>27</sup>Rouquerol, J., Partylra, S., *J. Chem. Tech. Bio-Tech*, **1981**, 31, 584.  
<sup>28</sup>Khan, M. N., Zareen, U., *J. of Hazard. Mater.*, **2006**, 133, 269.  
<sup>29</sup>Purakayastha, P. D., Pal A., *J. Environ. Sci. Health*, **2001 A**, 37, 925.  
<sup>30</sup>Beltran, F. J, Garcia-Araya, J. F, Alvarez, P. M, *Ind. Eng. Chem. Res*, **2000**, 39, 2214.  
<sup>31</sup>Tianyong, Z., Toshiyuki, O., Satoshi, H., Jincal Z., Nick S., Hisao H., *Appl Catal. B: Environ*, **2003**, 42, 13.  
<sup>32</sup>Sheng, H. L., Lin, C. M., Leu, H. G., *Water Res.*, **1999**, 33 (7) 1735.  
<sup>33</sup>Suárez-Ojeda, M. E., Kimb, J., Carrera, J., Metcalf, I. S., Font, J., *J. Hazard. Mater*, **2007**, 144, 655.  
<sup>34</sup>Kong, W., Wang, B., Ma, H., Gu, L., *J. Hazard. Mater. B*, **2006**, 137, 1532.

- <sup>35</sup>Lissens, G., Pieters, J., Verhaege, M., Pinoy, L., Verstraete, W., *Electrochim. Acta*, **2003**, *48*, 1655.
- <sup>36</sup>APHA-AWWA-WPCF, *American Public Health Association*, New York, **1989**.
- <sup>37</sup>Ansari, R., Mosayebzadeh, Z., Mohammad-khah, A., *J. Ads Sci Res*, **2011**, *2(3)*, 25.
- <sup>38</sup>Lagergren, S., *Kungliga Svenska Vetenskapsakad Handlingar*, **1898**, *24*, 1.
- <sup>39</sup>Ho, Y. S., McKay, G., *Process Biochem.* **1999**, *34(5)* 451.
- <sup>40</sup>Bulut, E., Özacar, M., Şengil, İ. A., *J. Hazard. Mater.*, **2008**, *154*, 613.
- <sup>41</sup>Benfield, L. D., Randall, C. W., Prentice-Hall Inc. **1980**.
- <sup>42</sup>Ansari, R., and Dezhampannah, H., *Eur. Chem. Bull.* **2013**, *2(4)* 220.

Received: 11.01.2013.

Accepted: 30.01.2013.





# CO<sub>2</sub> CAPTURE FROM COAL FIRED ELECTRIC POWER GENERATION IN CHINA

Zhang Yongmei<sup>[a]\*</sup>

**Keywords:** CO<sub>2</sub>; capture; coal fired electric power generation; china

Nowadays environmental issues due to emission of greenhouse gases such as CO<sub>2</sub> are discussed. CO<sub>2</sub> capture has also been introduced. Large amount of CO<sub>2</sub> is discharged from Chinese coal fired electric power generation, so CO<sub>2</sub> capture is mainly studied in order to protect the environment. Four types of CO<sub>2</sub> capture technologies such as decarbonation before burning, CO<sub>2</sub> capture after burning, oxygen-rich technologies and chemical looping combustion have been discussed. CO<sub>2</sub> capture is improved by using the above methods. The complete development of CO<sub>2</sub> capture technologies has resulted in good economic and social benefits around the world.

\* Corresponding Author

Fax: 86-24-56860869

E-Mail: zh6688551@163.com

[a] Liaoning Shihua University, Fushun, Liaoning, P.R. China.

## Introduction

More and more people around the world are paying attention to the effect of greenhouse gases (CO<sub>2</sub>, CH<sub>4</sub>, NO<sub>x</sub>, hydrofluorocarbon, perfluorocarbon and SF<sub>6</sub>) on the environment. The effects of global warming mainly come from CO<sub>2</sub>. Chinese Government promises to reduce 40 – 45 % of the amount of CO<sub>2</sub> emissions by 2020 based on 1.8 billion tons of CO<sub>2</sub> discharge in 2005.<sup>1</sup> Ratio of coal used as a fuel to other energies is 7 : 3 in China. Furthermore, coal used to generate electricity is above half of total coal consumption. Coal fired electric power generation is one of the main source of CO<sub>2</sub> discharge places in China, so it is very important to control the amount of CO<sub>2</sub> discharge from the coal fired electric power generation.<sup>2</sup>

In the present paper, four types of CO<sub>2</sub> capture technologies such as decarbonation before burning, CO<sub>2</sub> capture after burning, oxygen-rich technologies and chemical looping combustion are discussed. Furthermore, the optimal CO<sub>2</sub> capture method has been also pointed out.

## Discussion

### Decarbonation before burning

Wang Xiaoliang<sup>3</sup> introduced the reaction principle of decarbonation before burning. It meant using the appropriate method to get rid of carbon from a feedstock before burning, and then carbon with energy was separated with other materials in order to take off carbon from the feedstock. An integrated gasification combined cycle (IGCC) is a technology that uses a gasifier to turn coal and other carbon based fuels into gas—synthesis gas (syngas)<sup>4</sup>. Integrated gasification combined cycle systems were advanced type systems. They consisted of air separation unit, gasifier, syngas purification units, water gas shift reactors and CO<sub>2</sub> separation unit. Combined cycle systems encompassed combustor, compressor, heat recovery steam generator and steam turbine, etc. Figure 1 showed an image for an integrated combined gasification.

Coal was sent to a rod mill to produce slurry, which was pumped into a gasifier to burn and generate syngas whose content was CO and H<sub>2</sub>. Syngas was transported to a reforming unit where it was transferred into CO<sub>2</sub> and H<sub>2</sub>. Furthermore, CO<sub>2</sub> and H<sub>2</sub> were separated. H<sub>2</sub> was burnt at a combustor, so this is the best way to reach zero discharge. This system not only got rid of H<sub>2</sub>S but also decreased investment expenditures and operating fees.

### CO<sub>2</sub> capture after burning

CO<sub>2</sub> capture after burning meant that CO<sub>2</sub> was separated from flue gas. Three types of methods for separating CO<sub>2</sub> were the chemical absorption method, the membrane separation method and the cryodistillation.<sup>5</sup> The solvent absorption method is one of the most popular chemical methods in the chemical plant. Figure 2 presented a diagram for CO<sub>2</sub> capture after burning.<sup>6</sup> These have the advantages of the solvent absorption method, adding CO<sub>2</sub> to capture unit without changing original units and widely used at coal fired electric power generation. On the other hand, this method had a lot of disadvantages such as consuming a lot of solvent, pretreating flue gas (getting rid of S, NO<sub>x</sub> and particles) before CO<sub>2</sub> capture, getting more volume of flue gas due to the existence of nitrogen, investing more money because of CO<sub>2</sub> capture and requiring high energy for separating CO<sub>2</sub> at high - pressure and high - temperature. Although CO<sub>2</sub> capture after burning was very good, it was very difficult to use this method in chemical plants due to poor profits.

### Oxygen-rich technologies

Wang Xiaoliang<sup>3</sup> introduced the principle of oxygen-rich technologies and compared between burning coal in an oxygen-rich environment and conventional coal combustion. The content of CO<sub>2</sub> in the flue gas was between 8 % and 16 % during the conventional coal combustion. It was very difficult to separate CO<sub>2</sub> due to low content of CO<sub>2</sub> in the flue gas and more investments were required. How to increase the content of CO<sub>2</sub> in the flue gas was one of the important factors to decrease the energy of CO<sub>2</sub> capture. Oxygen-rich technologies also called combustion in an O<sub>2</sub>/CO<sub>2</sub> mixture or an air separation/ flue gas recycle technology. High purity oxygen obtained by using the air separation and partial flue gas instead of air reacted with coal, so the content of CO<sub>2</sub> in the flue gas was improved.

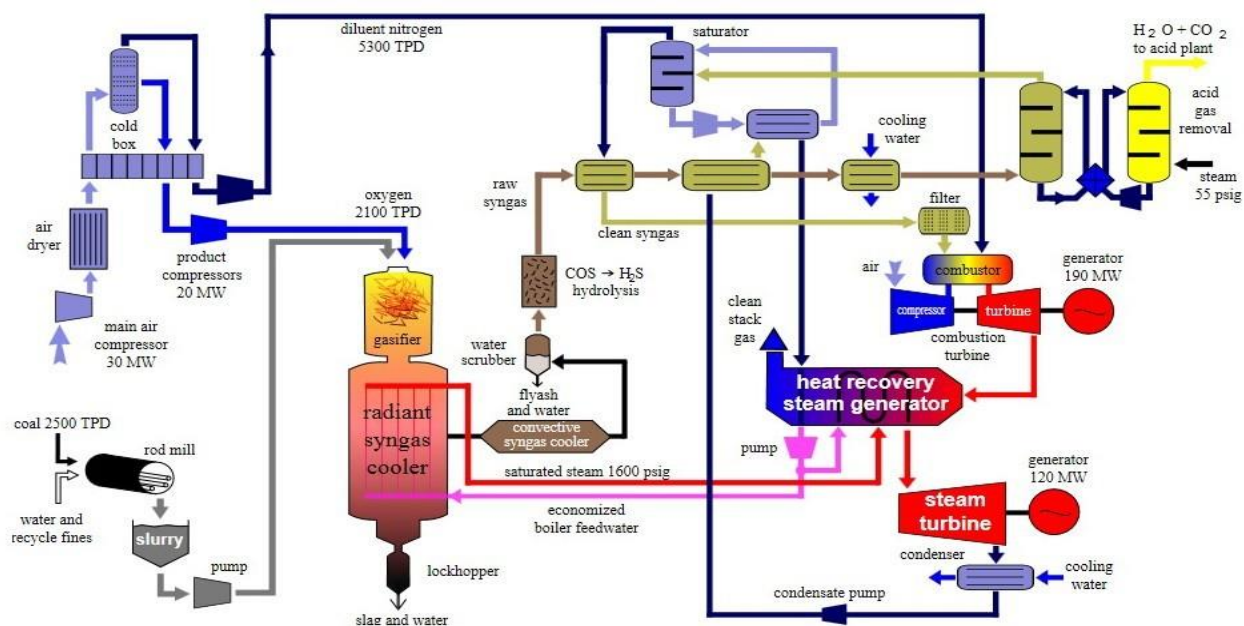


**Figure 1.** An integrated gasification combined cycle

Reusing the flue gas adjusted the boiler's temperature. At the same time the boiler thermal efficiency was increased due to reusing the flue gas instead of nitrogen in the air. Oxygen-rich technologies not only got high purity oxygen but also controlled coal pollution.

They are new type of coal burning technologies. Oxygen-rich technologies consisted of four types of combustion technologies such as aerobic combustion, oxygen combustion, oxy-fuel combustion and air-oxygen combustion. These advantages for oxygen-rich technologies were listed as follows. The content of

CO<sub>2</sub> in the flue gas reached 95 % and CO<sub>2</sub> was directly liquefied to recovery without the flue gas separation. High purity SO<sub>2</sub> existed in the boiler due to reusing the flue gas, so it improved desulfuration efficiency. The amount of the flue gas discharge was decreased about 80 % due to reusing the flue gas, so the heat loss was decreased and the boiler efficiency was improved. The radiant efficiency for burning coal in an oxygen-rich environment is better than that of the conventional coal combustion because high purity CO<sub>2</sub> and H<sub>2</sub>O in the boiler made the flue gas have high specific heat and radiation coefficient. Figure 3 showed an image for oxygen-rich technologies.

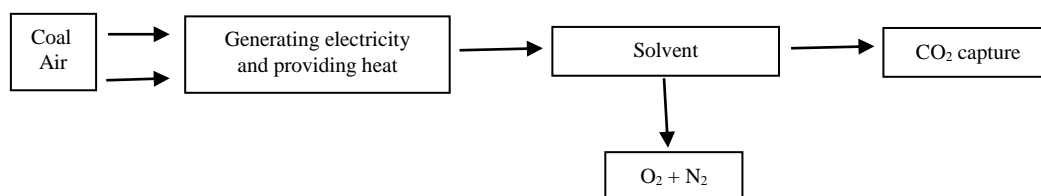


**Figure 2.** General scheme of CO<sub>2</sub> capture after burning

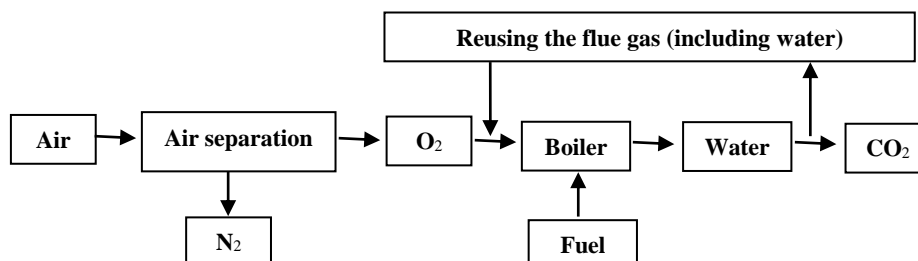
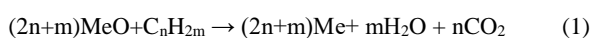


**Figure 3.** General scheme of oxygen-rich technologies

### Chemical looping combustion

Lyngfelt<sup>7</sup> discussed the principle of the chemical looping combustion. The chemical looping combustion was a new type of the burning method. It broke the conventional combustion method. The chemical looping combustion did not directly burn fuel with O<sub>2</sub> in the air. Oxygen carriers (metallic oxides) were used to move between the air reactor and the fuel reactor so the chemical energy from fuel was released. Figure 4 presented a diagram for chemical looping combustion. The fuel was pumped into the fuel reactor and reacted with metallic oxides (MeO). Eqn. (1) was written as follows. CO<sub>2</sub> and H<sub>2</sub>O were discharged from the top of the fuel reactor. High purity CO<sub>2</sub> was almost obtained when H<sub>2</sub>O was condensed. The reduced metal oxide (Me) was transported from the fuel reactor to the air reactor. Me reacted with O<sub>2</sub> in the air reactor, so Me was reused several times. Eqn. (2) was written as follows.



These are having the advantages of the chemical looping combustion, such as getting high purity CO<sub>2</sub>, increasing combustion efficiency due to two step chemical reactions and decreasing the heat loss and effectively controlling the produced NO<sub>x</sub> and its discharge.

### Conclusion

Based on the above discussion and review, four types of CO<sub>2</sub> capture technologies such as decarbonation before burning, CO<sub>2</sub> capture after burning, oxygen-rich technologies and chemical looping combustion have been introduced. The decarbonation before burning is one of best ways because H<sub>2</sub> is produced to burn at a combustor and this way, probably, reaches zero discharge. Furthermore, this system not only gets rid of H<sub>2</sub>S but also decreases investment expenditures and operating fees. CO<sub>2</sub> capture after burning is one of the worst methods because chemical plants obtain less income.

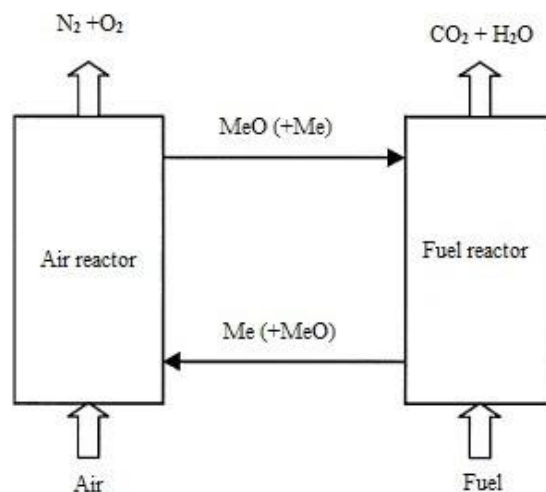


Figure 4. Diagram of chemical looping combustion

### References

- <sup>1</sup>Yang, H. Q., Xu, Z. H. and Fan, M. H., *J. Environ. Sci.*, **2008**, 20, 14.
- <sup>2</sup>Huang, B., Liu, L. B. and Xu, S. S., *Electrical Equip.*, **2008**, 19(5), 3.
- <sup>3</sup>Wang, X. L., Wu, J. H. and Zhao, Q., *Dongfang Electrical Rev.*, **2011**, 25(98), 1.
- <sup>4</sup>[http://en.wikipedia.org/wiki/integrated\\_gasification\\_combined\\_cycle](http://en.wikipedia.org/wiki/integrated_gasification_combined_cycle).
- <sup>5</sup>Olajire, A. A., *Energy*, **2010**, 35(6), 2610.
- <sup>6</sup>Zhang, H., Re, H. W., Lu, J. G. and Ji, Y., *J. Nanjing Univ. Inform. Sci. Technol.*, **2009**, 1(2), 129.
- <sup>7</sup>Lyngfelt, A., Leckner, B. and Mattisson, T., *Chem. Eng. Sci.*, **2001**, 56, 3101.

Received: 10.12.2012.

Accepted: 31.01.2013.



# EFFECT OF CITRATE IONS ON THE ELECTROCHEMICAL BEHAVIOUR OF MILD STEEL IN TIPA – Zn<sup>2+</sup> SYSTEM (TIPA=TRIIISOPROPANOLAMINE)

Y. Brightson Arul Jacob<sup>[a],\*</sup>, R. Sayee Kannan<sup>[b]</sup>, J. Jeyasundari<sup>[c]</sup>

**Keywords:** Electrochemical study, Corrosion inhibition, Triisopropanolamine, Trisodium citrate, FTIR spectra.

The inhibition efficiency (IE) of various concentrations of a TIPA(triisopropanolamine)-TSC(trisodium citrate)-Zn<sup>2+</sup> system in controlling corrosion of mild steel immersed in aqueous solution containing 60 ppm Cl<sup>-</sup> was evaluated by a weight loss study. The formulation consisting of 100 ppm of TIPA and 50 ppm of Zn<sup>2+</sup> showed 62% inhibition efficiency. When TSC (250 ppm) is added the inhibition efficiency increases to 100%. In the presence of TSC has excellent inhibition efficiency. Polarization studies reveal that TIPA-TSC-Zn<sup>2+</sup> function as an anodic inhibitor. AC impedance spectra suggest that a protective film is formed on the metal surface. FTIR spectra reveal that the protective film consists of Fe<sup>2+</sup> - TIPA, Fe<sup>2+</sup> - TSC complex and Zn(OH)<sub>2</sub>.

## Corresponding Authors

\*E-Mail: brightson\_hai@yahoo.co.in

- [a] Department of chemistry, NMSSVN College, Madurai-625019, Tamilnadu, India  
 [b] Department of Chemistry, Thiagarajar College, Madurai-625009, Tamilnadu, India, Email:rsamkannan@yahoo.co.in  
 [c] Department of chemistry, NMSSVN College, Madurai-625019, Tamilnadu, India, Email: jjsundari16@yahoo.com

cases, it appears that adsorption inhibitors affect both the anodic and cathodic process although in many cases the effect is unequal.<sup>7</sup>

## Materials and Methods

### Sample Preparation

Carbon steel specimens (0.026% S, 0.067 % P, 0.4% Mn, 0.1% C and the rest iron) of the dimensions 1.0 cm x 4.0 cm x 0.2 cm were polished to mirror finish and degreased with Acetone and used for weight loss method.

### Weight Loss Method

Mild steel specimens in triplicate were immersed in 100 ml of aqueous solution containing 60 ppm Cl<sup>-</sup> and various concentrations of Triisopropanolamine in the presence and absence of Zn<sup>2+</sup> (as ZnSO<sub>4</sub>.7H<sub>2</sub>O) for a period of one day. The corrosion products were cleaned with Clark's solution.<sup>8</sup> The weight of the specimens before and after immersion was determined using Shimadzu balance AY62. The corrosion inhibition efficiency was calculated with

$$IE(\%) = 100 \left( 1 - \frac{W_2}{W_1} \right) \quad (1)$$

Where W<sub>1</sub> is the corrosion rate in the absence of the inhibitor and W<sub>2</sub> is the corrosion rate in the presence of inhibitor. From the weight loss, the corrosion rates was calculated ρ- density of the metal is g cm<sup>-3</sup>.

### Electrochemical Study

Polarization studies were carried out using a CHI electro chemical impedance analyzer, model 660 A. A three electrode cell assembly was used. The working electrode was a rectangular specimen of mild steel with one face of electrode (1 cm<sup>2</sup> area) exposed and the rest shielded with red

## Introduction

Studies on the corrosion of metals in organic medium have attracted considerable interest in recent years due to their wide applications. It has been reported that the overvoltage for the cathodic reaction on metals in contact with such medium is lower than to the aqueous medium. Hence it causes accelerated, uniform and localized types of corrosion attack. It has been found earlier that the corrosion caused by the aqueous organic solvents can be effectively controlled by the use of corrosion inhibitors for a system can not only extend the life of the reaction vessels in use but could also enable the use of a less expense.<sup>1-5</sup>

Therefore, in this investigation, the authors have chosen mild steel to study corrosion inhibition, in contact with a very important aqueous organic medium petroleum having acetic acid and NaCl, Amines that are reported as good organic inhibitor for aqueous acid solutions have been used as inhibitor in this study. The aim of our study was to propose surface protection that will be able both to act in the corrosive medium having petroleum, and to have a tumble rule to chosen a best chemical structure for such mediums.

In previous work the mode of action of some alkyl amines to protect of mild steel was studied. It was shown that two intermediates adsorbed on the steel surface. Because these amines are different in attached groups, we choose to investigate the electrochemical corrosion behavior of carbon steel inhibited by amines with different structures.<sup>6</sup>

These organic compounds adsorb on the metal surface and suppress metal dissolution and reduction reactions. In most



lacquer. A saturated calomel electrode (SCE) was used as the reference electrode and a rectangular platinum foil was used as the counter electrode. Polarization curves were recorded using iR compensation. The results, such as tafel slopes and  $I_{\text{corr}}$ ,  $E_{\text{corr}}$ , and LPR values were calculated. During the Polarization study, the scan rate (V/S) was 0.01, hold time at E f(s) was zero, and quit time (s) was 2.

### AC impedance measurement

A time interval of 5 to 10 minutes was give for the system to attain a steady state open circuit potential. The AC frequency was varied from 100 mHZ to 100 Khz. The real part ( $Z'$ ) and imaginary part ( $Z''$ ) of the cell impedance were measured in ohms for various frequencies. The  $R_t$ (charge transfer resistance) and  $C_{dl}$  (double layer capacitance) were calculated.  $C_{dl}$  values were calculated by using the following relationship.

$$C_{dl} = \frac{1}{2\pi R_t f_{\text{max}}} \quad (2)$$

### FT-IR spectra

These spectra were recorded in a perki-Elmer 1600spectrophotometer. The film was carefully removed, mixed thoroughly with Kbr and made in to pellets and the FTIR spectra were recorded

## Results and Discussion

### Analysis of the Weight Loss Method

Corrosion rates (CR) of mild steel(MS) immersed in aqueous solution containing 60 ppm Cl<sup>-</sup> in the absence and presence of inhibitors triisopropanolamine, Zn<sup>2+</sup>, trisodium citrate are given in Table 1-3. The inhibition efficiencies (IE) are also given in this table. It is observed from table 1 that triisopropanolamine(TIPA) shows some inhibition efficiency of 47%. 100 ppm of TIPA and 50 ppm of Zn<sup>2+</sup> shows 63% inhibition efficiency. After the addition of trisodium citrate(TSC) 250 ppm the increase in inhibition efficiency of the system (TIPA + TSC+ Zn<sup>2+</sup>) is 100% IE.

**Table 1.** Corrosion rates of (CR mdd) mild steel immersed in an aqueous solution containing 60 ppm of Cl<sup>-</sup> and the inhibition efficiencies (IE %) obtained by weight loss method (pH=8.2)

Cl <sup>-</sup> ppm	TIPA ppm	IE %	CR mdd
60	50	28	8.12
60	100	47	13.34
60	150	31	8.99
60	200	31	8.99
60	250	25	7.25

**Table 2.** Corrosion rates (CR mdd) mild steel immersed in an aqueous solution containing 60 ppm Cl<sup>-</sup> and the inhibition efficiencies (IE%) obtained by weight loss method (pH=8.2)

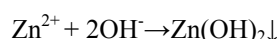
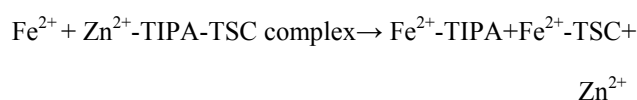
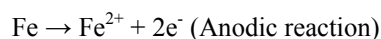
Cl <sup>-</sup> ppm	TIPA ppm	Zn <sup>2+</sup> ppm	IE %	CR mdd
60	0	0	-	29
60	0	50	23	6.67
60	50	50	18	5.04
60	100	50	63	18.13
60	150	50	38	10.8
60	200	50	34	10
60	250	50	18	5.22

**Table 3.** Corrosion rates (CR mdd) mild steel immersed in an aqueous solution containing 60 ppm Cl<sup>-</sup> and the inhibition efficiencies (IE%) obtained by weight loss method (pH=8.2)

Cl <sup>-</sup> ppm	TIPA ppm	Zn <sup>2+</sup> ppm	TSC ppm	IE %	CR mdd
60	100	50	50	68.75	9.06
60	100	50	100	87.50	3.62
60	100	50	150	97.81	0.63
60	100	50	200	96.80	0.92
60	100	50	250	100	-

### Influence of TSC on the inhibition efficiencies of TIPA

The inhibitory<sup>17</sup> and co-inhibitory effect<sup>18</sup> of trisodium citrate has been described recently. The influence of TSC on the inhibition efficiencies of TIPA + Zn<sup>2+</sup> system is given in table 3. It is observed that as the concentration of TSC increases the IE increases. It is also observed that a synergistic effect exists between TSC and TIPA + Zn<sup>2+</sup> system. For example 100 ppm of TIPA, 50 ppm of Zn<sup>2+</sup> and 250 ppm of TSC has 100% IE. On the metal surface Fe<sup>2+</sup>-TIPA complex and Fe<sup>2+</sup>-TSC complex is formed on the anodic sites of the metal surface. Thus the anodic reaction is controlled. The cathodic reaction is the generation of OH<sup>-</sup>, which is controlled the formation of Zn(OH)<sub>2</sub> on the cathodic sites of the metal surface. Thus the anodic reaction and cathodic reaction are controlled effectively. This accounts for the synergistic effect existing between TIPA-Zn<sup>2+</sup> and TSC.



### Corrosion Measurement

Polarization study has been to confirm the formation of protective film formed on the metal surface during corrosion inhibition process.<sup>9-14</sup> If a protective film is formed on the metal surface. The linear polarization resistance value (LPR) increases and the corrosion current value ( $I_{\text{corr}}$ ) decreases.

The potentiodynamic polarization curves of mild steel immersed in aqueous solution containing 60 ppm Cl<sup>-</sup> in the absence and presence of inhibitors are shown in figure 1. The corrosion parameters are given in table 4. When mild steel was immersed in 60 ppm Cl<sup>-</sup> the corrosion potential was -583mV versus SCE. When TIPA (100 ppm), Zn<sup>2+</sup> (50 ppm) and TSC (250 ppm) were added to the above system, the corrosion potential shifted to the noble side -436 mV versus SCE. This indicates that a film is formed on the anodic sites of the metal surface. This film controls the anodic reaction of metal dissolution by forming Fe<sup>2+</sup>-TIPA, Fe<sup>2+</sup>-TSC complex on the anodic sides of the metal surface. The formation of protective film on the metal surface is further supported by the fact that the anodic Tafel slope ( $b_a$ ) increases from 170 to 197 mV. Further, the LPR value increases from  $1.693 \times 10^4$  ohm cm<sup>2</sup> to  $4.6 \times 10^4$  ohm cm<sup>2</sup>. The corrosion current decreases from  $1.873 \times 10^{-10}$  A cm<sup>-2</sup> to  $7.54 \times 10^{-7}$  A cm<sup>-2</sup>. Thus Polarization study confirm the formation of a protective film on the metal surface

**Table 4.** Corrosion parameters of mild steel immersed in A obtained from polarization study

System	$E_{corr}$ mV*	$b_a$ mV**	$b_c$ mV**	LPR $\Omega$ cm <sup>2</sup>	$I_{corr}$ A cm <sup>-2</sup>
A	-583	127	170	$1.693 \times 10^4$	$1.873 \times 10^{-10}$
A+B	-436	135	197	$4.6 \times 10^4$	$7.54 \times 10^{-7}$

A=Aqueous solution containing 60 ppm Cl<sup>-</sup>; B= TIPA (100 ppm); Zn<sup>2+</sup> (50 ppm); TSC (250 ppm); \*mV vs SCE; \*\* mV in one decade.

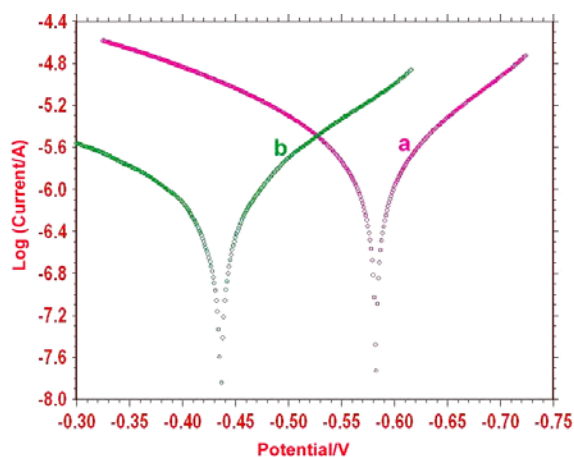


**Figure 1.** Polarization curves of MS is immersed in a) 60 ppm Cl<sup>-</sup> (Blank) b) TIPA (100 ppm) + Zn<sup>2+</sup> (50 ppm) + TSC (250 ppm)

### Analysis of AC impedance spectra

AC impedance spectra (electro chemical impedance spectra) have been used to confirm the formation of protective film on the metal surface. If a protective film is formed on the metal surface, charge transfer resistance ( $R_t$ ) increases, double layer capacitance value ( $C_{dl}$ ) decreases, and the impedance  $\log(Z \text{ ohm}^{-1})$  value increases. The AC impedance spectra of mild steel immerse in an aqueous solution containing 60 ppm Cl<sup>-</sup> in the presence and absence of inhibitors (TIPA – Zn<sup>2+</sup> -TSC) are shown in figure-2 (a) and (b) (Nyquist Plots) and figure - 3a and 3b (Bode plots). The AC impedance parameter, namely, charge transfer resistance ( $R_t$ ) and double layer capacitance ( $C_{dl}$ ) derived from Nyquist plots are given in table 5.

It is observed that when the inhibitors (TIPA (100 ppm) - Zn<sup>2+</sup> (50 ppm) –TSC (250 ppm) are added the charge transfer resistance ( $R_t$ ) increases from  $3149 \text{ cm}^2$  to  $2398 \text{ cm}^2$ . The  $C_{dl}$  value decreases from  $5.07 \times 10^{-7} \text{ F cm}^{-2}$  to  $6.66 \times 10^{-10} \text{ F cm}^{-2}$ . The impedance value [ $\log(Z \text{ ohm}^{-1})$ ] increases from 3.3411 to 3.4620. These results lead to the conclusion that a protective film is formed on the metal surface.

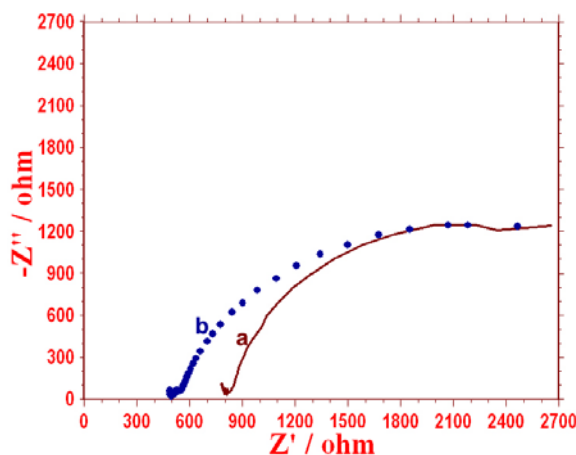


**Figure 2.** AC impedance spectra(Nyquist plot) of MS immersed in a) 60 ppm Cl<sup>-</sup> (Blank) b) TIPA (100 ppm) + Zn<sup>2+</sup> (50 ppm) + TSC (250 ppm)

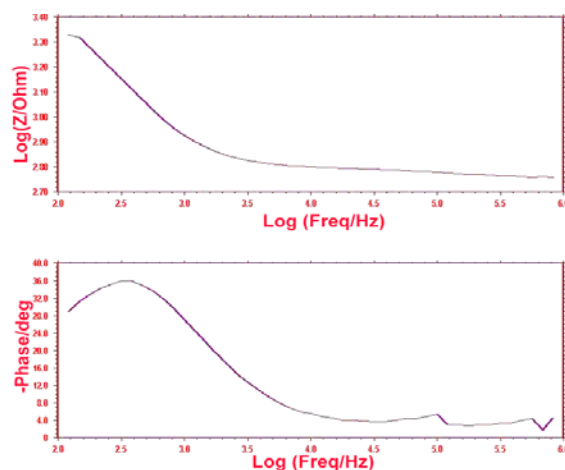


**Figure 3a.** AC impedance spectra of MS immersed in various test solutions (Bode Plot) a) 60 ppm Cl<sup>-</sup>(Blank)

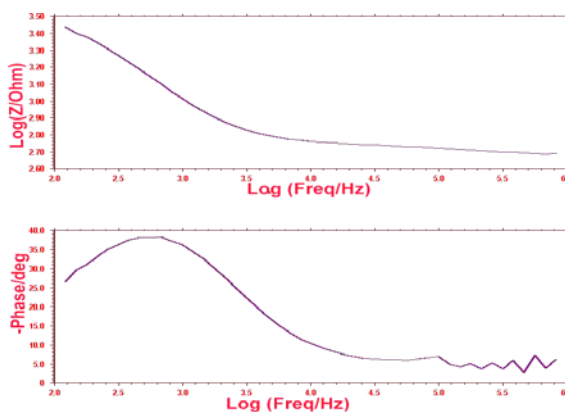


**Figure 3b.** AC impedance spectra of MS immersed in various test solutions (Bode Plot) a) TIPA (100 ppm) + Zn<sup>2+</sup> (50 ppm) + TSC (250 ppm)

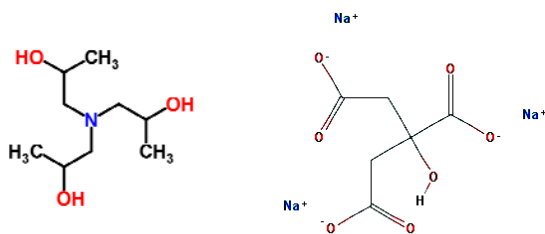
**Table 5.** Corrosion parameters of mild steel immersed in aqueous solution containing 60 ppm Cl<sup>-</sup> obtained by AC impedance spectra.

System	R <sub>t</sub> ohm cm <sup>2</sup>	C <sub>dl</sub> F cm <sup>-2</sup>	Impedance [log(Z ohm <sup>-1</sup> )]
A	3149	5.07×10 <sup>-7</sup>	3.3411
A+B	2398	6.66×10 <sup>-10</sup>	3.4620

A= Aqueous solution containing 60 ppm Cl<sup>-</sup>; B= TIPA (100 ppm); Zn<sup>2+</sup> (50 ppm); TSC (250 ppm)

### FT-IR spectra

FT-IR spectra of TIPA+ Zn<sup>2+</sup> is shown in figure 4a. The –NH stretching and –OH stretching frequency have overlapped and appear at 3350 cm<sup>-1</sup>. The –CN stretching frequency appears 1042 cm<sup>-1</sup>. The FTIR spectra of film formed on the metal surface after immersion in solution containing 60 ppm Cl<sup>-</sup>, 100 ppm of TIPA and 50 ppm Zn<sup>2+</sup>, 250 ppm of TSC is shown in figure 4b. The –OH stretching frequency has shifted from 3350 cm<sup>-1</sup> to 3427 cm<sup>-1</sup>. The CN stretching frequency has shifted 1042 cm<sup>-1</sup> to 1115 cm<sup>-1</sup>. This suggest that TSC and TIPA coordinated with Fe<sup>2+</sup> through their polar groups resulting in the formation of Fe<sup>2+</sup>-TSC complex and Fe<sup>2+</sup>-TIPA complex. The peak at 1416 cm<sup>-1</sup> is due to Zn-O stretching.<sup>15-16</sup> The –OH stretching frequency appears at 3427 cm<sup>-1</sup>. The C=O stretching frequency of TSC has shifted from 1599 cm<sup>-1</sup> to 1562 cm<sup>-1</sup>. This shift indicates that the carboxyl oxygen atom was coordinated to Fe<sup>2+</sup> results in the formation of Fe<sup>2+</sup>-TSC complex on the anodic sites of the metal surface. These results suggest the formation of Zn(OH)<sub>2</sub> on cathodic sites of the metal surface.



**Scheme 1.** Triisopropanolamine    **Scheme 2.** Trisodiumcitrate

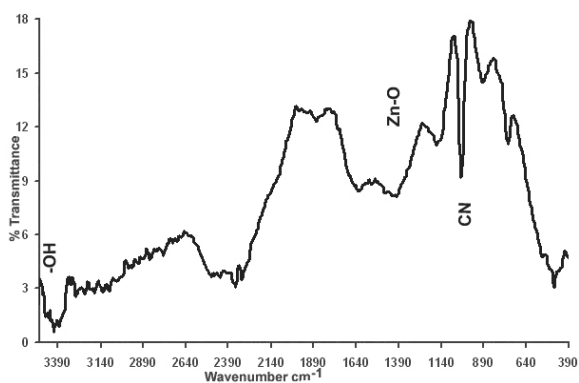


**Figure 4a.** Aqueous solution containing 60 ppm of Cl<sup>-</sup> + 100 ppm of TIPA + 50 ppm of Zn<sup>2+</sup>

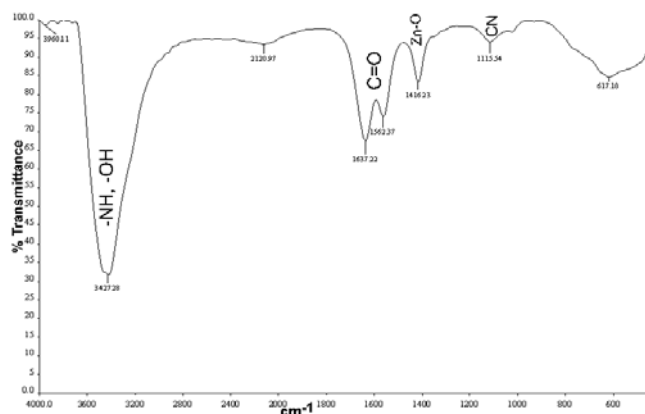
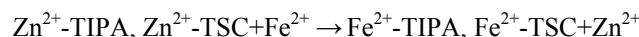


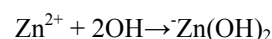
**Figure 4b.** Aqueous solution containing 60ppm of Cl<sup>-</sup> + 100 ppm of TIPA + 50 ppm of Zn<sup>2+</sup> + 250 ppm of TSC

### Conclusion

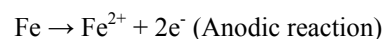
With these discussions, a mechanism may be proposed for the corrosion inhibition of carbon steel immersed in aqueous solution containing 60 ppm Cl<sup>-</sup> by TIPA (100 ppm) – Zn<sup>2+</sup>(50 ppm) - TSC (250 ppm) system. When the formulation consisting 60 ppm Cl<sup>-</sup>, 100 ppm TIPA and 50 ppm of Zn<sup>2+</sup>, there is formation of TIPA-Zn<sup>2+</sup>, TSC-Zn<sup>2+</sup> complex in solution. When mild steel immersed in this solution TIPA-Zn<sup>2+</sup>, TSC-Zn<sup>2+</sup> complex diffuses from the bulk of the solution towards the metal surface. TIPA-Zn<sup>2+</sup>, TSC-Zn<sup>2+</sup> complex are converted in to TIPA-Fe<sup>2+</sup>, TSC-Fe<sup>2+</sup> complex on the anodic sites of the metal surface with release of Zinc ion.



The released Zn<sup>2+</sup> combines with OH<sup>-</sup> to form Zn(OH)<sub>2</sub> on the cathodic sites of the metal surface



Thus the protective film consists of TIPA-Fe<sup>2+</sup>, TSC-Fe<sup>2+</sup> complex and Zn(OH)<sub>2</sub>. In aqueous solution the anodic reaction is the formation of Fe<sup>2+</sup>. This anodic reaction is controlled by the formation of TIPA-TSC-Fe<sup>2+</sup> complex on the anodic sites of the metal surface. The cathodic reaction is the formation of OH<sup>-</sup> which is controlled by the formation of Zn(OH)<sub>2</sub> on the cathodic sites of the metal surface



FTIR spectra reveal that protective film formed on the metal surface. This accounts for the synergistic effect of TIPA-Zn<sup>2+</sup>-TSC system function as an anodic inhibitor.

### Acknowledgement

The authors are thankful to Head, chemistry department, Thiagarajar College and Head, chemistry department, NMSSVN College, Madurai, Tamilnadu, for their encouragement and necessary laboratory facilities.

## References

- <sup>1</sup>Altoe, P., Pimenta, G., Moulin, C. F., Diaz, S. L. and Mattor, O. R., *Electrochim. Acta.*, **1996**, *41*, 1165.
- <sup>2</sup>Roberse, P. R. and Sastri, V. S., *Corros. Sci.*, **1993**, *35*, 1503.
- <sup>3</sup>Gauveric, L., *Corrosion in the Photo Chemical Industry, ASM International.*, **1995**.
- <sup>4</sup>Matsunami, K., Kato, T., Sugimoto, K., *Int. J. Pressure Vessels Piping.*, **1991**, *45*, 179.
- <sup>5</sup>Paty, B. B. and Singh, D. D. N., *Corros. Sci.*, **1992**, *489*, 442.
- <sup>6</sup>Ashassi-Sorkhabi, H. and Nabavi-Amri, S. A., *Acta Chim. Sloven.*, **2000**, *47(4)* 507-518.
- <sup>7</sup>Fontana, M. G., *Corrosion Engineering, 3<sup>rd</sup> Edition*, M. C. Graw-Hill, **1982**.
- <sup>8</sup>Eddy, N. O., Ibok, U. J. and Ita, B. I., *J. Comput. Methods Sci. Eng.*, **2011**, *2*, 25-43.
- <sup>9</sup>Ormellese, M., Bolzoni, F., Lazzari, I., Brenna, A. and Predeterri, M., *Mater. Corros.*, **2011**, *62*, 170-172.
- <sup>10</sup>Helal, N. H. and Badawy, W. A., *Electrochim. Acta*, **2011**, *56*, 19.
- <sup>11</sup>Wranglen, G., *An Introduction to corrosion and Protection of Metals*, Chapman & Hall, **1985**.
- <sup>12</sup>Bawal, A. and Engelken, R. D., *Environ. Sci. Policy*, **2002**, *5*, 2 121-133.
- <sup>13</sup>EI-Eme, A. Y., *Corros. Sci.*, **2003**, *45(11)*, 2485-2495.
- <sup>14</sup>EI-Eme, A. Y., *Corros. Sci.*, **1998**, *40(11)*, 1845-1850.
- <sup>15</sup>Silverstein, R. M., Basler, G. C. and Morrill, T. C., *Spectroscopic Identification of Organic Compounds, 4th Edition*, John Wiley and Sons, **1981**.
- <sup>16</sup>Cross, A. D., *Introduction to Practical Infrared Spectroscopy*, Butterworths Scientific Publication, **1990**.
- <sup>17</sup>Shyamala Devi, B. and Rajendran, S., *Eur. Chem. Bull.*, **2012**, *1(5)*, 150-157.
- <sup>18</sup>Vijaya, N., Peter Pascal Regis, A., Rajendran, S., Pandiarajan, M. and Nagalakshmi, R., *Eur. Chem. Bull.* **2013**, *2(5)*, 275-278.

Received: 20.01.2013.

Accepted: 03.02.2013.





# STRUCTURAL CHARACTERIZATION AND HYDROLYSIS STUDIES OF REBAUDIOSIDE E, A MINOR SWEET COMPONENT OF *STEVIA REBAUDIANA*

Venkata Sai Prakash Chaturvedula<sup>[a]\*</sup> and Indra Prakash<sup>[a]</sup>

**Keywords:** *stevia rebaudiana*, compositae, asteraceae, rebaudioside A, spectral data, chemical studies.

From the commercial extract of the leaves of *Stevia rebaudiana*, a diterpene glycoside was isolated which was characterized as 13-[(2-*O*-β-D-glucopyranosyl-β-D-glucopyranosyl)oxy] *ent*-kaur-16-en-19-oic acid-(2-*O*-β-D-glucopyranosyl-β-D-glucopyranosyl) ester (**1**); also known as rebaudioside E. The complete <sup>1</sup>H and <sup>13</sup>C NMR assignments of rebaudioside E was achieved by the extensive 1D and 2D NMR (<sup>1</sup>H and <sup>13</sup>C, COSY, HMQC, HMBC) as well as mass spectral data. Further, hydrolysis studies were performed on rebaudioside E using acid and enzymatic studies to identify aglycone and sugar residues in its structure.

\* Corresponding Authors

E-Mail: [ychaturvedula@coca-cola.com](mailto:ychaturvedula@coca-cola.com)

[a] Organic Chemistry Department, The Coca-Cola Company, Global Research and Development, One Coca-Cola Plaza, Atlanta, GA 30313, USA Chapters

## Introduction

*Stevia rebaudiana* (Bertoni) is a perennial shrub belonging to the family of Asteraceae (Compositae) native to Brazil and Paraguay, but now grown commercially in a number of countries, particularly in Japan, Taiwan, Korea, Thailand and Indonesia.<sup>1-2</sup> Extracts of the leaves of *S. rebaudiana* have been used for decades to sweeten food and beverages in Japan, South America and China. The major constituents in the leaves of *S. rebaudiana* are the potently sweet glycosides namely steviolbioside, stevioside, rebaudiosides A and E, dulcoside A and rubusoside; which are glycosides of the diterpene steviol, *ent*-13-hydroxykaur-16-en-19-oic acid.<sup>3-4</sup> These compounds are also known as Stevia sweeteners. Rebaudioside E is minor component of *S. rebaudiana* and tastes about 150-200 times sweeter than sucrose and is non-caloric.

In our continuing research to discover natural sweeteners, we have collected commercial extracts of *S. rebaudiana* from various suppliers all over the World and isolated several novel diterpene glycosides.<sup>5-12</sup> Apart from isolating novel compounds from *S. rebaudiana* and utilizing them as possible natural sweeteners or sweetness enhancers, we are also engaged in understanding the stability of the steviol glycosides in various systems of interest and identification of degradation products using various spectroscopic techniques as well as synthesis using naturally occurring starting materials and their taste evaluation.<sup>13-18</sup> In this article, we are describing the isolation, characterization and complete <sup>1</sup>H and <sup>13</sup>C NMR spectral assignments for the diterpene glycoside 13-[(2-*O*-β-D-glucopyranosyl-β-D-glucopyranosyl)oxy] *ent*-kaur-16-en-19-oic acid-(2-*O*-β-D-glucopyranosyl-β-D-glucopyranosyl) ester (**1**) which is also known as rebaudioside E (Figure 1). The complete NMR assignments were achieved on the basis of 1D (<sup>1</sup>H and <sup>13</sup>C) and 2D (COSY, HMQC and HMBC) NMR as well as high resolution mass spectroscopic data. Acid, and enzymatic

hydrolysis studies on compound **1** were carried out to identify aglycone and sugar residues.

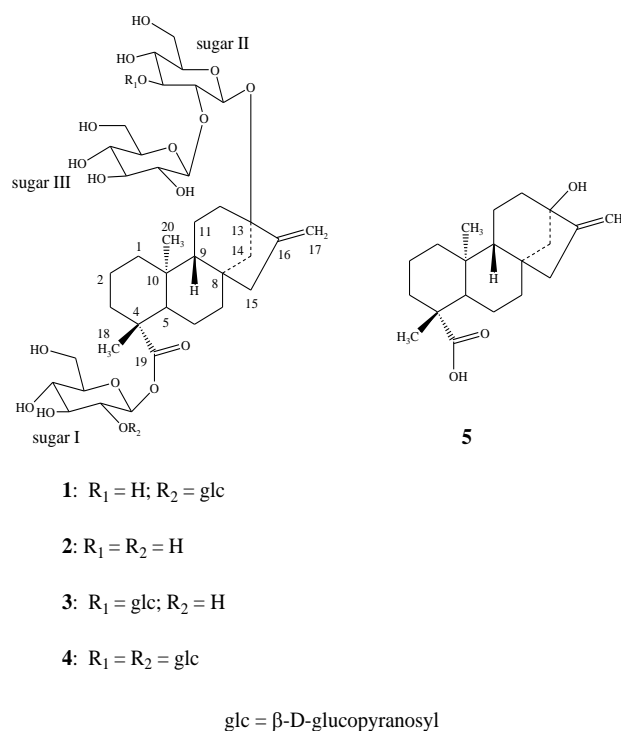


**Figure 1.** Structure of rebaudioside E (**1**) and other compounds

## EXPERIMENTAL

### General Instrumentation Procedures

Melting points were measured using a SRS Optimelt MPA 100 instrument and are uncorrected. Optical rotation was performed using Rudolph Autopol V at 25 °C and IR spectral data was acquired using a Perkin Elmer 400 Fourier Transform Infrared (FT-IR) Spectrometer with Universal attenuated total reflectance (UATR) polarization accessory. HPLC analysis was performed using an Agilent (Wilmington, DE) 1200 system, including a quaternary

pump, a temperature controlled column compartment with additional 6-port switching valve, an autosampler and a UV absorbance detector. Phenomenex Prodigy (Torrance, CA) ODS (3) with a Phenomenex guard column, 250 x 21.2 mm, 5  $\mu\text{m}$  (p/n 00G-4097-P0); and Phenomenex Synergi (Torrance, CA) Hydro RP, 250 x 10 mm, 4  $\mu\text{m}$  (p/n 00G-4336-N0) were used for the purification of rebaudioside E (**1**).

Analytical HPLC was carried out with a Waters 600E multisolvent delivery system using a Phenomenex Luna C<sub>18</sub> (150 x 4.6 mm, 5  $\mu\text{m}$ ) column for sugar identification.

NMR spectra were acquired on a Bruker DRX 500 MHz instrument with a 5 mm inverse detection probe using standard pulse sequences. The NMR spectra were performed in CD<sub>3</sub>OD and C<sub>5</sub>D<sub>5</sub>N; chemical shifts are given in  $\delta$  (ppm), and coupling constants are reported in Hz. The spectral data was referenced to the residual solvent signal ( $\delta_{\text{H}}$  3.30, and  $\delta_{\text{C}}$  49.0 for CD<sub>3</sub>OD or  $\delta_{\text{H}}$  7.19, and  $\delta_{\text{C}}$  123.5 for pyridine-d<sub>5</sub>).

MS and MS/MS data were generated with a Waters Premier QToF mass spectrometer equipped with an electrospray ionization source. Samples were diluted with H<sub>2</sub>O:acetonitrile (1:1) containing 0.1% formic acid and introduced via infusion using the onboard syringe pump. The samples were diluted to yield good signal to noise (s/n) which occurred at an approximate concentration of 0.01 mg mL<sup>-1</sup>.

#### Plant Material

SG95, the commercial aqueous extract consisting of a mixture of diterpenoid glycosides of the leaves of *S. rebaudiana* was obtained from the Pure Circle (Kuala Lumpur, Malaysia). The authenticity of the crude extract was confirmed by performing its retention time ( $t_{\text{R}}$ ) comparison with the internal standard compounds of known steviol glycosides isolated from *S. rebaudiana* using the preparative HPLC method as reported earlier.<sup>19</sup> A voucher specimen is deposited at The Coca-Cola Company, No. VSPC-3166-002.

#### Isolation and Characterization

Compound **1** was purified in two rounds by using an Agilent HPLC 1200 system equipped with a reversed phase (RP) HPLC. The initial round of purification using reversed phase HPLC is summarized below:

Column: Phenomenex Prodigy (Torrance, CA) ODS (3) with a Phenomenex guard column, 250 x 21.2 mm, 5  $\mu\text{m}$  (p/n 00G-4097-P0); Mobile Phase A: H<sub>2</sub>O; Mobile Phase B: Acetonitrile; Flow Rate: 20 mL min<sup>-1</sup>; Injection volume: 1000  $\mu\text{L}$  at 77 mg/mL, prepared in Acetonitrile / H<sub>2</sub>O (1:1). UV detection at 210 nm was used for obtaining a fraction rich of the steviol glycoside **1** with a total run time of 46 min (Table 1).

All of the baseline material eluting between retention time ( $t_{\text{R}}$ ) 11 and 18 min was collected and dried by rotary evaporation under reduced pressure for second round of purification.

**Table 1.** RP-HPLC method utilized for the purification of fraction rich in Rebaudioside E (**1**)

Time, min	% A	% B
0.0	75	25
8.5	75	25
10.0	71	29
15.5	70	30
17.5	66	34
23.5	66	34
25.5	48	52
28.5	48	52
29.5	30	70
35.0	30	70
35.1	75	25
45.0	75	25
46.0	75	25

A second round of purification was used using an Agilent HPLC 1200 system equipped with a reversed phase (RP) HPLC using the method given below: Column: Phenomenex Synergi Hydro RP, 250 x 10 mm, 4  $\mu\text{m}$  (p/n 00G-4336-N0); UV Detection: 210 nm; Mobile Phase A: H<sub>2</sub>O (0.01156% HOAc, 0.02844% NH<sub>4</sub>OAc); Mobile Phase B: Acetonitrile; Flow Rate: 5.0 mL/min; Injection volume: 250  $\mu\text{L}$ , prepared in H<sub>2</sub>O.

**Table 2.** RP-HPLC method utilized for the purification of pure rebaudioside E (**1**)

Time, min	%A	%B
0.0	75	25
8.5	75	25
10.0	71	29
16.5	70	30
16.51	0	100
21	0	100
21.1	75	25
28	75	25

Using the above mentioned HPLC method shown in Table 2, collected the peak eluting at  $t_{\text{R}}$  7.05 min; and dried the corresponding solution under nitrogen yielded **1**.

#### 13-[(2-O- $\beta$ -D-glucopyranosyl- $\beta$ -D-glucopyranosyl)oxy] ent-kaur-16-en-19-oic acid-(2-O- $\beta$ -D-glucopyranosyl- $\beta$ -D-glucopyranosyl) ester (Rebaudioside E, **1**)

White powder; IR  $\nu_{\text{max}}$ : 3315, 2943, 1722, 1055, 910 cm<sup>-1</sup>; <sup>1</sup>H-NMR (600 MHz, CD<sub>3</sub>OD,  $\delta$  ppm) and <sup>13</sup>C-NMR (150 MHz, CD<sub>3</sub>OD,  $\delta$  ppm) spectroscopic data see Table 3; HRMS (M+H)<sup>+</sup>  $m/z$  967.4418 (calcd. for C<sub>44</sub>H<sub>71</sub>O<sub>23</sub>: 967.4386); (M+NH<sub>4</sub>)<sup>+</sup>  $m/z$  984.4690 (calcd. for C<sub>44</sub>H<sub>74</sub>O<sub>23</sub>N: 984.4652); (M+Na)<sup>+</sup>  $m/z$  989.4237 (calcd. for C<sub>44</sub>H<sub>70</sub>O<sub>23</sub>Na: 989.4206).

#### Acid hydrolysis of **1**

To a solution of compound **1** (2 mg) in MeOH (3 ml) was added 3 ml of 5% H<sub>2</sub>SO<sub>4</sub> and the mixture was refluxed for 8 hours. The reaction mixture was then neutralized with saturated sodium carbonate and extracted with ethyl acetate (EtOAc) (2 x 25 ml) to give an aqueous fraction containing sugars and an EtOAc fraction containing the aglycone part.

The aqueous phase was concentrated and compared with standard sugars using the TLC systems EtOAc/*n*-butanol/water (2:7:1) and CH<sub>2</sub>Cl<sub>2</sub>/MeOH/water (10:6:1),<sup>20-22</sup> the sugar was identified as glucose.

#### Determination of sugar configuration in **1**

Compound **1** (1 mg) was hydrolyzed with 0.5 M HCl (2 mL) for 1.5 h. After cooling, the mixture was passed through an Amberlite IRA400 column and the eluate was lyophilized. The residue was dissolved in pyridine (1 mL) and heated with L-cysteine methyl ester HCl (5 mg) at 60°C for 1.5 h, and then *O*-tolyl isothiocyanate (25 µL) was added to the mixture and heated at 60 °C for an additional 1.5 h. The reaction mixture was analyzed by HPLC: column Phenomenex Luna C18, 150 x 4.6 mm (5 µ); 25% acetonitrile-0.2% TFA water, 1 mL min<sup>-1</sup>; UV detection at 250 nm. The sugar was identified as D-glucose (*t*<sub>R</sub>, 12.32 min) [authentic samples, D-glucose (*t*<sub>R</sub>, 12.38) and L-glucose (*t*<sub>R</sub>, 11.16 min)].<sup>23</sup>

#### Enzymatic hydrolysis of **1**

Compound **1** (1 mg) was dissolved in 10 ml of 0.1 M sodium acetate buffer, pH 4.5 and crude pectinase from *Aspergillus niger* (50 µL, Sigma-Aldrich, P2736) was added. The mixture was stirred at 50 °C for 48 hr. The product precipitated out during the reaction and was filtered and then crystallized. The resulting product obtained from the hydrolysis of **1** was identified as steviol (**5**) by comparison of its co-TLC with standard compound and <sup>1</sup>H NMR spectral data.<sup>24</sup>

### Results and Discussion

Compound **1** was isolated as a colorless powder and its positive mode of ESI ToF mass spectrum indicated an [M+H]<sup>+</sup> ion at *m/z* 967.4418 together with [M+NH<sub>4</sub>]<sup>+</sup> and [M+Na]<sup>+</sup> adducts at *m/z* 984.4690 and 989.4237, respectively. The mass of the [M+H]<sup>+</sup> ion was in good agreement with the molecular formula C<sub>44</sub>H<sub>70</sub>O<sub>23</sub> (calcd for C<sub>44</sub>H<sub>71</sub>O<sub>23</sub>: 967.4386) for rebaudioside E (**1**) and this composition was supported by <sup>13</sup>C NMR spectral data. The negative mode of ESI mass spectrum gave an [M-H]<sup>-</sup> ion at *m/z* 965.4263 which was in good agreement with the molecular formula C<sub>44</sub>H<sub>70</sub>O<sub>23</sub> (calcd for C<sub>44</sub>H<sub>69</sub>O<sub>23</sub>: 965.4230) supported further its molecular weight. The +ESI and -ESI data indicated that compound **1** has a nominal mass of 966 Daltons with the molecular formula C<sub>44</sub>H<sub>70</sub>O<sub>23</sub> and is, therefore, an isomer of rebaudioside A (**3**). The MS/MS spectrum of **1**, fragmenting on the [M+H]<sup>+</sup> ion at *m/z* 967 indicated the sequential loss of four hexose moieties at *m/z* 805.3868, 643.3336, 481.2813, and 319.2299.

The <sup>1</sup>H NMR spectrum of **1** showed the presence of two methyl singlets at δ 1.08 and 1.40, two olefinic protons as singlets at δ 5.06 and 5.73 of an exocyclic double bond, nine methylene and two methine protons between δ 0.71-2.52 characteristic for the *ent*-kaurane diterpenoids isolated earlier from the genus *Stevia*.<sup>3-10</sup> The basic skeleton of *ent*-kaurane diterpenoids was supported by COSY (H-1/H-2; H-2/H-3; H-5/H-6; H-6/H-7; H-9/H-11; H-11/H-12) and HMBC (H-1/C-2, C-10; H-3/C-1, C-2, C-4, C-5, C-18, C-19; H-5/C-4, C-6, C-7, C-9, C-10, C-18, C-19, C-20; H-9/C-8, C-10, C-11, C-12, C-14, C-15; H-14/C-8, C-9, C-13, C-

15, C-16 and H-17/C-13, C-15, C-16) correlations. The presence of four sugar units in its structure was supported by the <sup>1</sup>H NMR spectrum of **1** which showed the anomeric protons at δ 5.14, 5.29, 5.45, and 6.28. Enzymatic hydrolysis of **1** furnished an aglycone which was identified as steviol (**5**) by comparison of <sup>1</sup>H NMR<sup>24</sup> and co-TLC with standard compound. Acid hydrolysis of **1** with 5% H<sub>2</sub>SO<sub>4</sub> afforded glucose which was identified by direct comparison with authentic samples by TLC.<sup>20-22</sup> The stereochemistry of the sugar was identified as D-glucose by preparing its corresponding thiocarbamoyl-thiazolidine carboxylate derivatives with L-cysteine methyl ester and *O*-tolyl isothiocyanate, and in comparison of their retention times with the standard sugars as described in the literature.<sup>23</sup> The <sup>1</sup>H and <sup>13</sup>C NMR values for all the carbons in **1** were assigned on the basis of COSY, HMQC and HMBC correlations (Table 3).

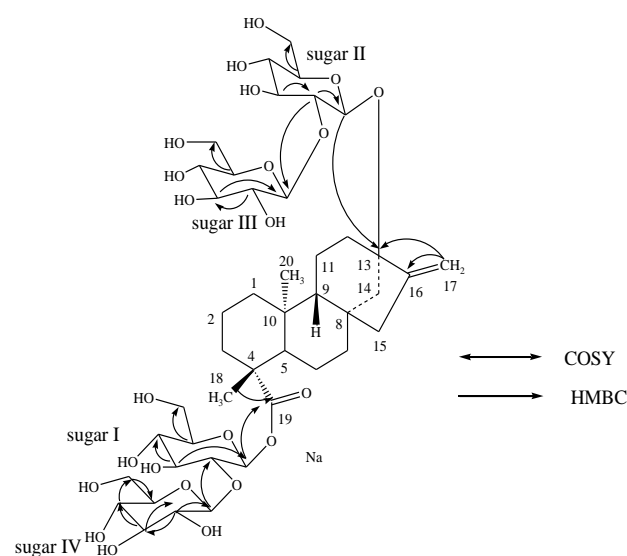


**Figure 2.** Key COSY and HMBC correlations of **1**

Based on the results from NMR spectral data and hydrolysis experiments of **1**, it was concluded that there are four β-D-glucosyl units in its structure similar to rebaudioside A (**3**). A close comparison of the <sup>1</sup>H and <sup>13</sup>C NMR values of **1** with stevioside (**2**) and rebaudioside D (**4**) suggested the presence of a 2-substituted β-D-glucosyl unit at C-13 in the form of ether and another 2-substituted β-D-glucosyl unit at C-19 position in the form of an ester. This was confirmed by the key HMBC correlations: H-2'''/C-1'', C-3'', C-1''''; H-1'''/C-2'', C-2''', C-3'''; H-2'/C-1', C-3', C-1'''' and H-1''''/C-2', C-2''''', C-3'''''. The large coupling constants observed for the four anomeric protons of the glucose moieties at δ 5.14 (d, *J*=7.6 Hz), 5.29 (d, *J*=7.7 Hz), 5.45 (d, *J*=7.8 Hz), and 6.28 (d, *J*=7.9 Hz), suggested their β-orientation as reported for steviol glycosides.<sup>5-12</sup> Based on the results from chemical and spectral studies, **1** was assigned as 13-[(2-*O*-β-D-glucopyranosyl-β-D-glucopyranosyl)oxy] *ent*-kaur-16-en-19-oic acid-(2-*O*-β-D-glucopyranosyl-β-D-glucopyranosyl) ester. The structure was further supported by the key COSY and HMBC correlations as shown in Figure 2.



**Table 3.** <sup>1</sup>H and <sup>13</sup>C NMR spectral data (chemical shifts and coupling constants) for rebaudioside E (**1**).<sup>a-c</sup>

Position	<sup>1</sup> H NMR	<sup>13</sup> C NMR
1	0.71 t (13.4), 1.68 m	40.3
2	1.42 m, 2.11 m	19.7
3	1.08 m, 2.75 d (13.1)	37.4
4	---	44.3
5	0.96 d (12.2)	57.1
6	1.84 d (12.1), 2.09 m	21.7
7	1.26 m, 1.32 m	41.3
8	---	42.5
9	0.86 m	53.7
10	---	39.2
11	1.64 m	20.3
12	1.94 m, 2.14 m	37.0
13	---	86.1
14	1.73 d (11.1), 2.52 d (11.1)	44.3
15	2.03 m, 2.07 m	47.6
16	---	154.5
17	5.06 s, 5.73 s	104.6
18	1.40 s	28.9
19	---	175.6
20	1.08 s	16.3
1'	6.28 d (7.9)	93.2
2'	4.38 m	80.9
3'	4.28 m	77.9
4'	4.24 m	71.4
5'	3.90 m	78.6
6'	4.33 m, 4.43 m	61.8
1''	5.14 d (7.6)	97.5
2''	4.17 m	84.2
3''	4.32 m	77.8
4''	4.20 m	71.1
5''	3.71 m	77.3
6''	4.24 m, 4.35 m	62.0
1'''	5.45 d (7.8)	105.4
2'''	4.04 t (8.2)	76.0
3'''	4.23 m	77.7
4'''	4.28 m	70.5
5'''	3.96 m	78.1
6'''	4.44 m, 4.52 m	62.4
1''''	5.29 d (7.7)	106.3
2''''	4.13 t (8.4)	76.9
3''''	4.23 m	77.7
4''''	4.32 m	71.3
5''''	3.96 m	78.1
6''''	4.44 m, 4.52 m	62.4

<sup>a</sup> assignments made on the basis of COSY, HMQC and HMBC correlations; <sup>b</sup> Chemical shift values are in  $\delta$  (ppm); <sup>c</sup> Coupling constants are in Hz.

Though partial NMR spectral data has been reported earlier for rebaudioside E (**1**) by Ohta *et al*<sup>25</sup>, this is the first report of the complete <sup>1</sup>H and <sup>13</sup>C NMR spectral assignments based on 1D (<sup>1</sup>H and <sup>13</sup>C) and 2D (COSY, HMQC and HMBC) NMR as well as high resolution mass spectroscopic data which was supported by hydrolysis studies.

## Conclusions

We are herewith reporting the complete <sup>1</sup>H and <sup>13</sup>C NMR spectral assignments for 13-[(2-*O*- $\beta$ -D-glucopyranosyl- $\beta$ -D-glucopyranosyl)oxy] *ent*-kaur-16-en-19-oic acid-(2-*O*- $\beta$ -D-

glucopyranosyl- $\beta$ -D-glucopyranosyl) ester (Rebaudioside E, **1**) that were made on the basis of extensive 1D and 2D NMR as well as high resolution mass spectral data. Further, acid hydrolysis furnished D-glucose suggesting the presence only sugar unit and enzymatic hydrolysis furnished steviol.

## Acknowledgements

We wish to thank AMRI, Bothell, WA, USA for obtaining some selected spectral data and Chris Mubarak, Analytical Sciences Department, The Coca-Cola Company, Atlanta, GA for providing IR spectral data.

## References

- Mosettig, E., Beglinger, U., Dolder, F., Lichiti, H., Quitt, P., Waters, J. A. *J. Am. Chem. Soc.*, **1963**, *85*, 2305.
- Mosettig, E., Beglinger, U., Dolder, F., Lichiti, H., Quitt, P., Waters, J. A. *J. Org. Chem.*, **1955**, *20*, 884-899.
- Wayne, E. S., Lin, L. *Carbohydr. Res.*, **2009**, *344*, 2533-2538.
- Brandle, J. E., Starratt, A.N., Gijen, M. *Can. J. Plant Sci.*, **1998**, *78*, 527-536.
- Chaturvedula, V. S. P., Prakash, I. *J. Med. Plants Res.*, **2011**, *5*, 4838-4842.
- Chaturvedula, V. S. P., Mani, U.; Prakash, I. *Molecules*, **2011**, *16*, 3552-3562.
- Chaturvedula, V. S. P., Prakash, I. *Molecules*, **2011**, *16*, 2937-2943.
- Chaturvedula, V. S. P., Prakash, I. *Carbohydr. Res.*, **2011**, *346*, 1057-1060.
- Chaturvedula, V. S. P., Rhea, J., Milanowski, D., Mocek, U., Prakash, I. *Nat. Prod. Commun.*, **2011**, *6*, 175-178.
- Chaturvedula, V. S. P., Prakash, I. *Nat. Prod. Commun.*, **2011**, *6*, 1059-1062.
- Chaturvedula, V. S. P., Clos, J. F., Rhea, J., Milanowski, D., Mocek, U., DuBois, G. E., Prakash, I. *Phytochemistry Lett.*, **2011**, *4*, 209-212.
- Chaturvedula, V. S. P., Mani, U., Prakash, I. *Carbohydr. Res.*, **2011**, *346*, 2034-2038.
- Chaturvedula, V. S. P., Klucik, J., Mani, U., Prakash, I. *Molecules*, **2011**, *16*, 8402-8409.
- Chaturvedula, V. S. P., Clos, J. F., Prakash, I. *Int. J. Pharm. Pharm. Sci.*, **2011**, *3*, 316-323.
- Chaturvedula, V. S. P., Clos, J. F., Prakash, I. *Int. J. Pharm. Pharm. Sci.*, **2011**, *3* (Suppl. 5), 421-425.
- Prakash, I., Clos, J. F., Chaturvedula, V. S. P. *Food Res. Int.* **2012**, *48*, 65-75.
- Chaturvedula, V. S. P., Campbell, M., Miguel, R. I. S., Prakash, I. *Molecules*, **2012**, *17*, 8908-8916.
- Chaturvedula, V. S. P., Campbell, M., Prakash, I. *Int. J. Mol. Sci.*, **2012**, *13*, 15126-15136.
- Clos, J. F., DuBois, G. E., Prakash, I. *J. Agric. Food Chem.* **2008**, *56*, 8507-8513.
- Bedir, E., Toyang, N. J., Khan, I. A., Walker, L. A., Clark, A. M., *J. Nat. Prod.*, **2001**, *64*, 95-97.
- Chaturvedula, V. S. P., Schilling, J. K., Miller, J. S., Andriantsiferana, R., Rasamison, V. E., Kingston, D. G. I. *Planta Med.*, **2003**, *69*, 440-444.
- Huan, V. D., Yamamura, S., Ohtani, K., Kasai, R., Yamasaki, K., Nham, N. T. *Phytochemistry*, **1998**, *47*, 451-457.

<sup>23</sup>Tanaka, T., Nakashima, T., Ueda, T., Tomii, K., Kouno, I. *Chem. Pharm. Bull.*, **2007**, *55*, 899-901.

<sup>25</sup>Ohta, M., Sasa, S., Inoue, A., Tamai, T., Fujita, I., Morita, K., Matsuura, F. *J. Appl. Glycosci.*, **2010**, *57*, 1553-1559.

<sup>24</sup>Ohtani, K., Aikawa, Y., Kasai, R., Chou, W., Yamasaki, K., Tanaka, O. *Phytochemistry*, **1992**, *31*, 1553-1559.

Received: 22.01.2013.

Accepted: 03.02.2013.